VII. SAMPLING IN SAN JOAQUIN VALLEY AND SAN FRANCISCO BAY AIR BASINS

A. Description of the Meteorology and 3-D Distribution of Pollutants in the San Joaquin Valley

1. Introduction

Aircraft sampling data in the San Joaquin Valley were analyzed for two days, representing sampling days for the Aerosol Characterization Study. These days were September 7 and September 13, 1972. Only two flights were made each day. Discussions of these days are given in the following sections. Complete data for the sampling flights are given in the 1972 Data Volume.

2. September 7, 1972 (Morning)

The streamline flow pattern for 0900 PST on September 7 is shown in Fig. VII-1. The flow at this time of day tends to be relatively complex with northwesterly winds along the western part of the valley and southeasterly winds in the eastern sections. A general convergence region is indicated to the north of Fresno (FAT) and to the west of Bakersfield (BFL). These zones appear to contribute to a complex structure in the mixing heights (Fig. VII-2a) with low mixing layer heights in the northwest sections of the valley and in the southeast. Values of integrated bscat (Fig. VII-2b) are largest where a deep mixing layer occurs near Lost Hills (LH). CO values during the morning (Fig. VII-3a) are rather uniformly distributed, but oxidants also peak in the Lost Hills area (Fig. VII-3b).

September 7, 1972 (Afternoon)

During the afternoon in the San Joaquin Valley, northwesterly winds predominate throughout the entire valley (Fig. VII-4). Mixing layer heights (Fig. VII-5a) are highest along the east, south, and southwest slopes of the valley while the intrusion of cooler, sea breeze air is indicated in the northwest near Modesto (MOD). This results in substantially reduced mixing layer depths in this region. Values of integrated bscat (Fig. VII-5b) are largest along the slopes to the east and south where mixing depths are great and a considerable vertical extent of particulates is being integrated. Otherwise, the b_{scat} values are relatively low. CO values (Fig. VII-6a) peak in the southern sections while maximum oxidant values occur (Fig. VII-6b) near Modesto.

3. September 13, 1972 (Morning)

The morning streamline flow pattern (Fig. VII-7) on September 13 was similar to September 7. Low mixing heights (Fig. VII-8a) occurred in the Los Banos (LOB) area with strongly upward

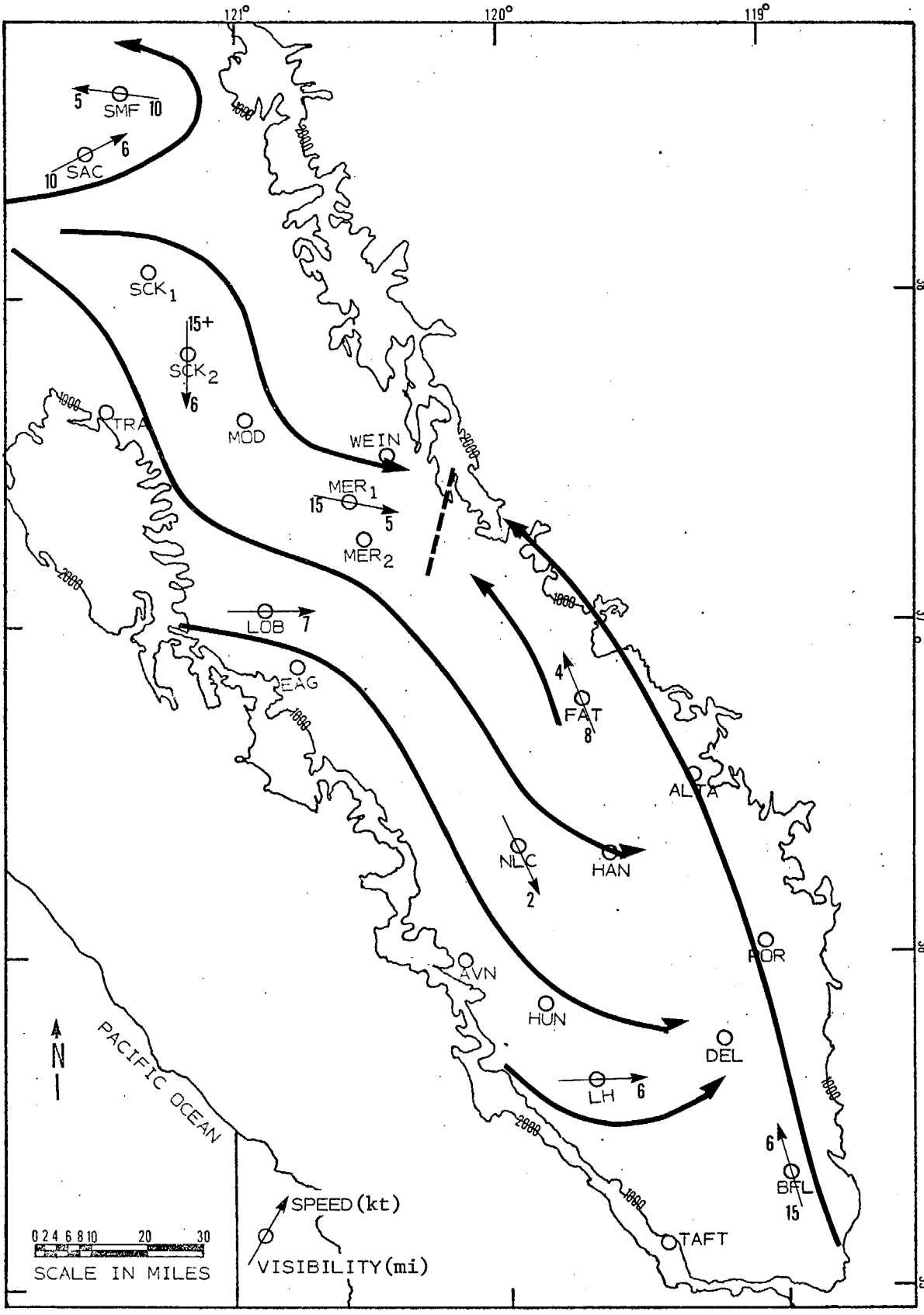

Fig. VII-1. STREAMLINE ANALYSIS - 0900 PST
September 7, 1972

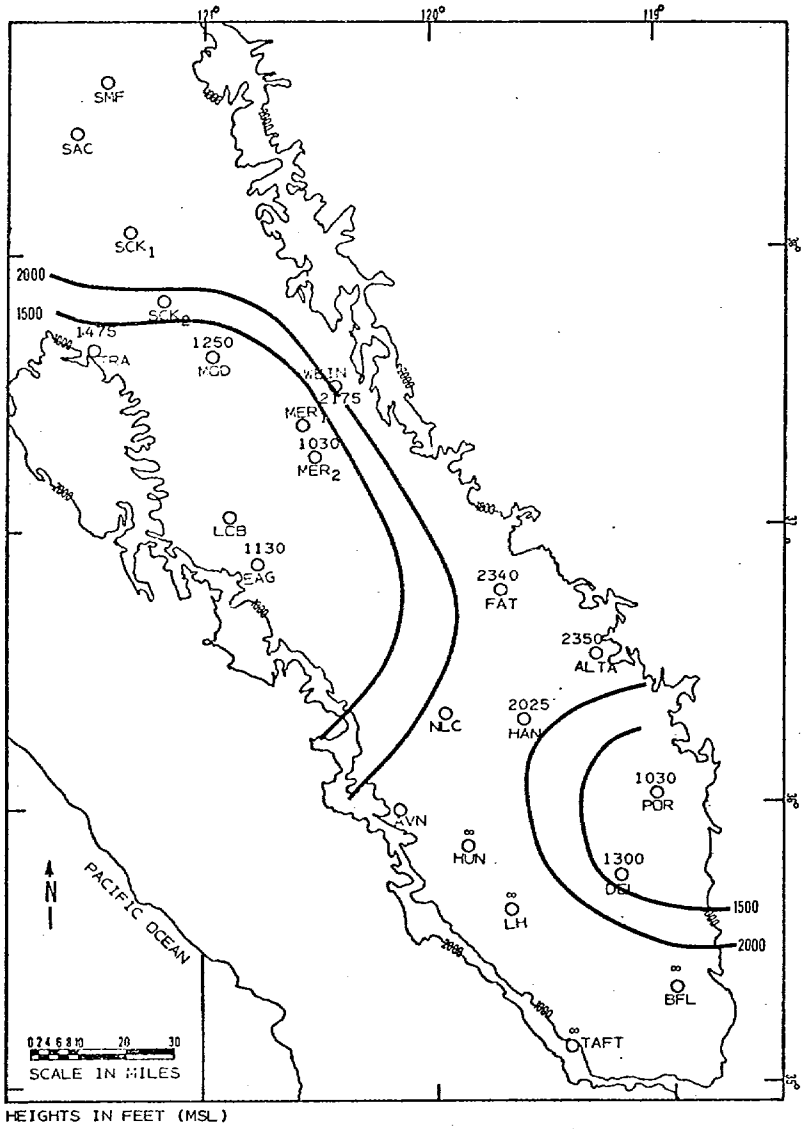

a. MIXING LAYER HEIGHTS - MORNING
September 7, 1972

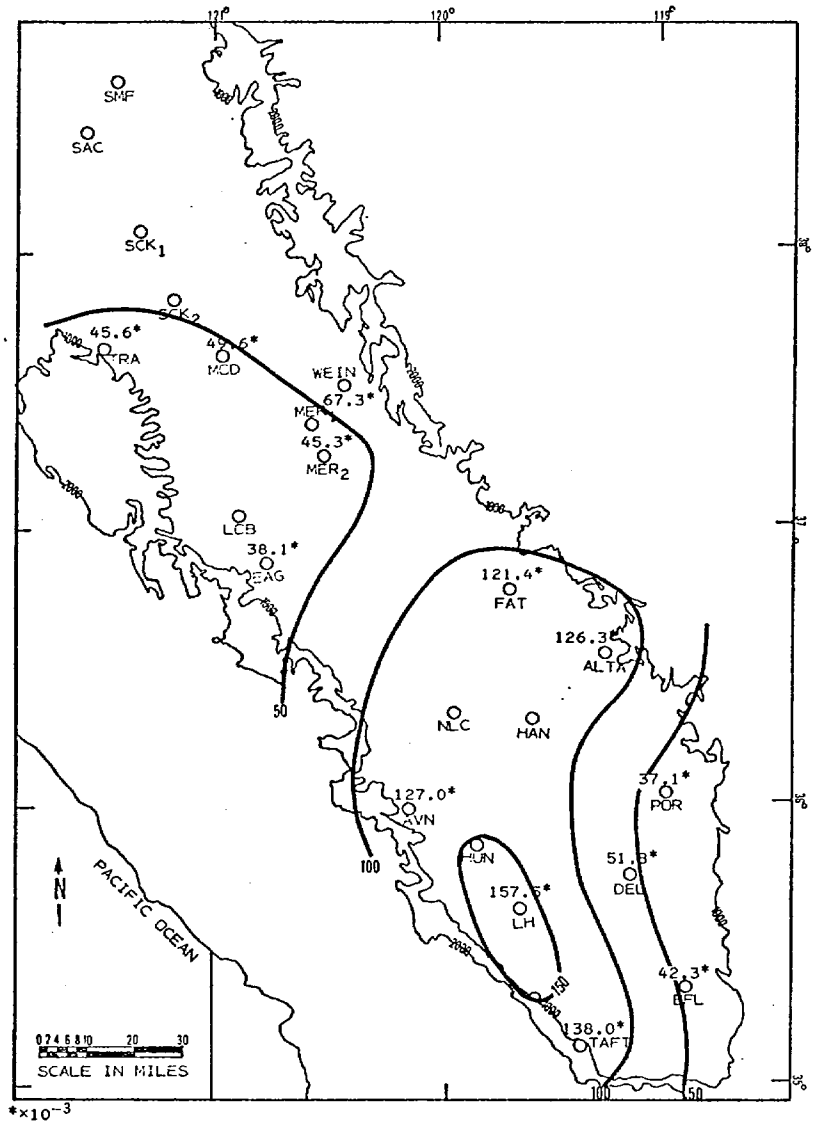

b. b_{scat} INTEGRATIONS - MORNING
September 7, 1972

Fig. VII-2.

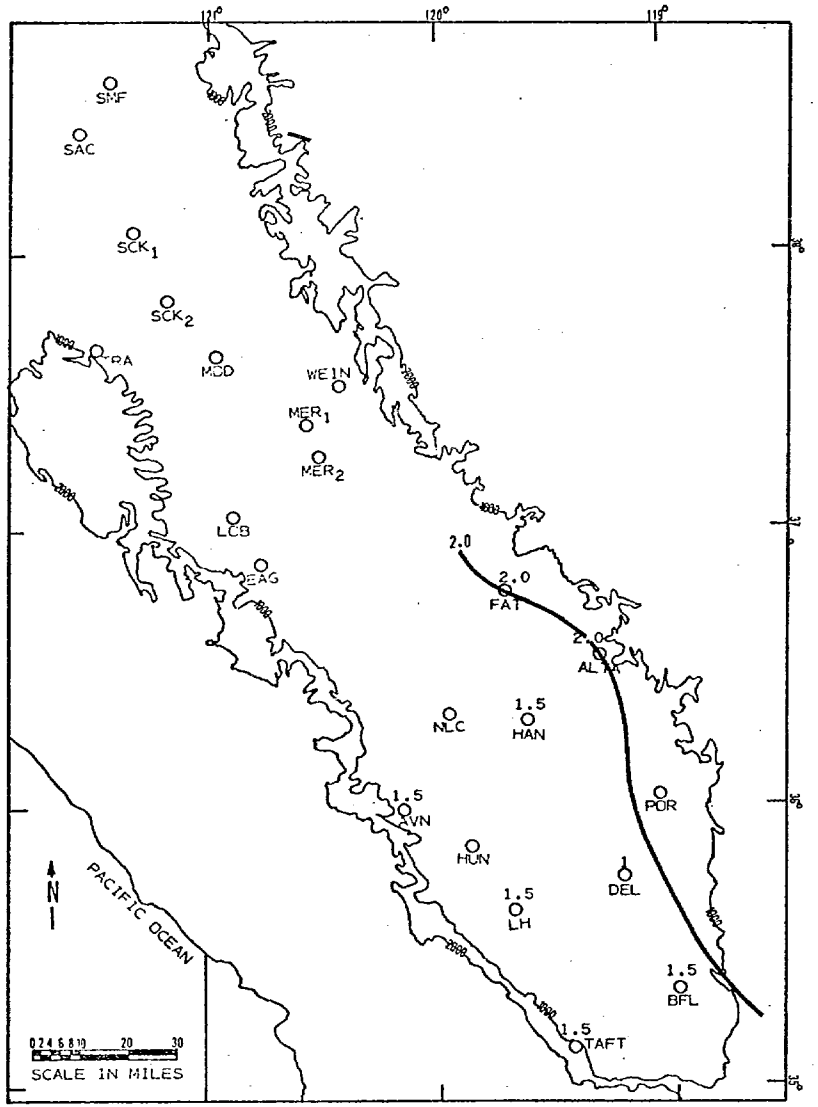

a. PEAK CO CONCENTRATIONS (ppm) WITHIN MIXING LAYER - MORNING
September 7, 1972

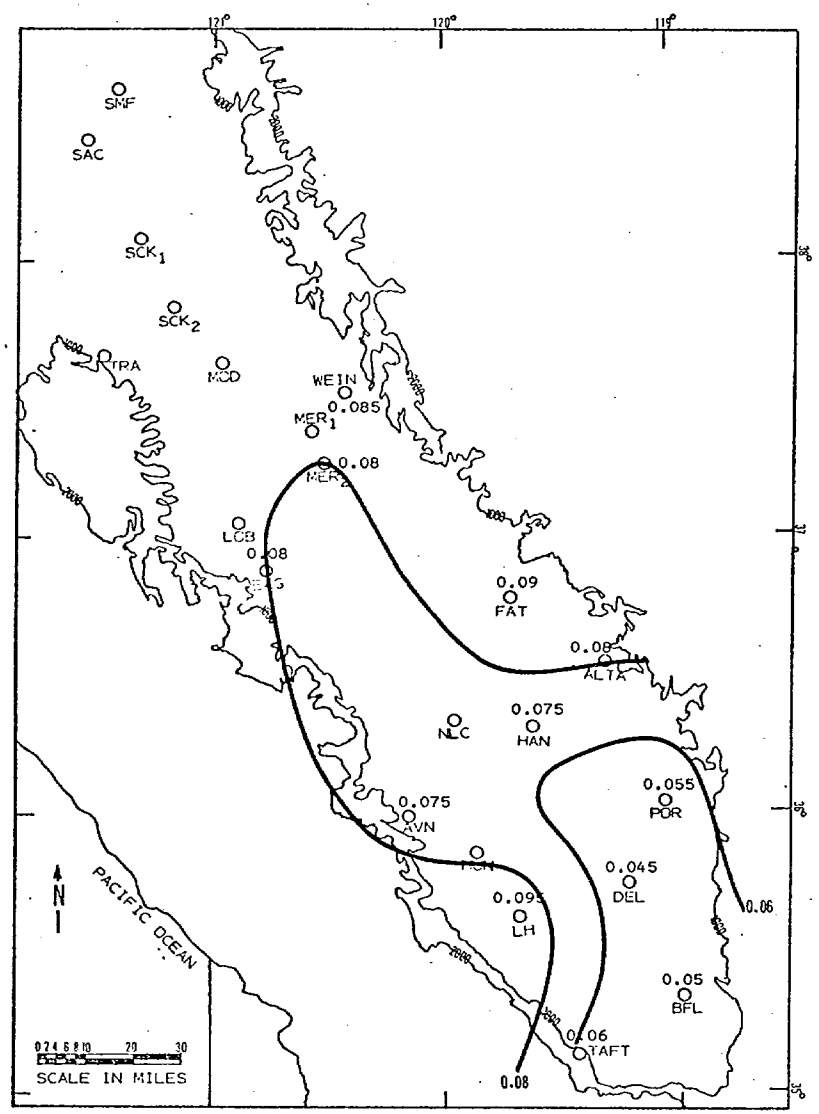

b. PEAK OZONE CONCENTRATIONS (ppm) WITHIN MIXING LAYER - MORNING
September 7, 1972

Fig. VII-3.

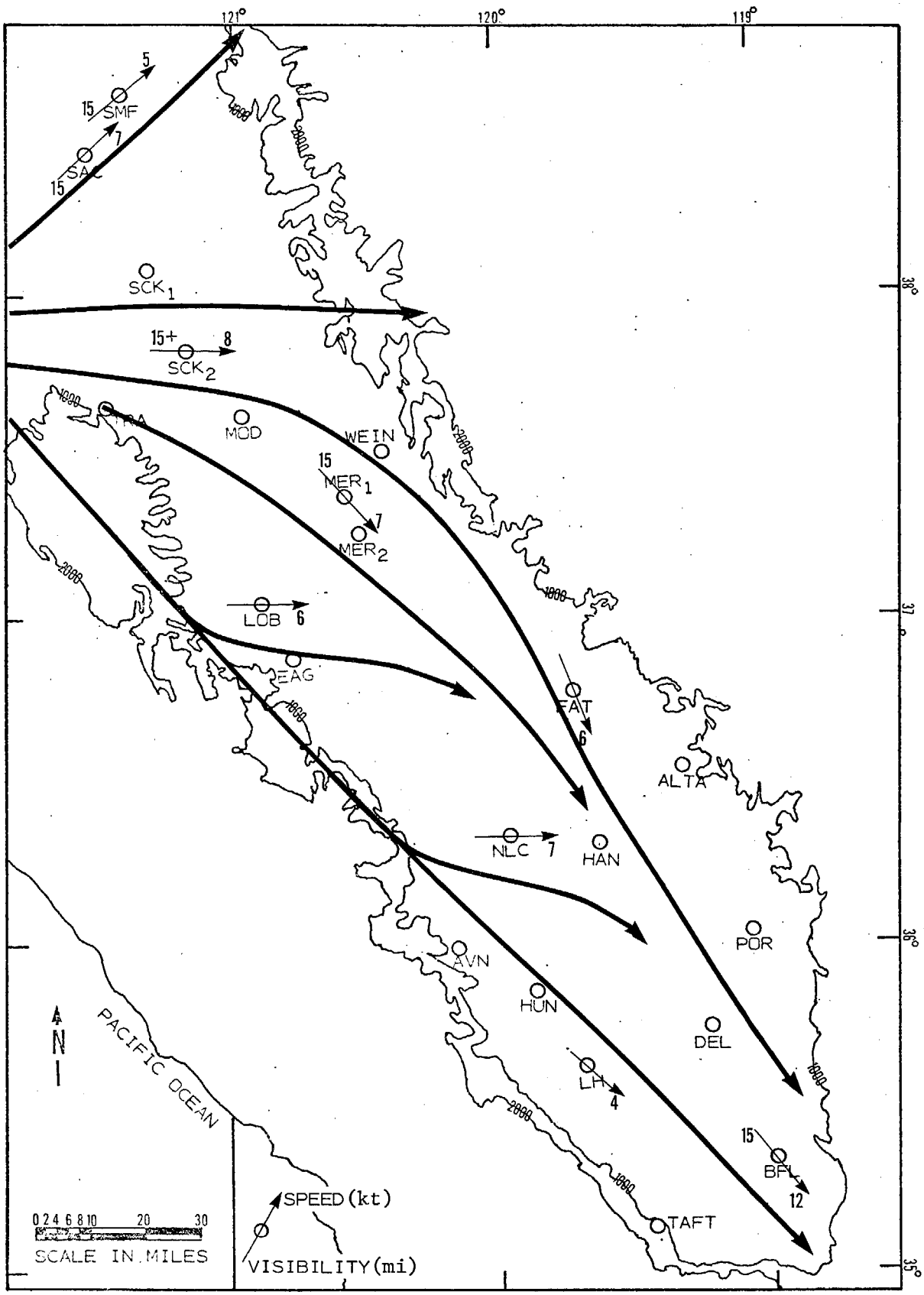

Fig. VII-4. STREAMLINE ANALYSIS - 1500 PST
September 7, 1972

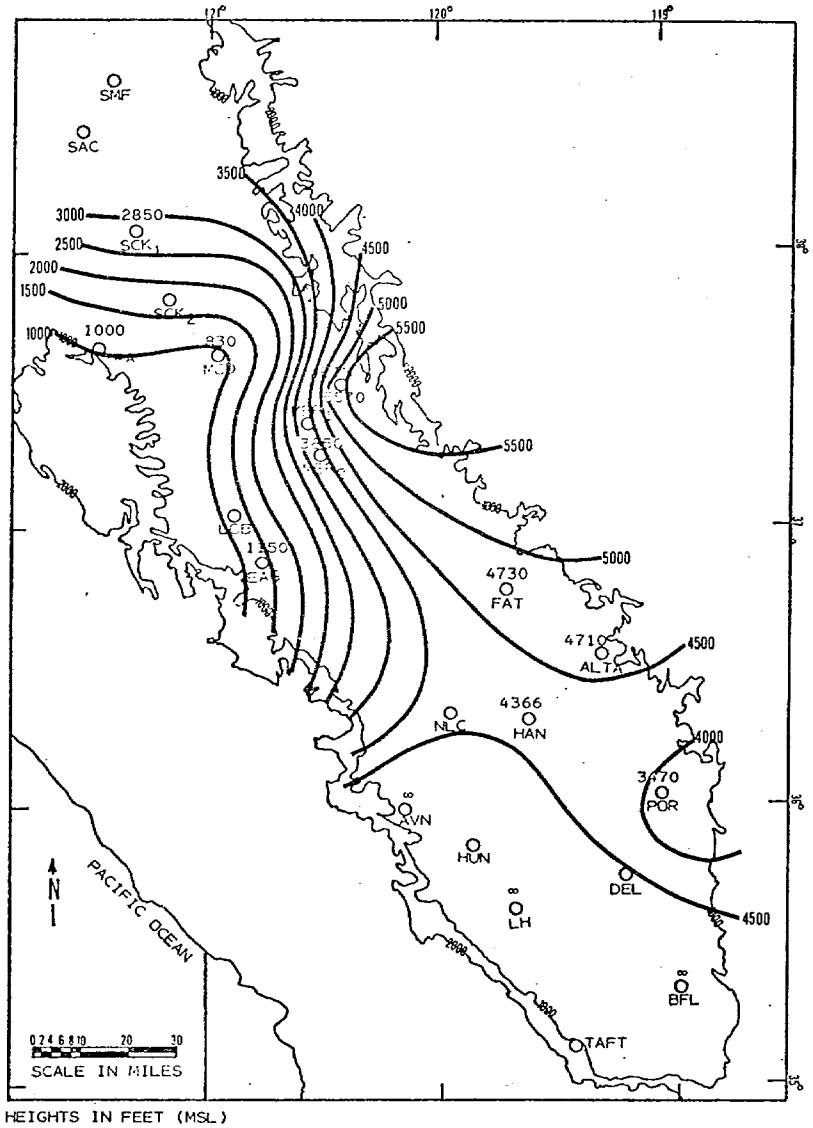

HEIGHTS IN FEET (MSL)

a. MIXING LAYER HEIGHTS - AFTERNOON
September 7, 1972

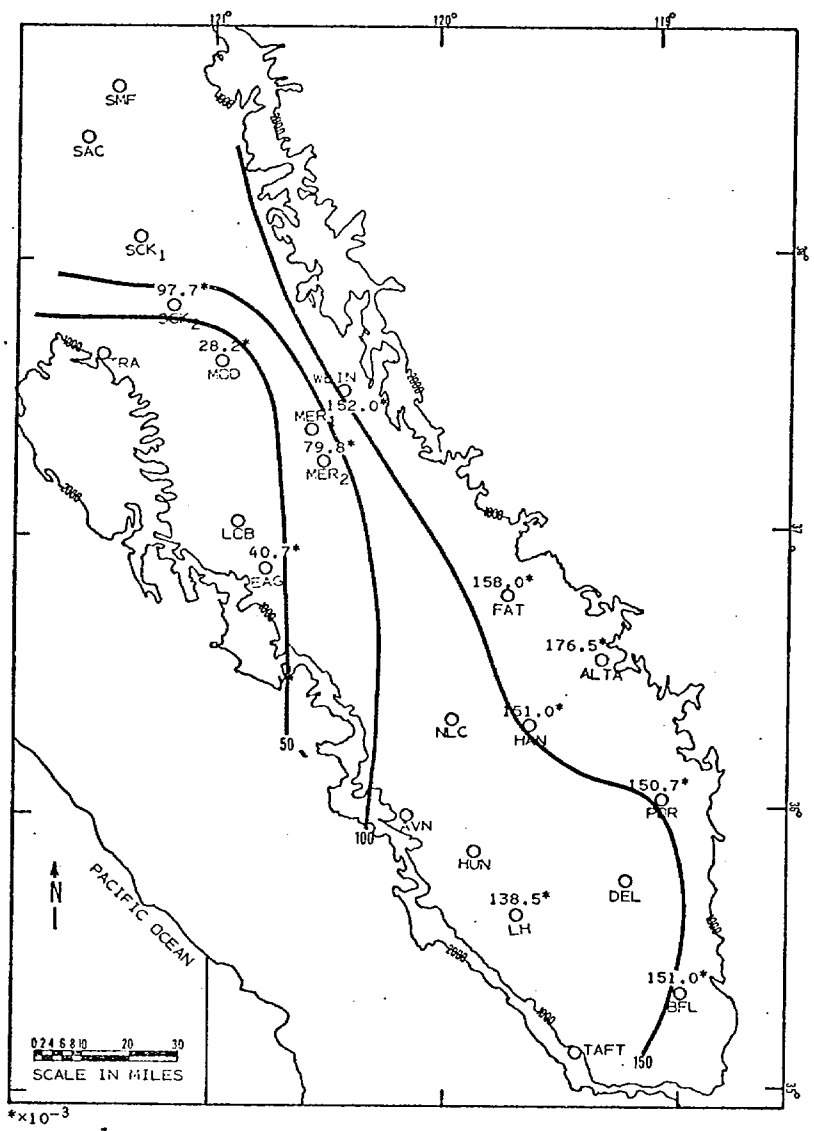

*×10⁻³

b. b_{scat} INTEGRATIONS - AFTERNOON
September 7, 1972

Fig. VII-5.

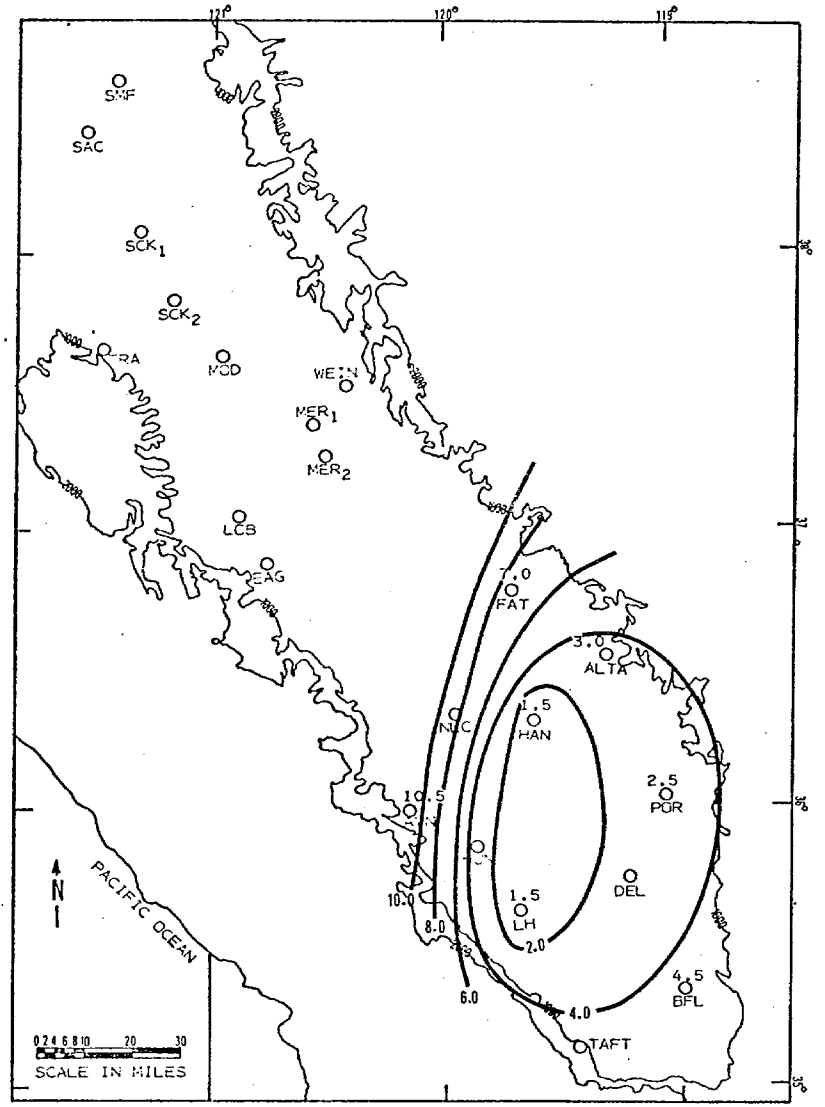

a. PEAK CO CONCENTRATIONS (ppm) WITHIN MIXING LAYER - AFTERNOON
September 7, 1972

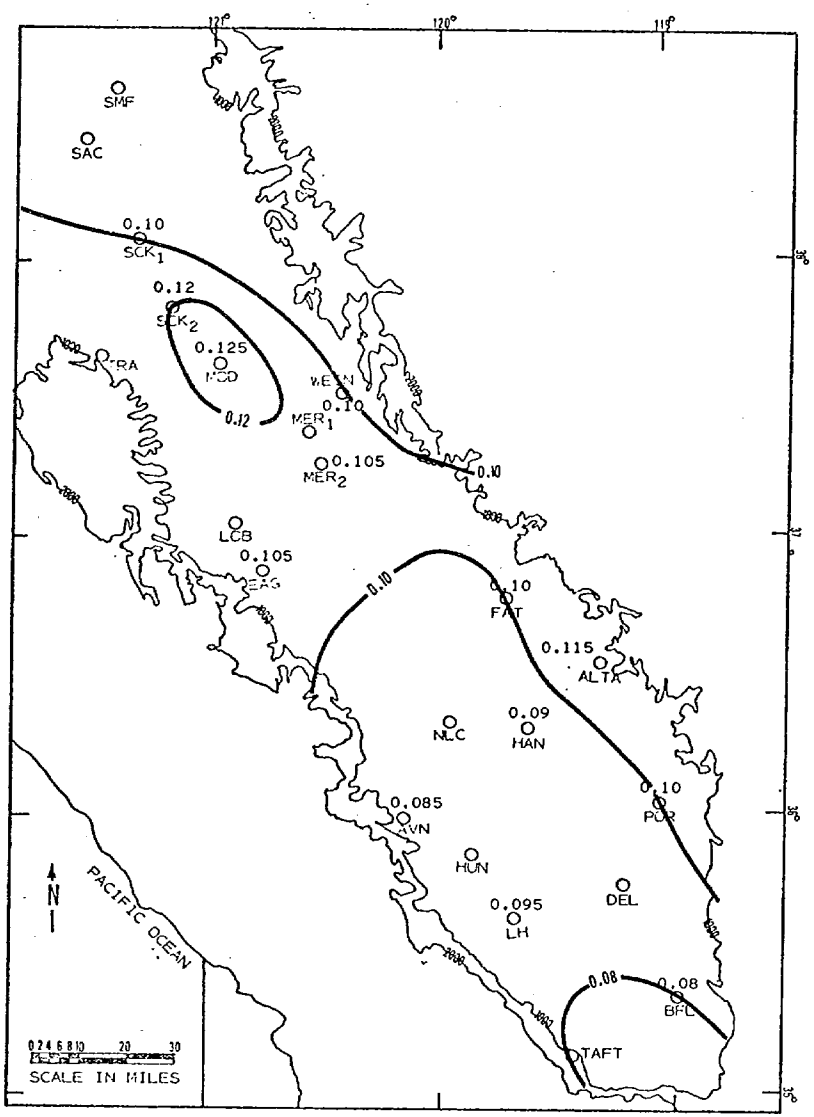

b. PEAK OZONE CONCENTRATIONS (ppm) WITHIN MIXING LAYER - AFTERNOON
September 7, 1972

Fig. VII-6.

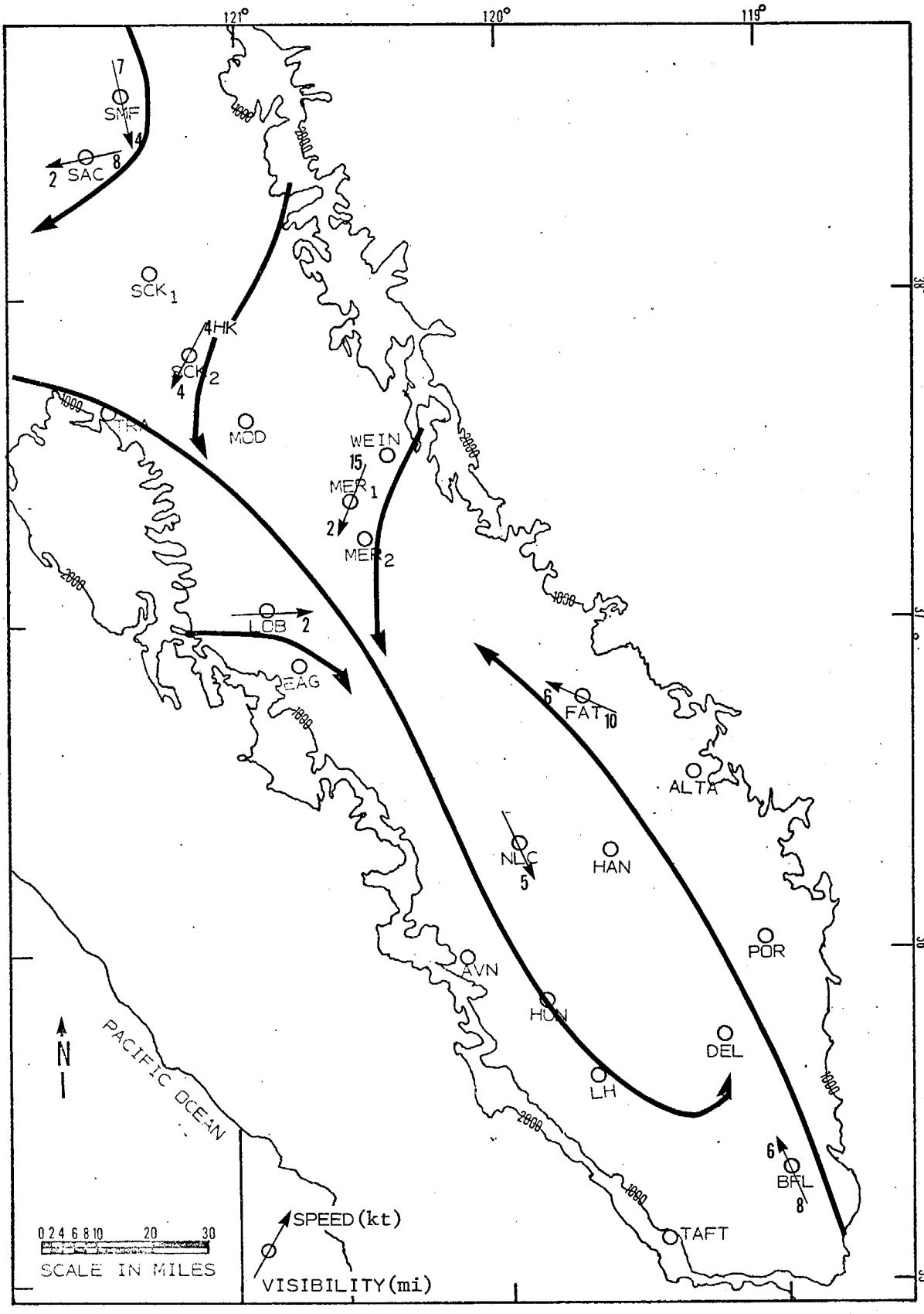

Fig. VII-7. STREAMLINE ANALYSIS - 0900 PST
September 13, 1972

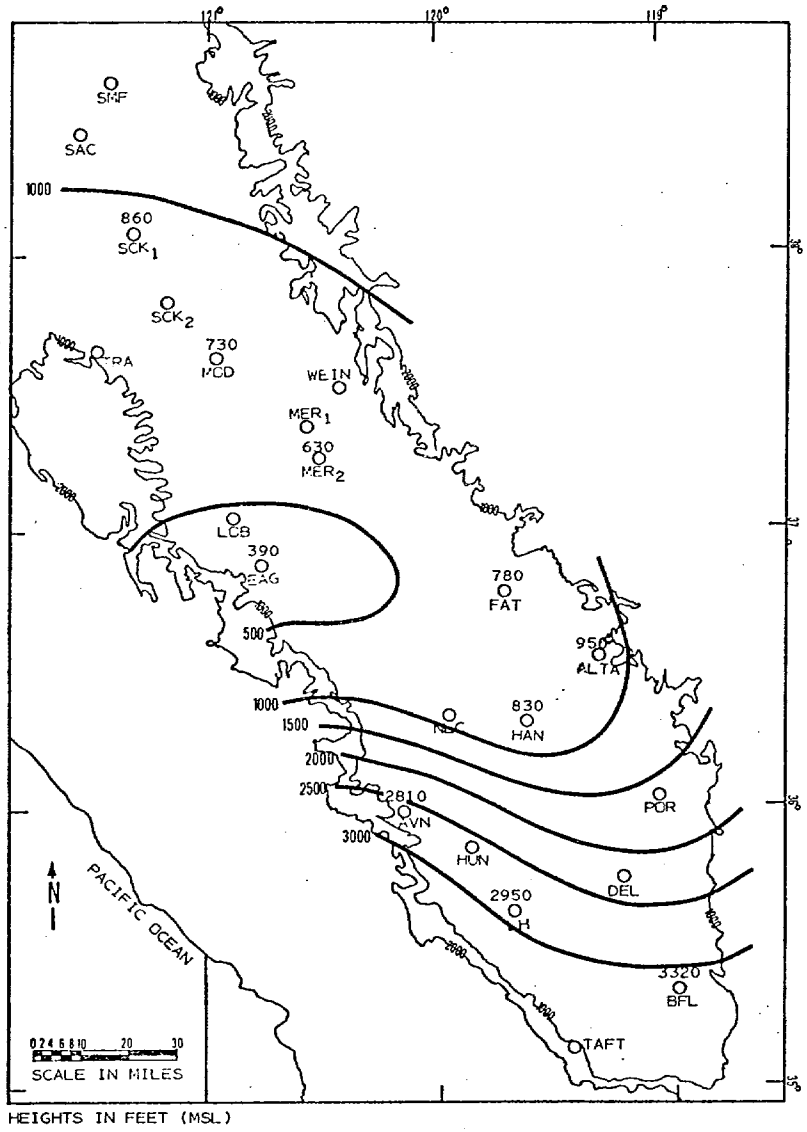

a. MIXING LAYER HEIGHTS - MORNING
September 13, 1972

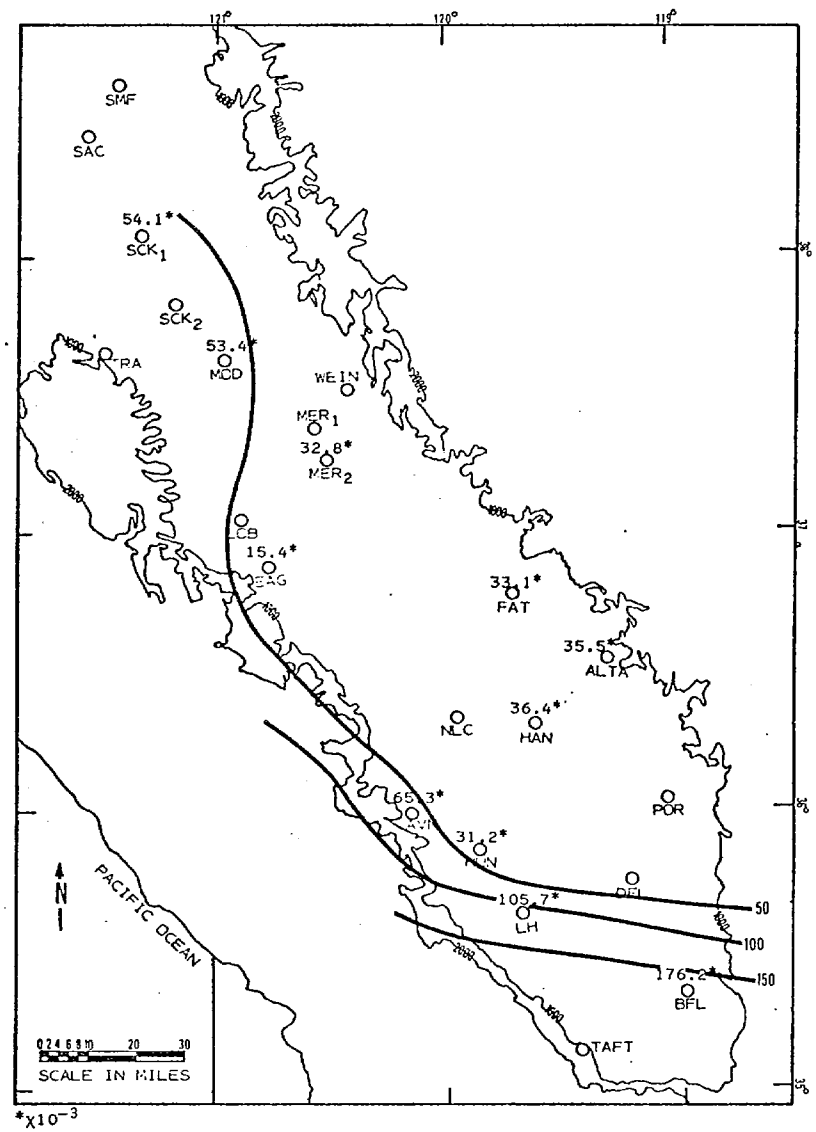

b. b_{scat} INTEGRATIONS - MORNING
September 13, 1972

Fig. VII-8.

heights toward the south. Values of b_{scat} (Fig. VII-8b) were largest in the southern sections.

September 13, 1972 (Afternoon)

During the afternoon of September 13, northwesterly winds again prevailed throughout the valley (Fig. VII-9). Mixing layer heights (Fig. VII-10a) show high values near the western slopes of the valley and low values in the sea breeze air near Stockton (SCK). Values of integrated b_{scat} (Fig. VII-10b) during the afternoon were again relatively low but largest in the area where mixing layer depths were greatest.

4. Summary

The meteorology of the San Joaquin Valley is complex and poorly understood. The valley tends to act as a closed system, at times, with circulating winds at the low levels. Afternoon heating of the slopes raises the mixing layers substantially. Sea breeze air intrudes into the northern part of the valley, creating extreme N-S differences in the mixing layer. In spite of the considerable similarity between the two sampling days, the characteristics of the valley are not clear, and additional data of a three-dimensional nature are needed.

B. Description of the Meteorology and 3-D Distribution of Pollutants in the San Francisco Bay Area

1. Introduction

Aircraft sampling data for August 25, 1972, in the San Francisco Bay area have been analyzed in the present study. This day had been selected as an intensive sampling day by the Aerosol Characterization Study. Details of the data analysis are described in the following sections. Complete data for August 25 appear in the 1972 Data Volume.

2. August 25, 1972 (Morning)

Low clouds and fog covered most of the Bay area during the morning hours. The streamline analysis shown in Fig. VII-11 indicates light southerly and southeasterly winds throughout the Bay area and the Santa Clara Valley. Mixing layer heights (Fig. VII-12a) generally show lowest values over the San Francisco and San Pablo Bays with increasing heights surrounding the bays. Integrated values of b_{scat} (within the mixing layer) during the morning are seen to be quite low at all sampling locations (Fig. VII-12b). CO data on the morning flights (Fig. VII-13a) show largest values from the San Francisco airport southeastward toward Palo Alto in response to the morning traffic. Ozone values (Fig. VII-13b) are less than 0.05 ppm at all sampling locations.

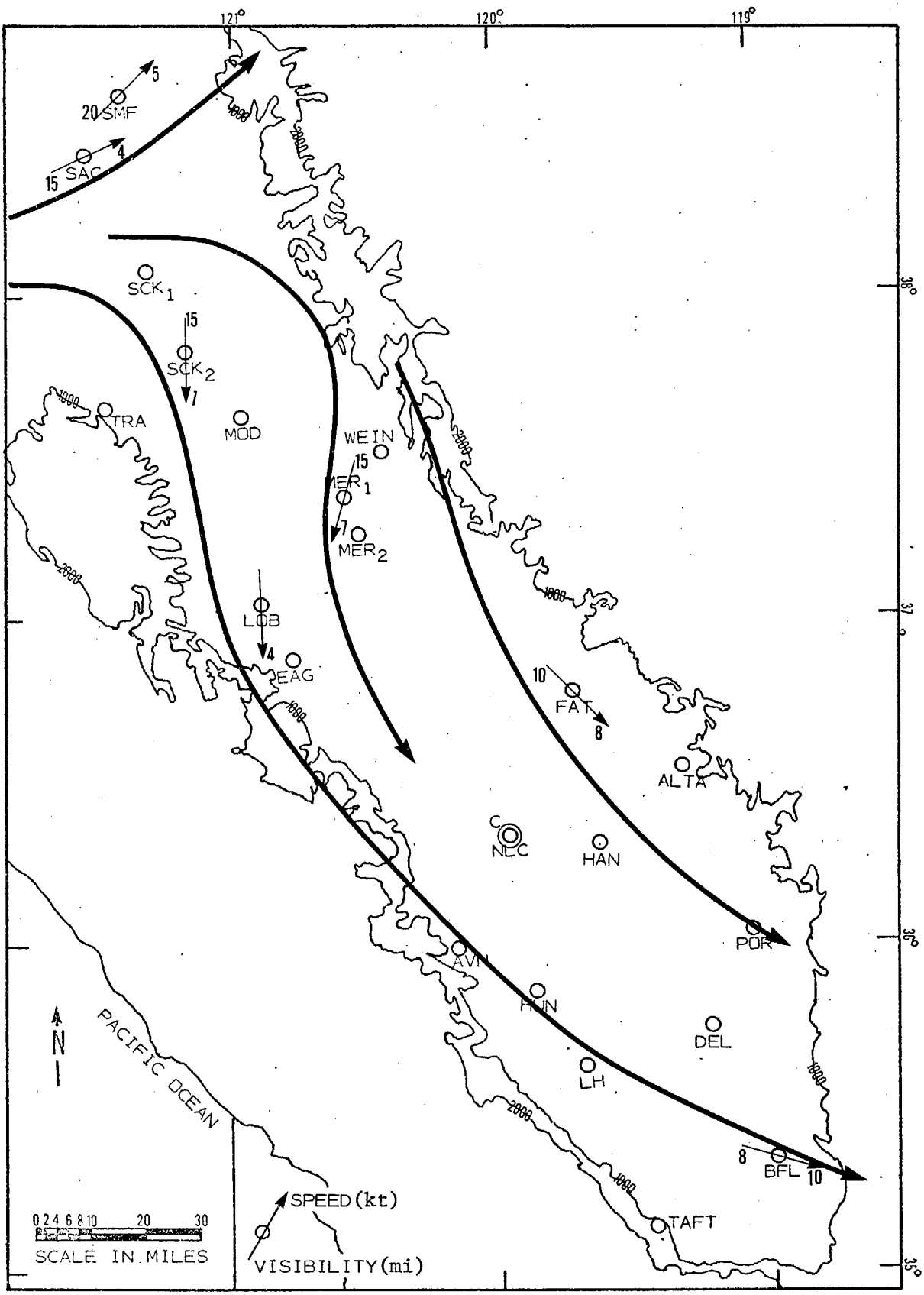

Fig. VII-9. STREAMLINE ANALYSIS - 1500 PST
September 13, 1972

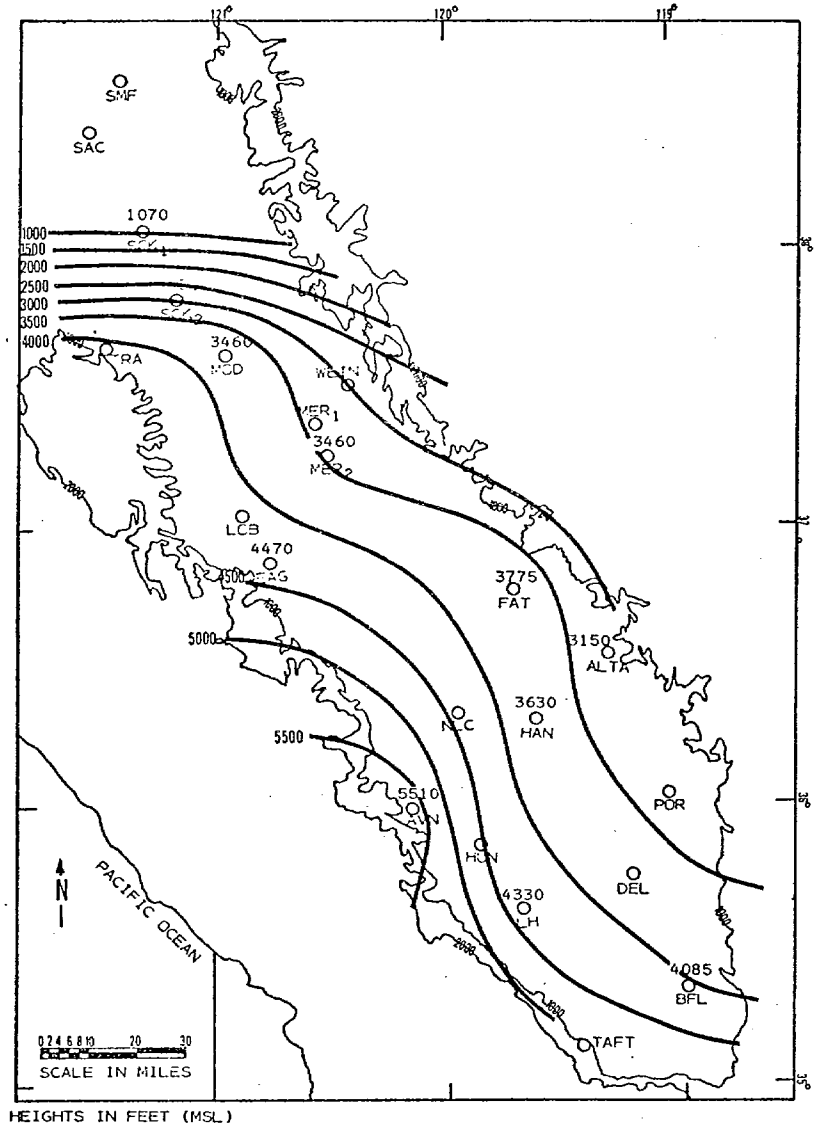

HEIGHTS IN FEET (MSL)

a. MIXING LAYER HEIGHTS - AFTERNOON
September 13, 1972

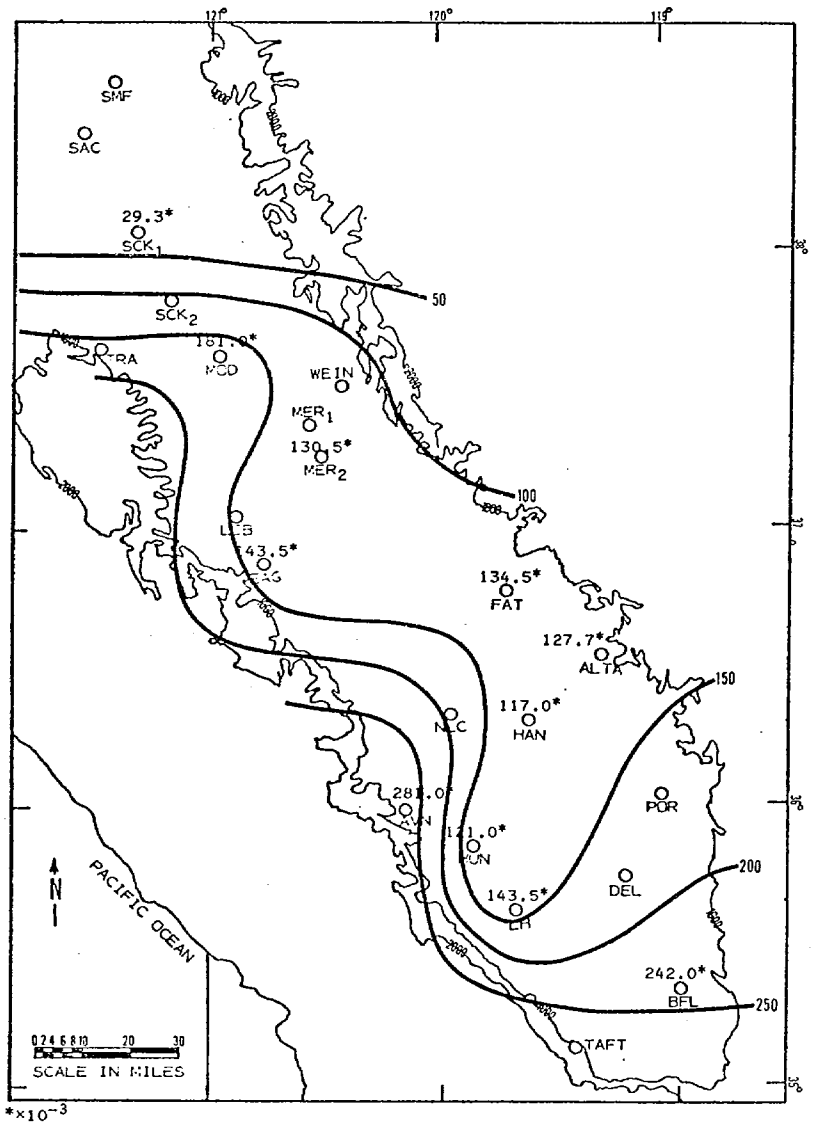

*×10⁻³

b. b_{scat} INTEGRATIONS - AFTERNOON
September 13, 1972

Fig. VII-10.

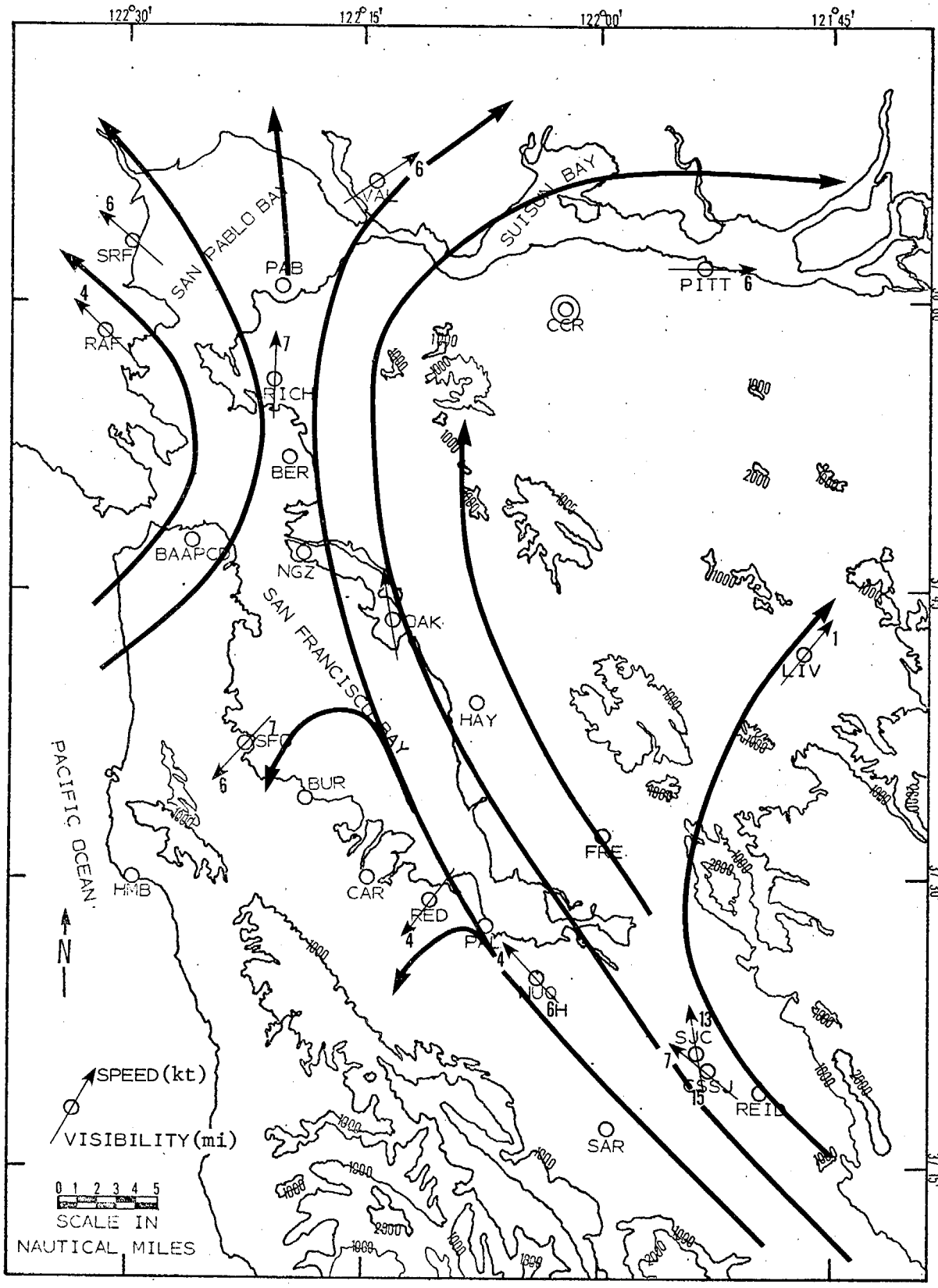

Fig. VII-11 STREAMLINE ANALYSIS - 0900 PST
August 25, 1972

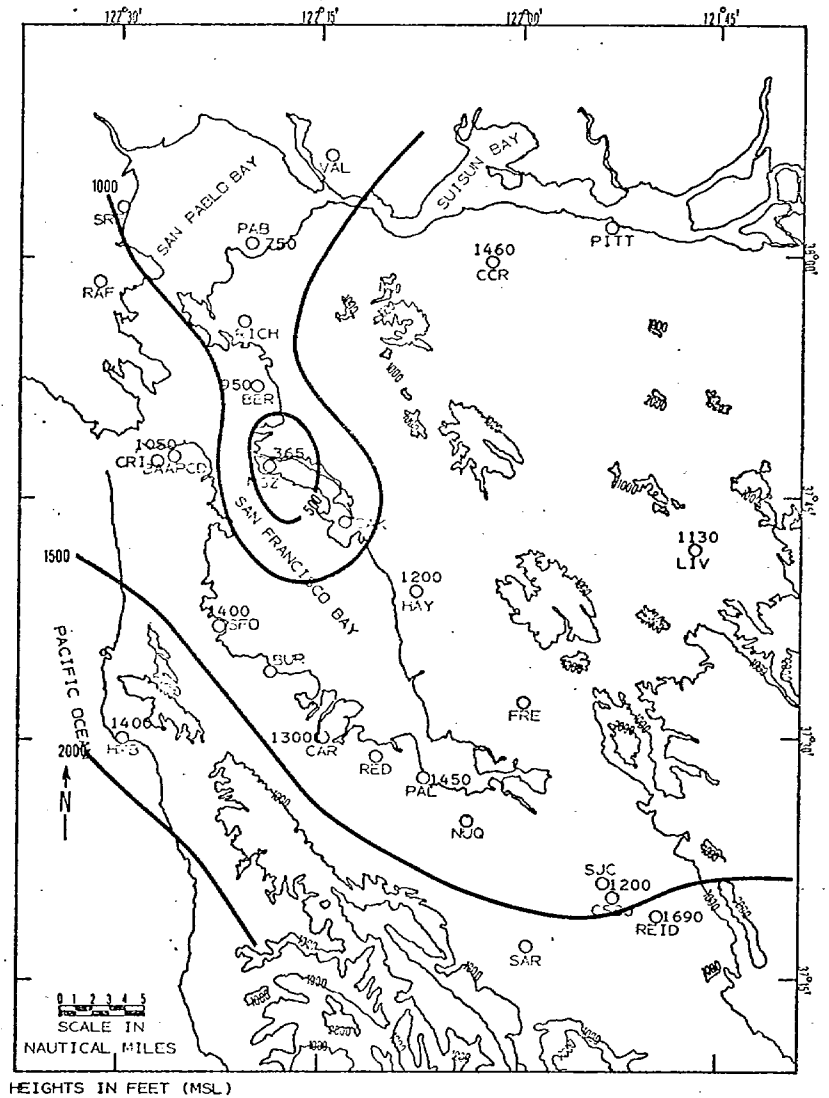

a. MIXING LAYER HEIGHTS - MORNING
August 25, 1972

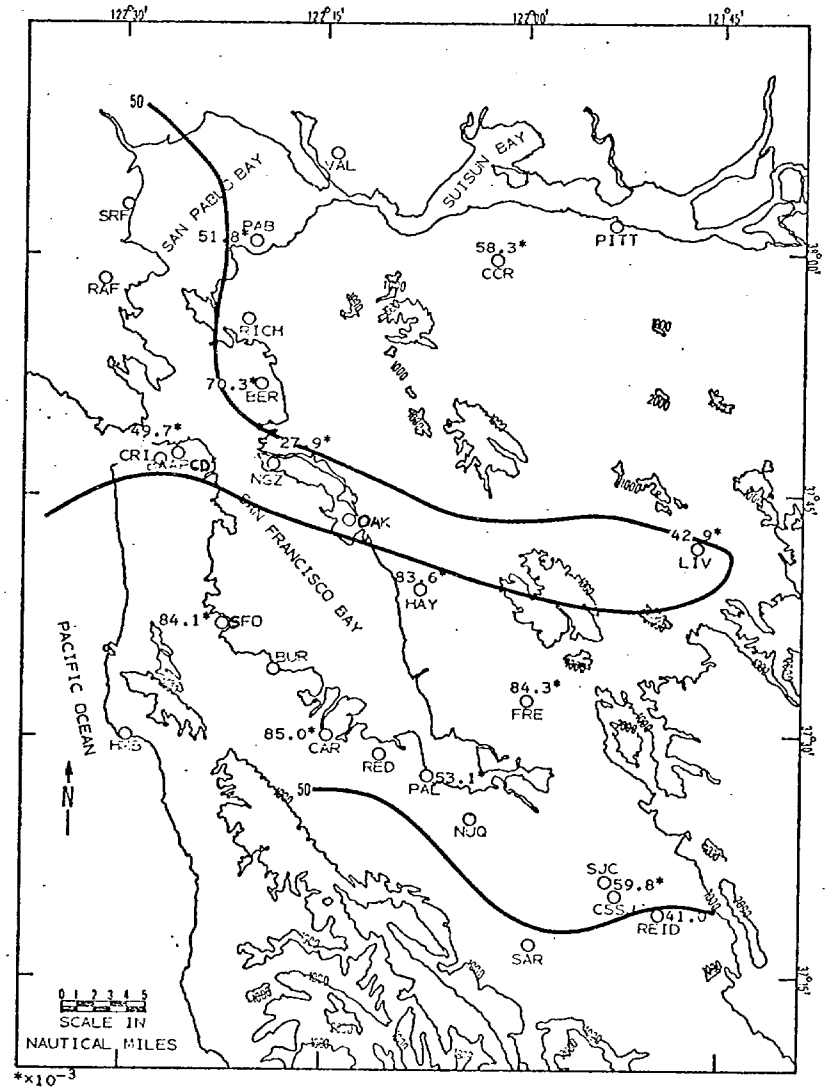

b. b_{scat} INTEGRATION - MORNING
August 25, 1972

Fig. VII-12

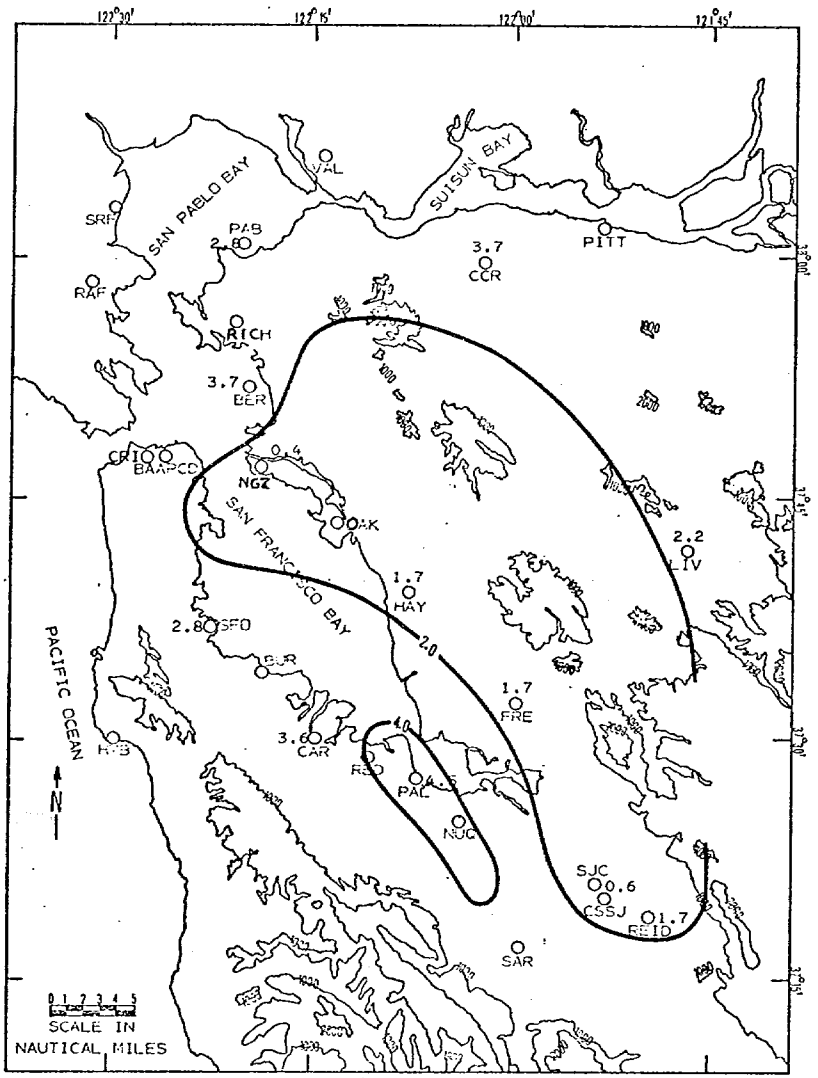

a. PEAK CO CONCENTRATIONS (ppm) WITHIN MIXING LAYER - MORNING
August 25, 1972

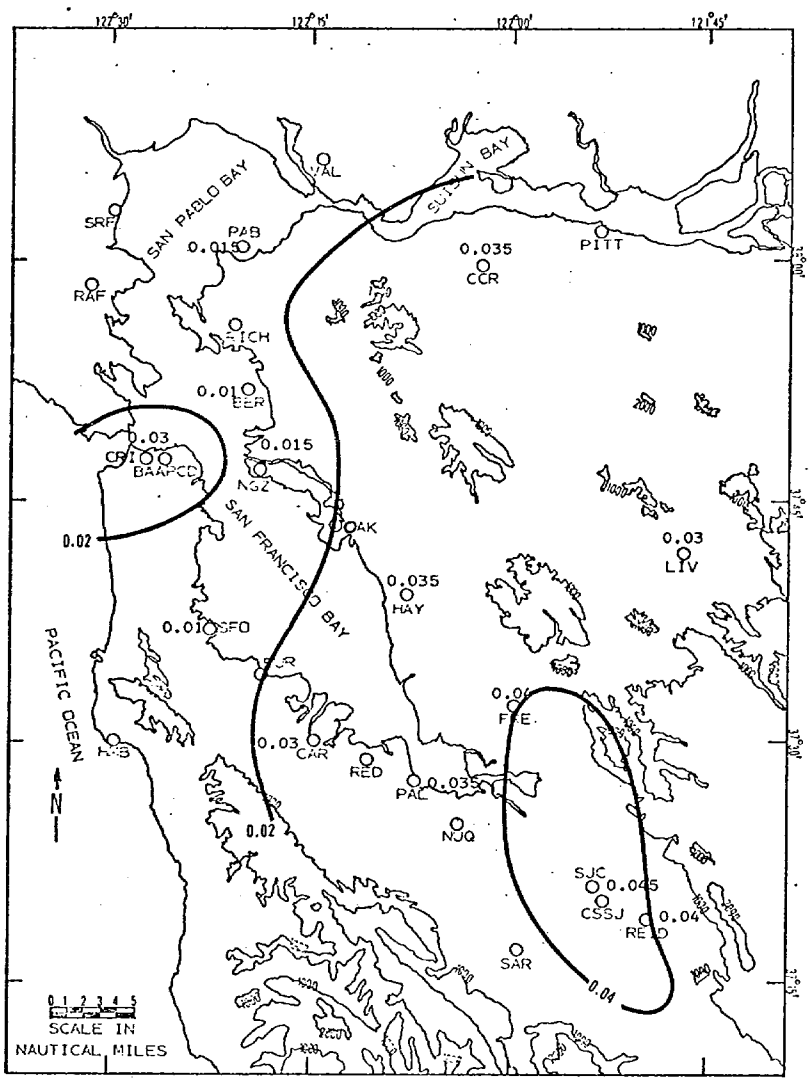

b. PEAK OZONE CONCENTRATIONS (ppm) WITHIN MIXING LAYER - MORNING
August 25, 1972

Fig. VII-13

August 25, 1972 (Midday)

By midday, a moderate sea breeze had established itself throughout the San Francisco area. Streamlines for 1200 PST are shown in Fig. VII-14. Westerly winds enter through the Golden Gate and split into a southwest flow moving up toward the Sacramento Valley and a northwest flow passing down into the Santa Clara Valley. Mixing layer heights (Fig. VII-15a) show well-defined minimum values over the water surfaces of the Bay with highest values near Livermore (LIV) where surface heating is more significant. The normal surface heating effects do not operate over the water areas, and mixing layer heights during the daytime tend to slope upward in all directions from South San Francisco Bay. Largest integrated b_{scat} values (Fig. VII-15b) at midday on August 25 occur near Livermore (LIV) and Hayward (HAY). It is of interest that the northern areas along the Sacramento River Valley show considerably lower integrated b_{scat} values than those which receive air passing over the metropolitan San Francisco-Oakland area. CO values (Fig. VII-16a) are less than 4 ppm at all sampling locations while oxidant values (Fig. VII-16b) peak in the area from downtown San Francisco to Palo Alto. At this time, b_{scat} and oxidant patterns do not agree particularly well.

August 25, 1972 (Afternoon)

By afternoon, the sea breeze flow had intensified throughout the area (Fig. VII-17), resulting in lower mixing heights (Fig. VII-18a), particularly at Livermore, while the heights increased in the vicinity of San Jose as a result of continued surface heating. Values of integrated bscat (Fig. VII-18b) during the afternoon flights were largest to the southeast of San Jose although the values dropped significantly at Livermore in the sea breeze air. CO values (Fig. VII-19a) were highest in the vicinity of San Jose and the San Francisco airport while oxidant peaks (Fig. VII-19b) exceeded 0.10 ppm in the region from Fremont (FREM) to San Jose (SJC).

3. Summary

Mixing layer heights tend to be lowest during the day over the waters of the San Francisco Bay, while in the surrounding areas the heights lift substantially due to surface heating. Pollutants from the metropolitan area follow the southern branch of the sea breeze flow being carried eastward through Livermore and southeastward past San Jose. During the late afternoon, there is reasonable agreement between b_{scat} and oxidant patterns in the Santa Clara Valley, apparently in the presence of aged aerosols from the San Francisco area.

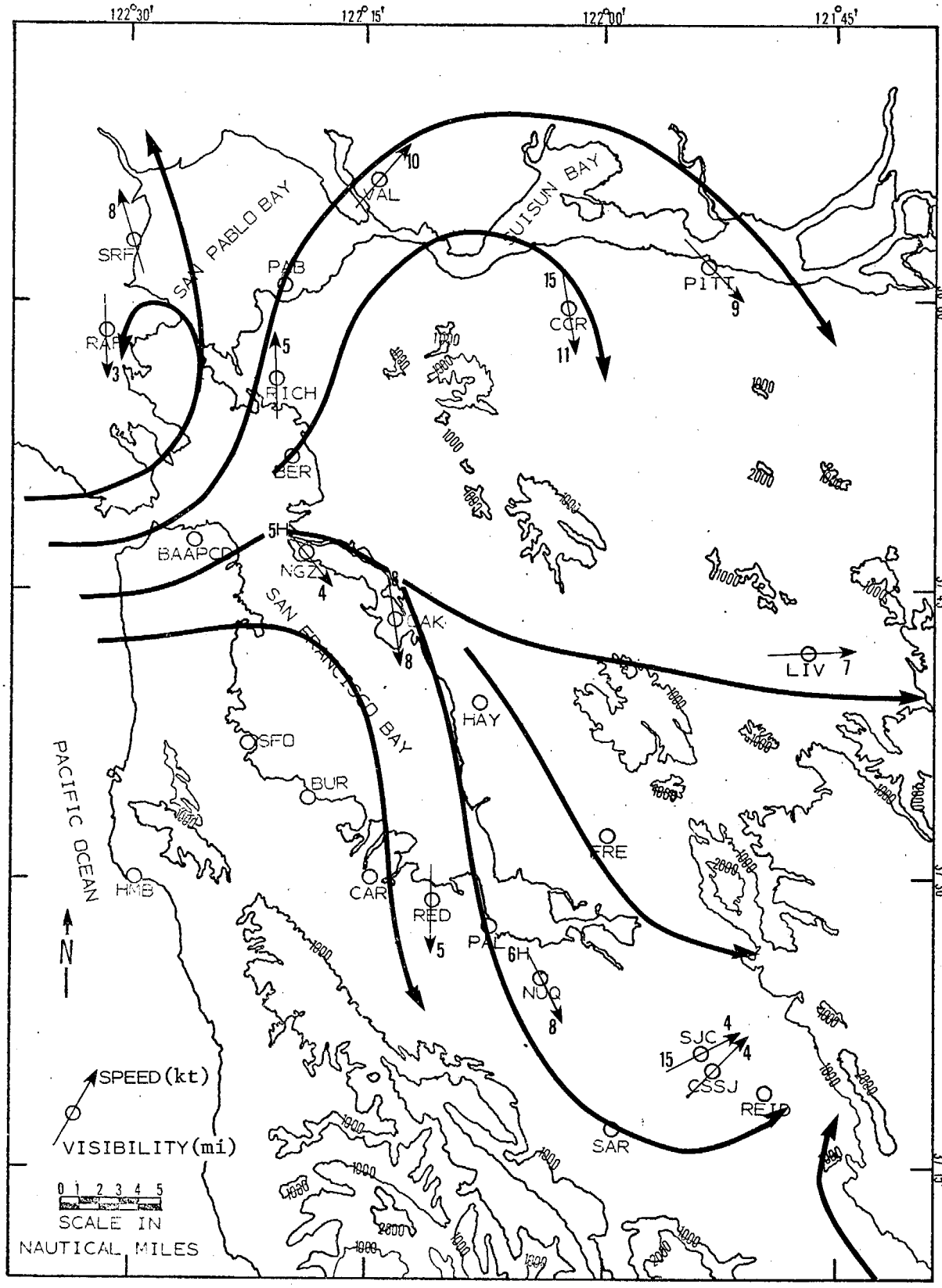

Fig. VII-14. STREAMLINE ANALYSIS - 1200 PST
August 25, 1972

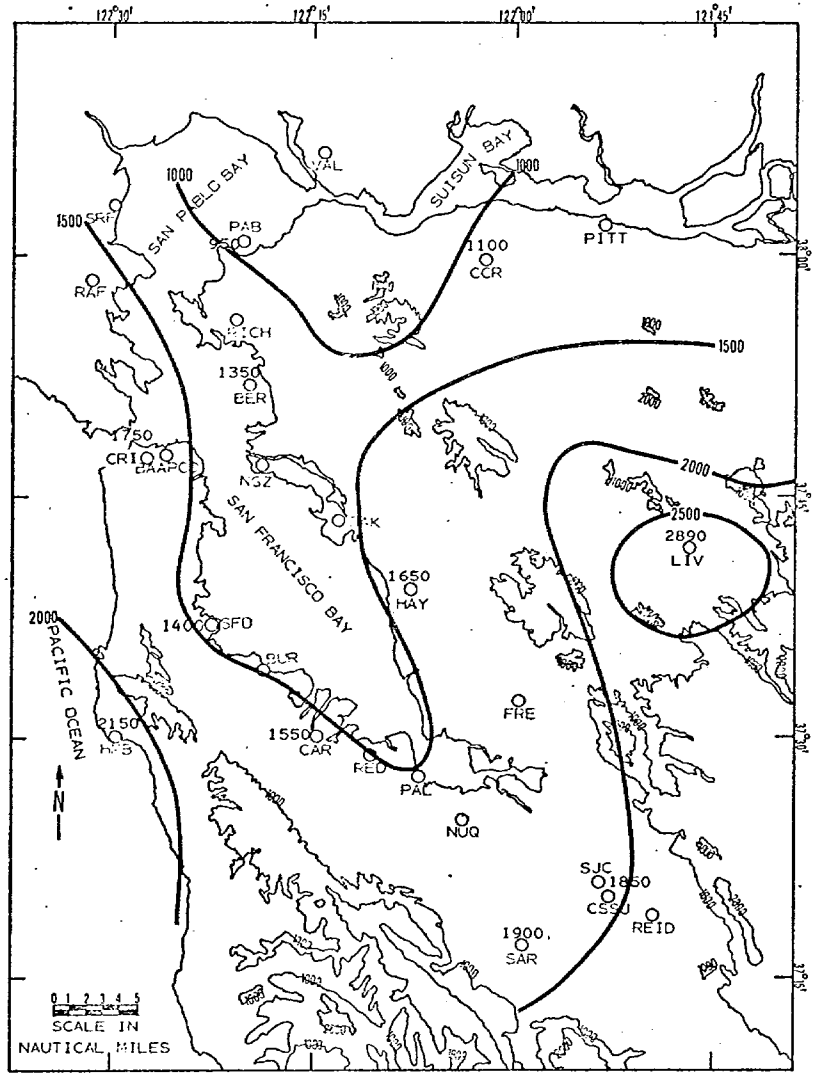

HEIGHTS IN FEET (MSL)

a. MIXING LAYER HEIGHTS - MIDDAY
August 25, 1972

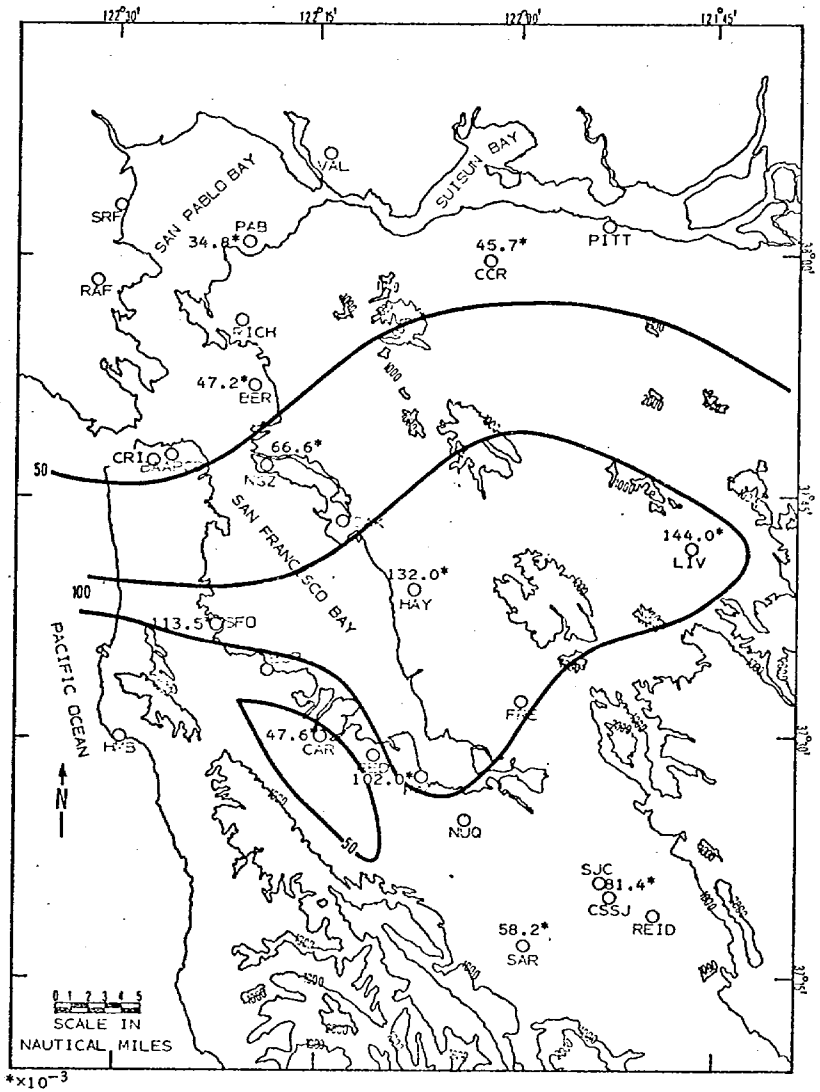

*×10⁻³

b. b_{scat} INTEGRATION - MIDDAY
August 25, 1972

Fig. VII-15

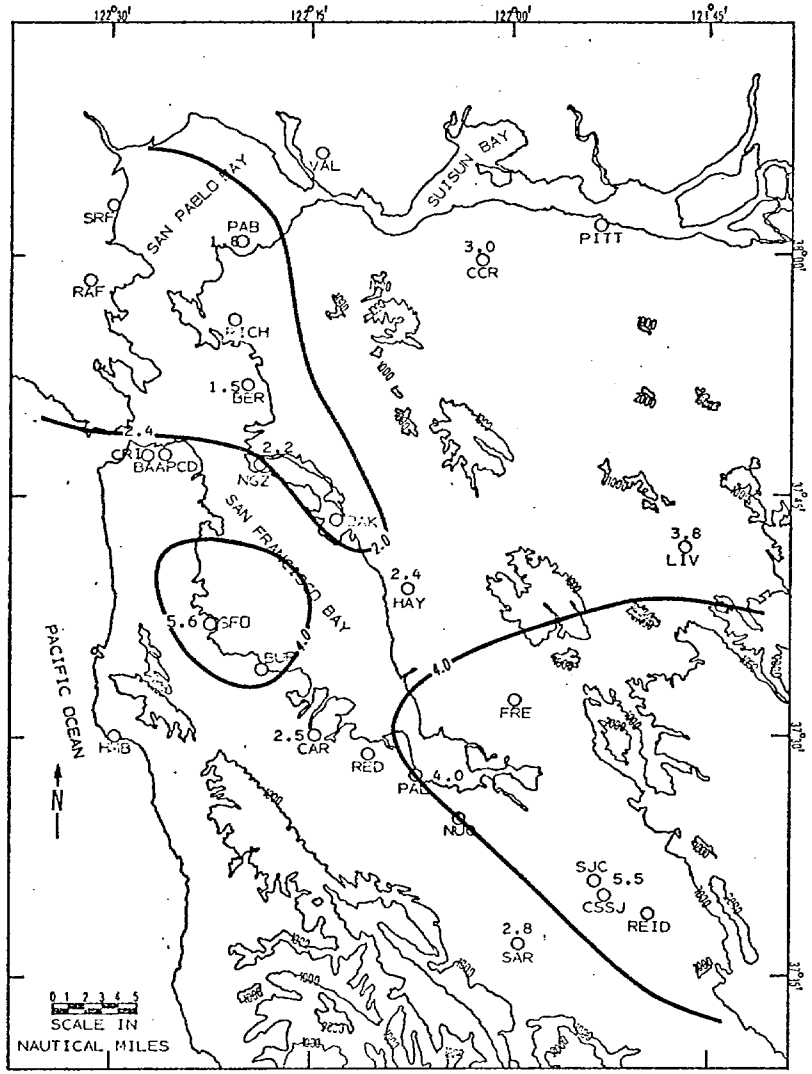

a. PEAK CO CONCENTRATIONS (ppm) WITHIN MIXING LAYER - MIDDAY
August 25, 1972

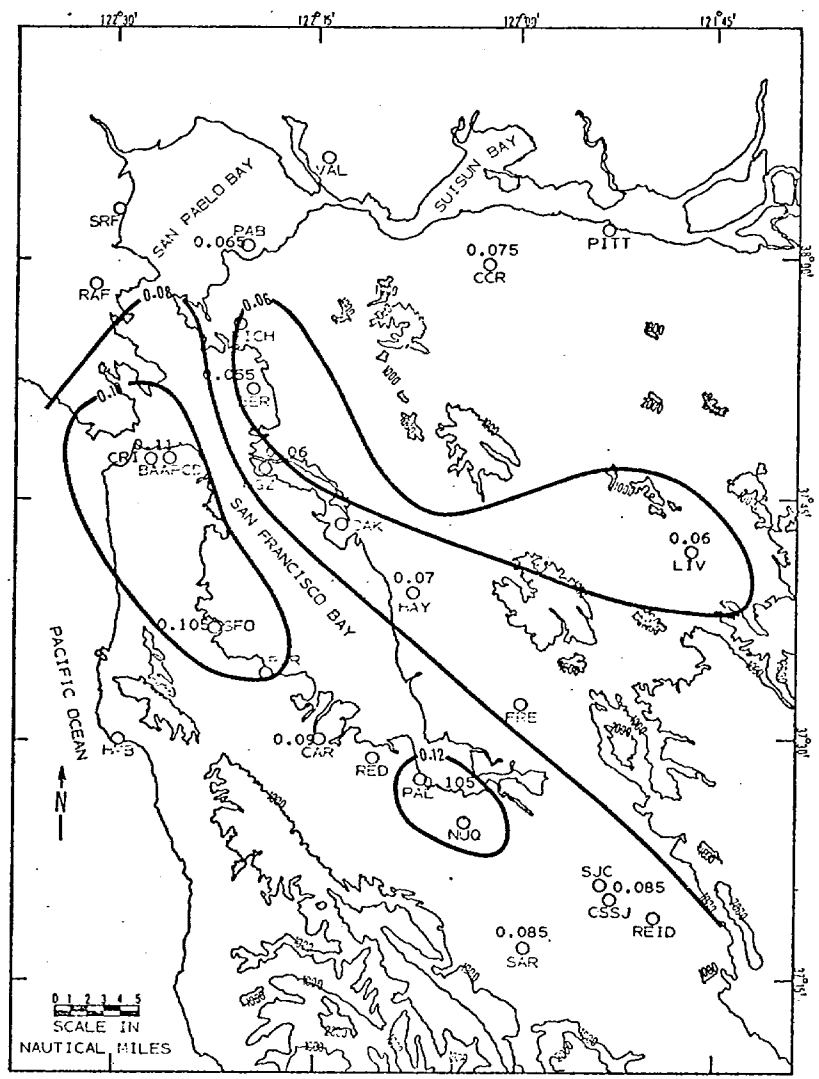

b. PEAK OZONE CONCENTRATIONS (ppm) WITHIN MIXING LAYER - MIDDAY
August 25, 1972

Fig. VII-16

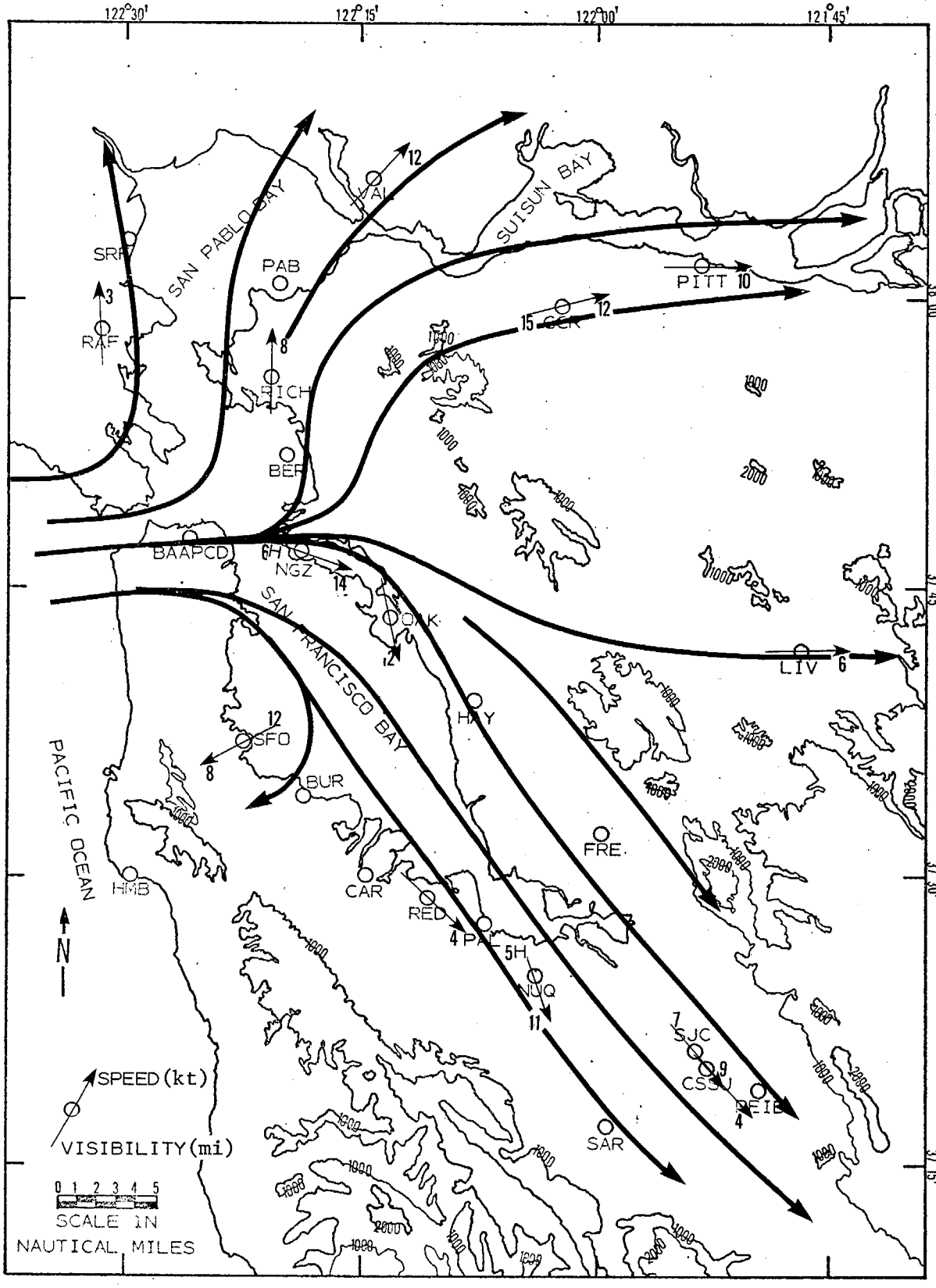

Fig. VII-17. STREAMLINE ANALYSIS - 1500 PST
August 25, 1972

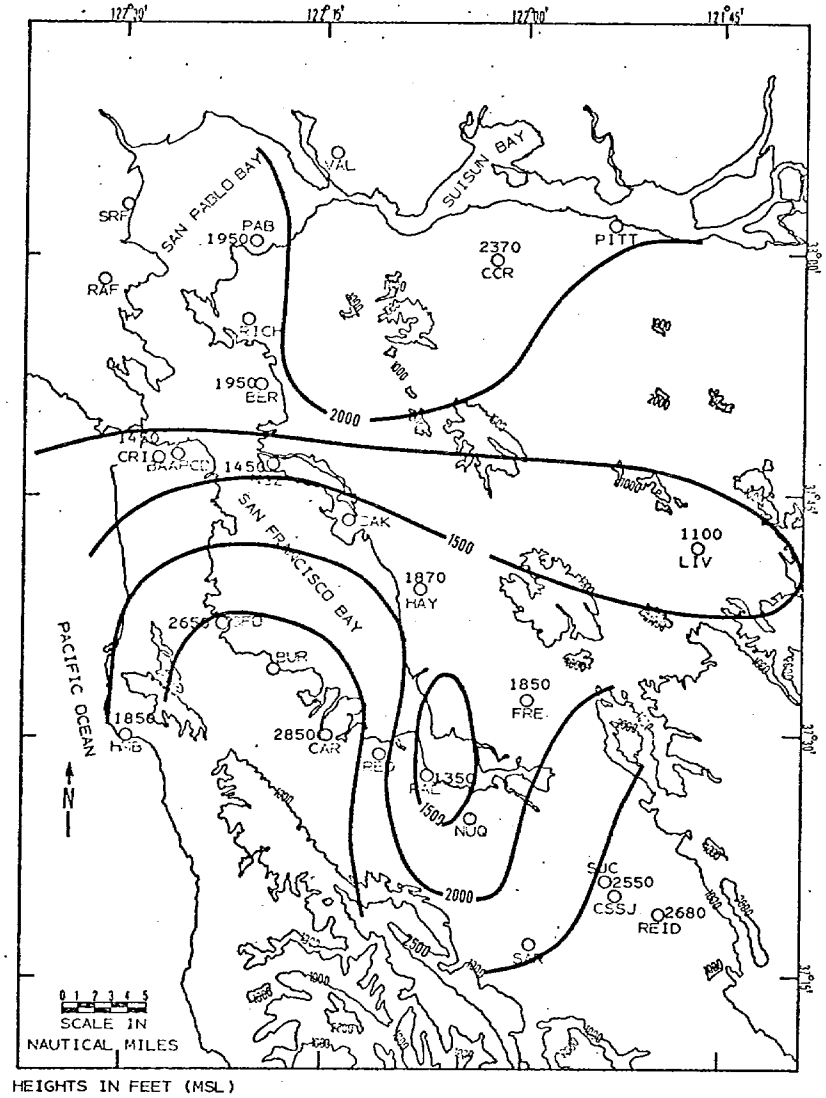

a. MIXING LAYER HEIGHTS - AFTERNOON
August 25, 1972

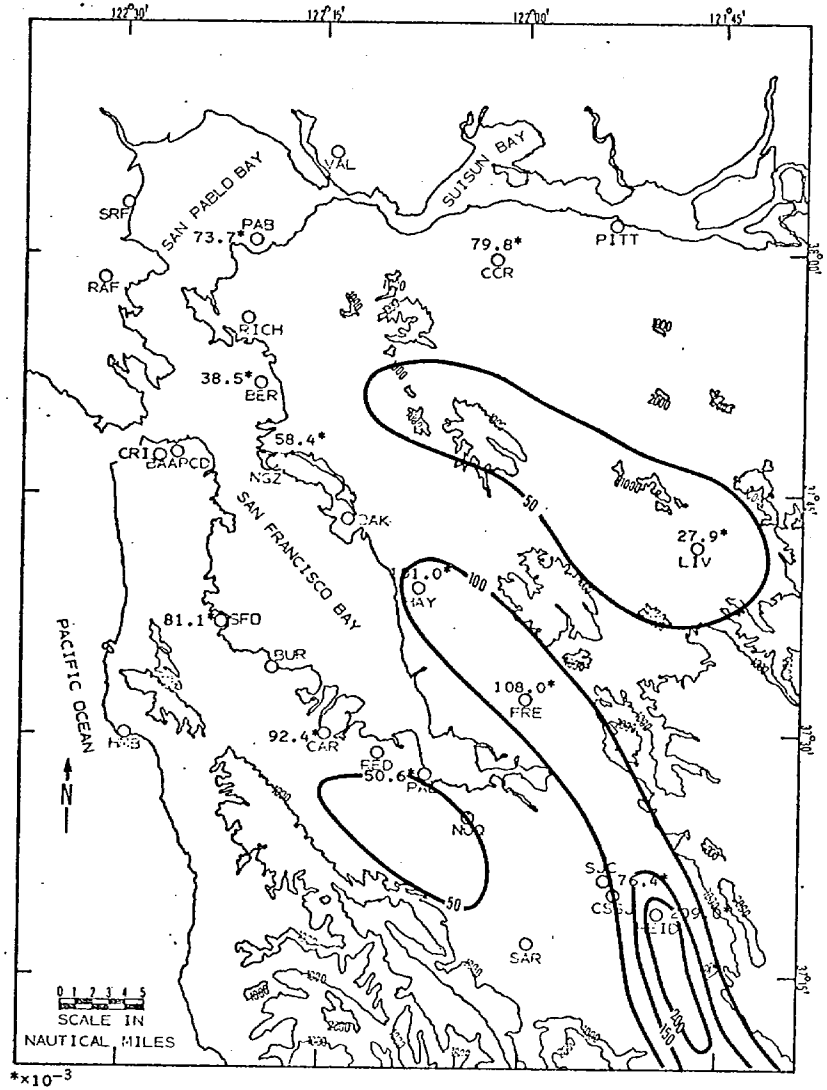

b. b_{scat} INTEGRATION - AFTERNOON
August 25, 1972

Fig. VII-18

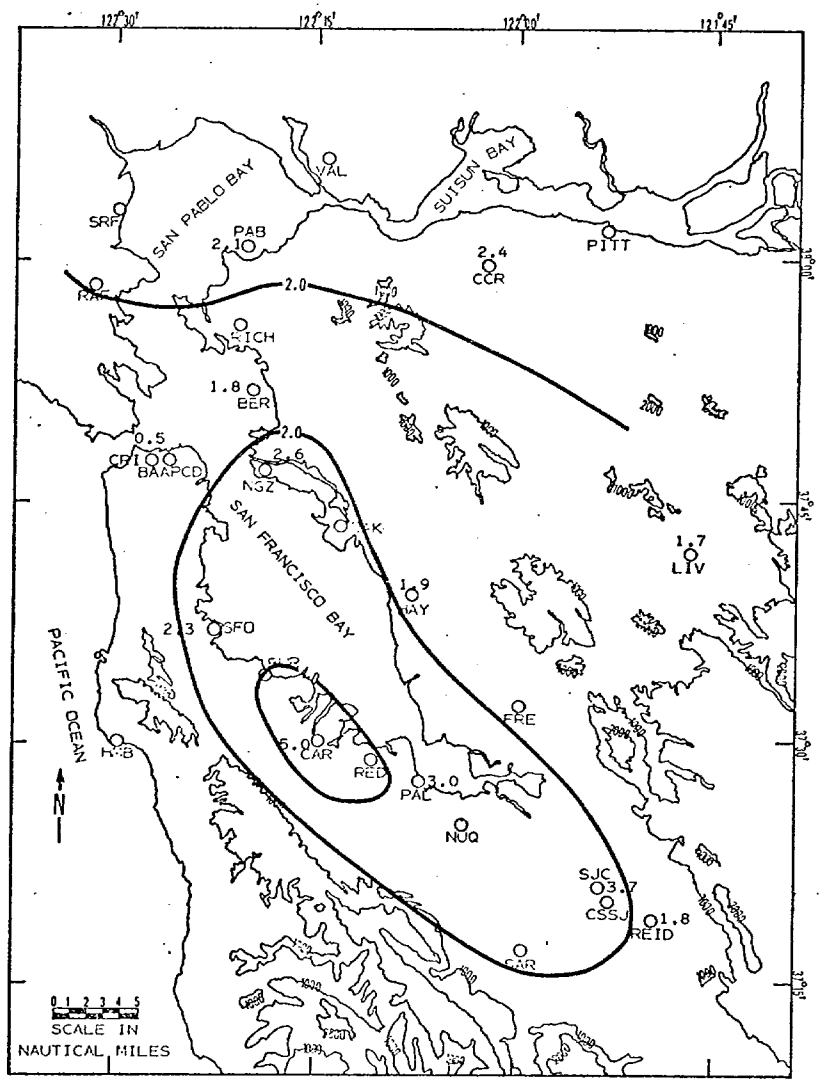

a. PEAK CO CONCENTRATIONS (ppm) WITHIN MIXING LAYER - AFTERNOON
August 25, 1972

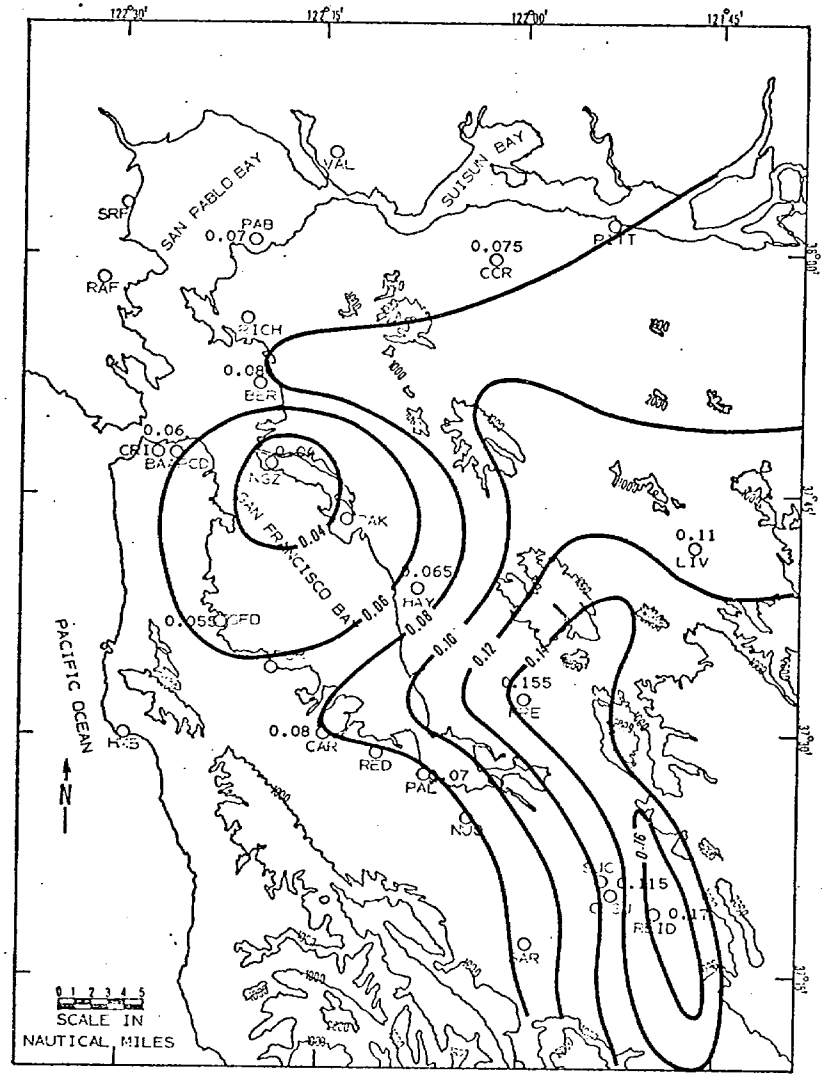

b. PEAK OZONE CONCENTRATIONS (ppm) WITHIN MIXING LAYER - AFTERNOON
August 25, 1972

Fig. VII-19

VIII. ATMOSPHERIC PHYSICAL AND CHEMICAL PROCESSES

A. Pollutant Analysis Along Air Trajectories

1. Introduction

The three-dimensional pollutant gradient study, like most air quality monitoring operations, was conducted within an Eulerian framework; that is, contaminant levels were measured at a number of fixed locations in the Los Angeles Basin. In this section, we will demonstrate how the Eulerian data obtained can be used to study the evolution of contaminants in a moving air mass. This Lagrangian interpretation of the data is of help in understanding the phenomena of pollutant aging and transport.

The afternoon of July 25, 1973, which is one of the days discussed in detail in Chapter VI, provides a good example of the differences between the perspective of a stationary observer and the perspective of a moving observer riding with the wind. As shown in Fig. VIII-1, the hourly average ozone concentrations measured at Upland on this day rose gradually to a maximum at 1600-1700 PDT and then fell rapidly. To a stationary observer, the ozone seemed to "disappear" late in the afternoon. As Figs. VIII-2 and VIII-3 make clear, the sharpness of the late afternoon drop in ozone concentration was due to the passage of a front, and an observer riding with the wind would have experienced no abrupt change in concentration.

2. Pollutant Loadings

The study of the pollutant budget within a moving air mass is simplified if concentrations are integrated with respect to height to obtain the total pollutant loading over a unit area on the ground. Loadings of primary pollutants can be related directly to emission rates and the loading of any pollutant is less sensitive to changes in the depth of the surface mixed layer than is the concentration.

We will define the loading of a pollutant by the following integral:

$$L_X = \int_{GL}^{MH} \left([X]_Z - [X]_{BG} \right) \, dZ,$$

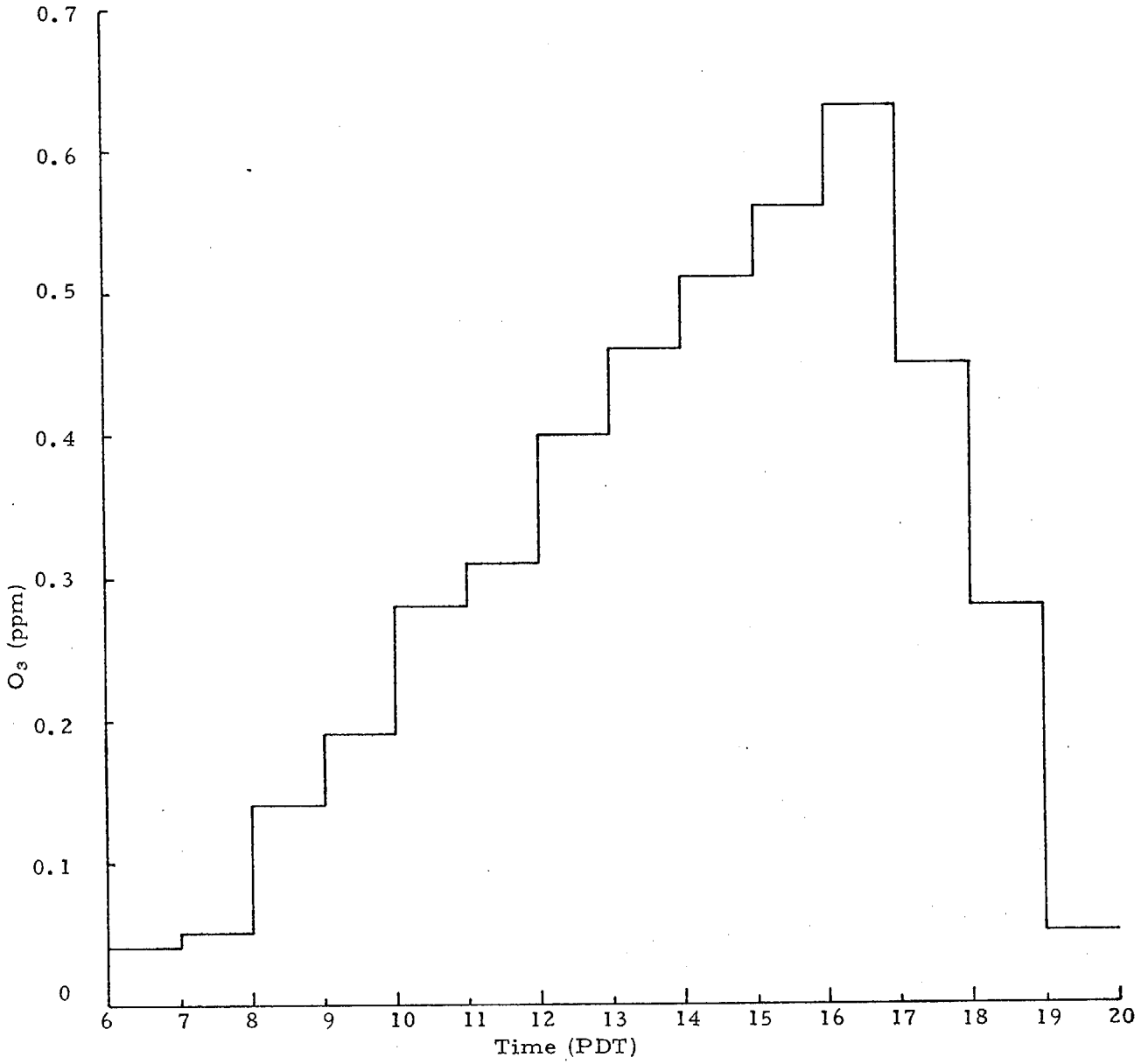

Fig. VIII-1. HOURLY AVERAGE OZONE CONCENTRATIONS MEASURED AT UPLAND, CALIFORNIA ARB STATION, JULY 25, 1973

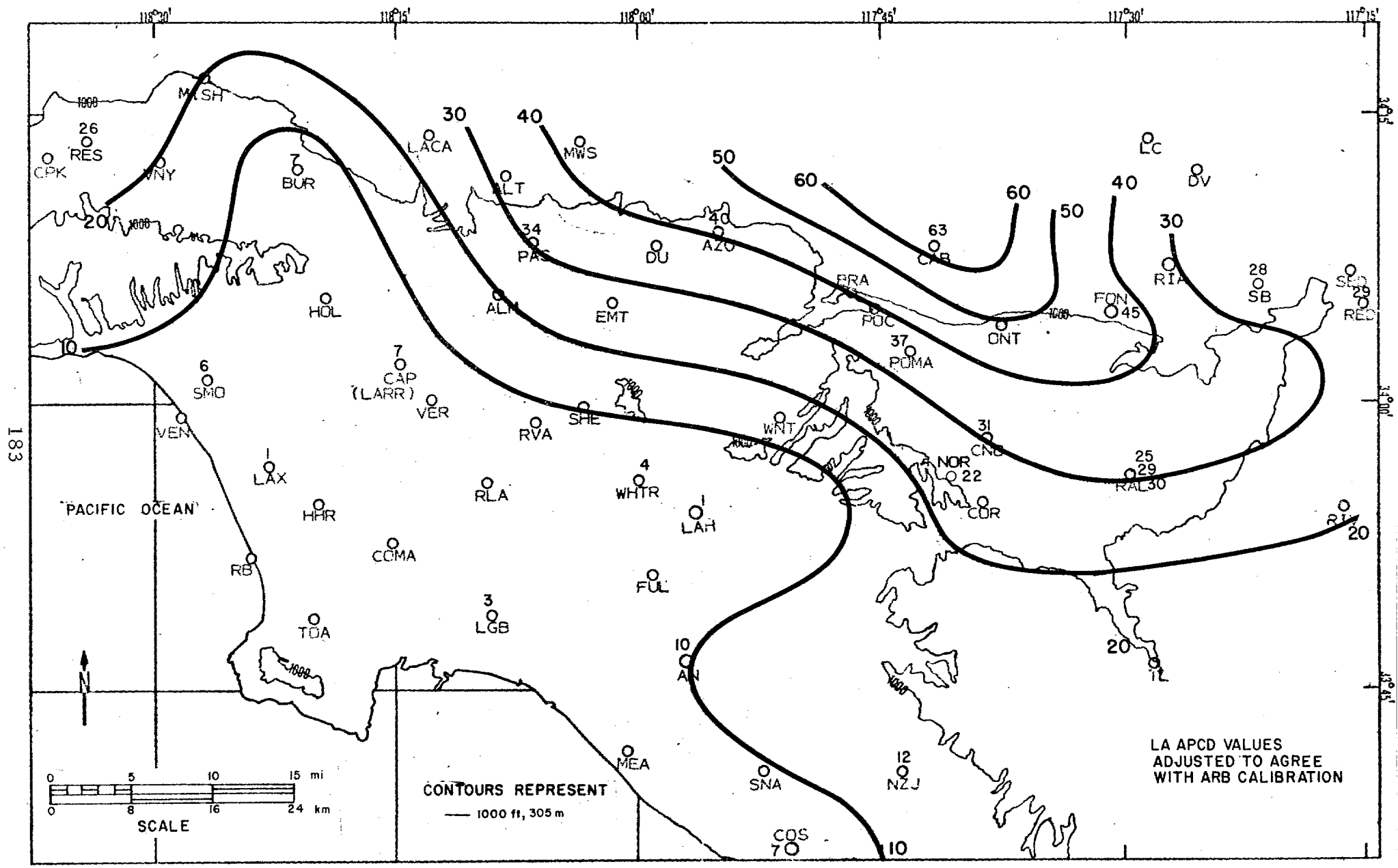

Fig. VIII-2. SURFACE OZONE CONCENTRATIONS (pphm), 1600-1700 PDT, JULY 25, 1973

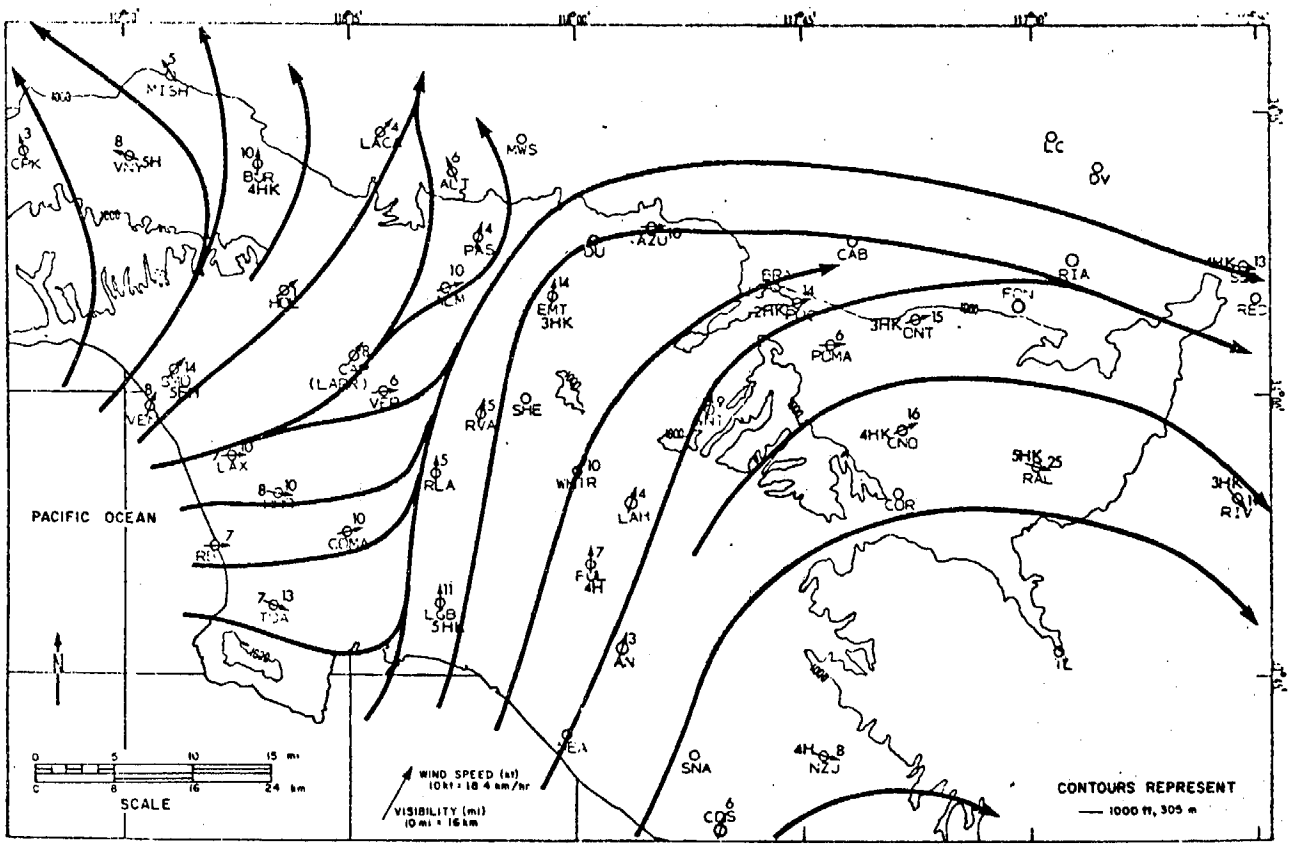

Fig. VIII-3. SURFACE WIND STREAMLINES - 1600 PDT, JULY 25, 1973

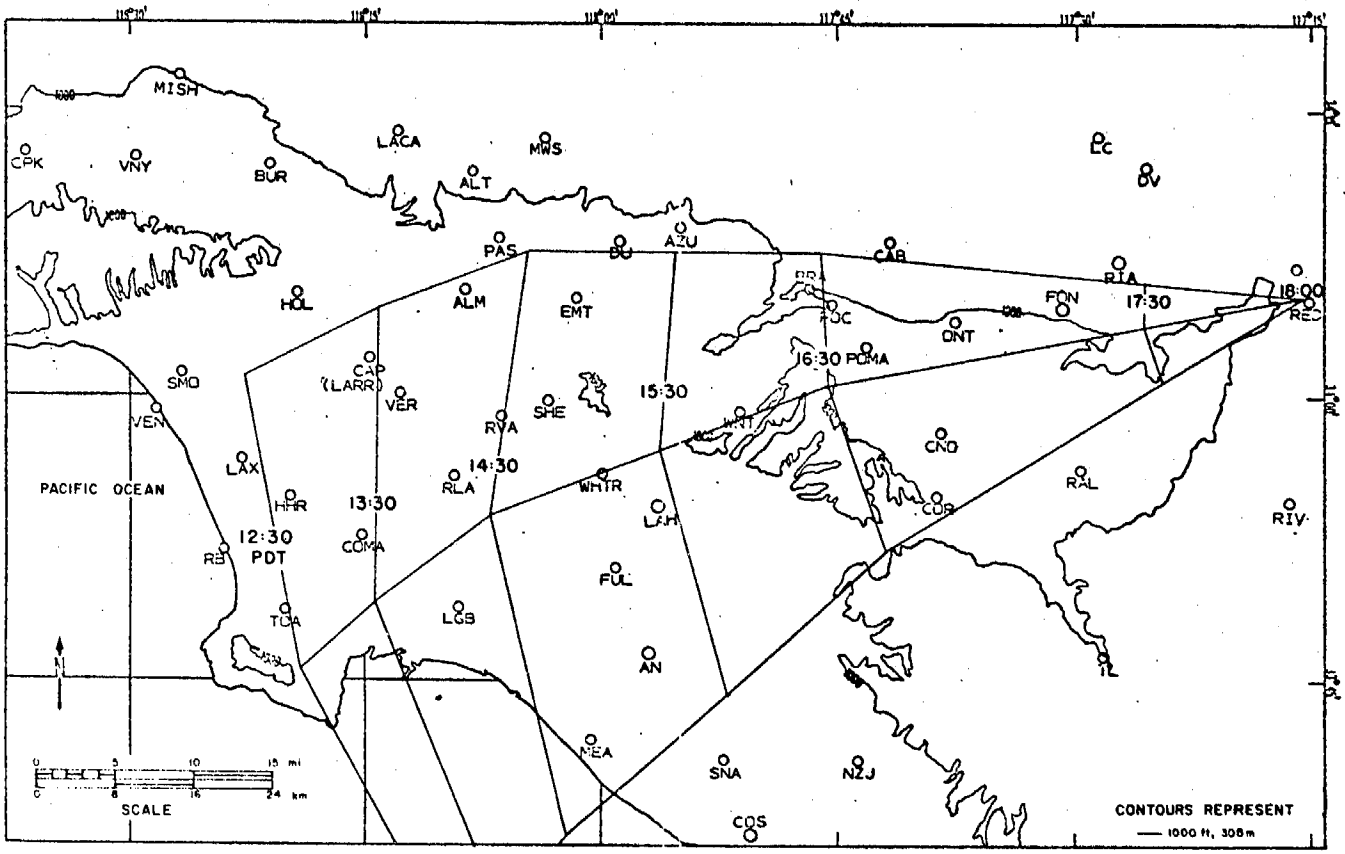

Fig. VIII-4. TRAJECTORY ENVELOPE FOR AIR ARRIVING OVER REDLANDS AT 1800 PDT, JULY 25, 1973

where

X = any pollutant

$[X]_Z$ = concentration of X at height Z

$[X]_{BG}$ = background concentration of X

GL = ground level

MH = mixing height.

The correction for the background concentration is made so that deepening of the surface mixed layer has no effect on calculated loadings if the air above is relatively clean. Background concentrations of 1 ppm for CO and 0.04 ppm for ozone are used in the analyses which follow.

3. Trajectory Analyses

a. July 25, 1973

Figure VIII-4 shows the calculated envelope of probable trajectories for air arriving over Redlands at 1800 PDT, just ahead of the advancing sea breeze front. These trajectories were derived from observed wind fields as described in Chapter VI. Figure VIII-5 shows how calculated pollutant loadings changed en route to Redlands. Loadings at aircraft sounding locations were obtained by integration of aircraft data, and loadings at surface monitoring locations were estimated by multiplying the concentration measured near the ground by the prevailing mixing height for the area.

Although there is considerable scatter in the data, certain trends are apparent. Loadings increase during the passage over the heavily urbanized western Los Angeles Basin as the air mass accumulates primary emissions and reaction products. The observed rate at which the CO loading increases during this period is comparable with the calculated rate at which CO is emitted (e.g., Roth et al., 1974). Later, as the air mass crosses the eastern basin, loadings decrease. The extent to which this decrease is due to meteorological factors such as dilution and spreading can be judged from the loadings of CO which is a relatively inert constituent of the atmosphere.

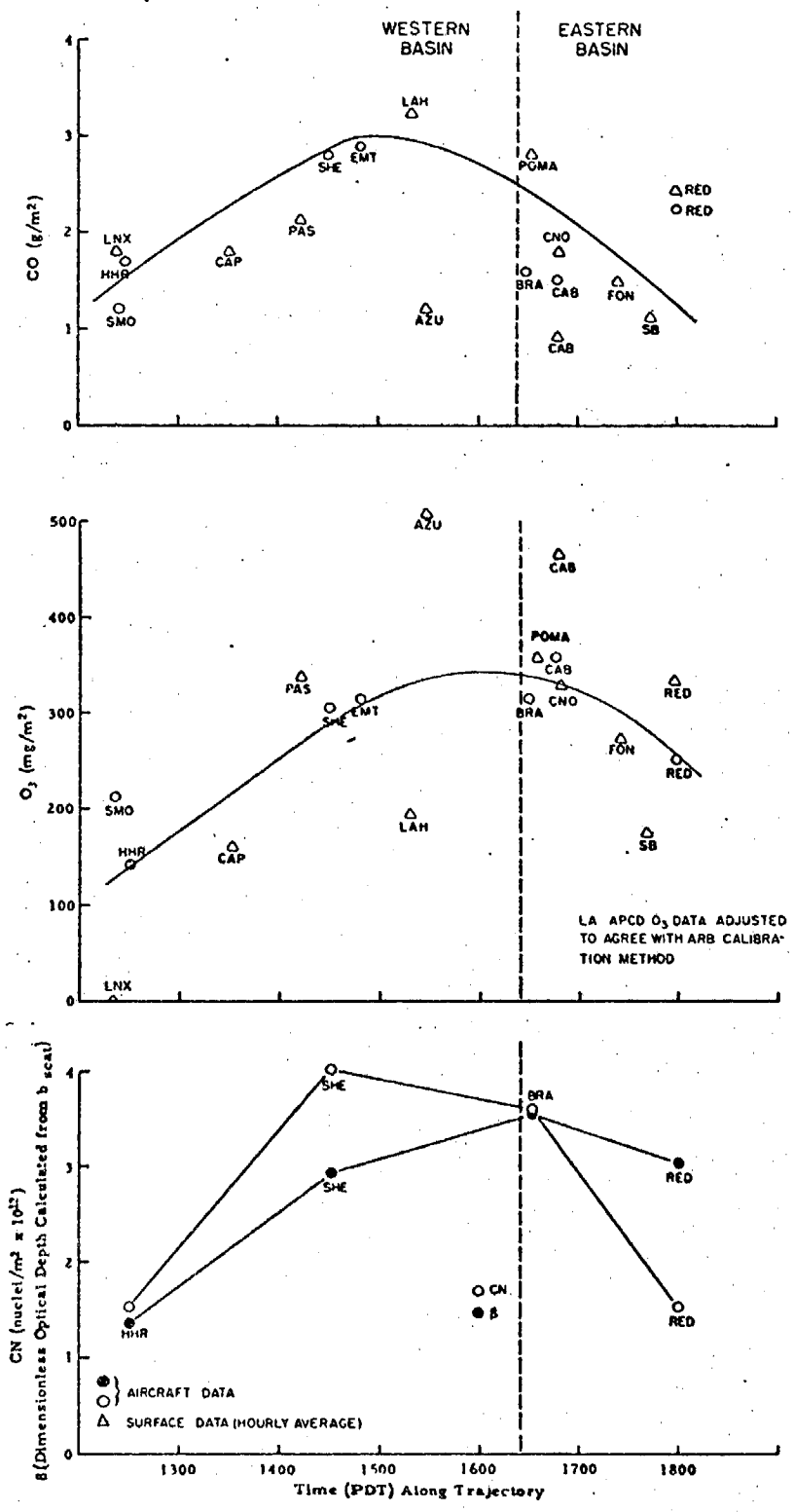

Fig. VIII-5. POLLUTANT LOADINGS IN SURFACE MIXED LAYER ALONG TRAJECTORY ARRIVING AT REDLANDS IN AFTERNOON OF JULY 25, 1973

(From aircraft measurements plus estimates made from ground data and mixing height.)

The plots of Fig. VIII-5 are most instructive when compared against each other. For example, the ratio of CN to b_{scat} first increases as primary aerosols with a high proportion of small particles are added to the air mass and then decreases as these small particles coagulate. Comparison of ozone and CO shows that the ozone loadings peak later in the trajectory than the CO loadings, production of ozone partially offsetting the general decrease in loadings due to meteorological factors.

b. September 21, 1972

Figures VIII-6 and VIII-7 show air trajectory envelopes and pollutant loadings calculated for another of the days discussed in detail in Chapter VI. A large amount of scatter is evident in the data due to the great depth of the surface mixed layer in the eastern basin on this day. The most interesting feature of the plots in Fig. VIII-7 is the increase in the ratio of ozone to CO along the trajectory, showing the increased rate of accumulation of ozone as the NO emitted early in the trajectory is oxidized.

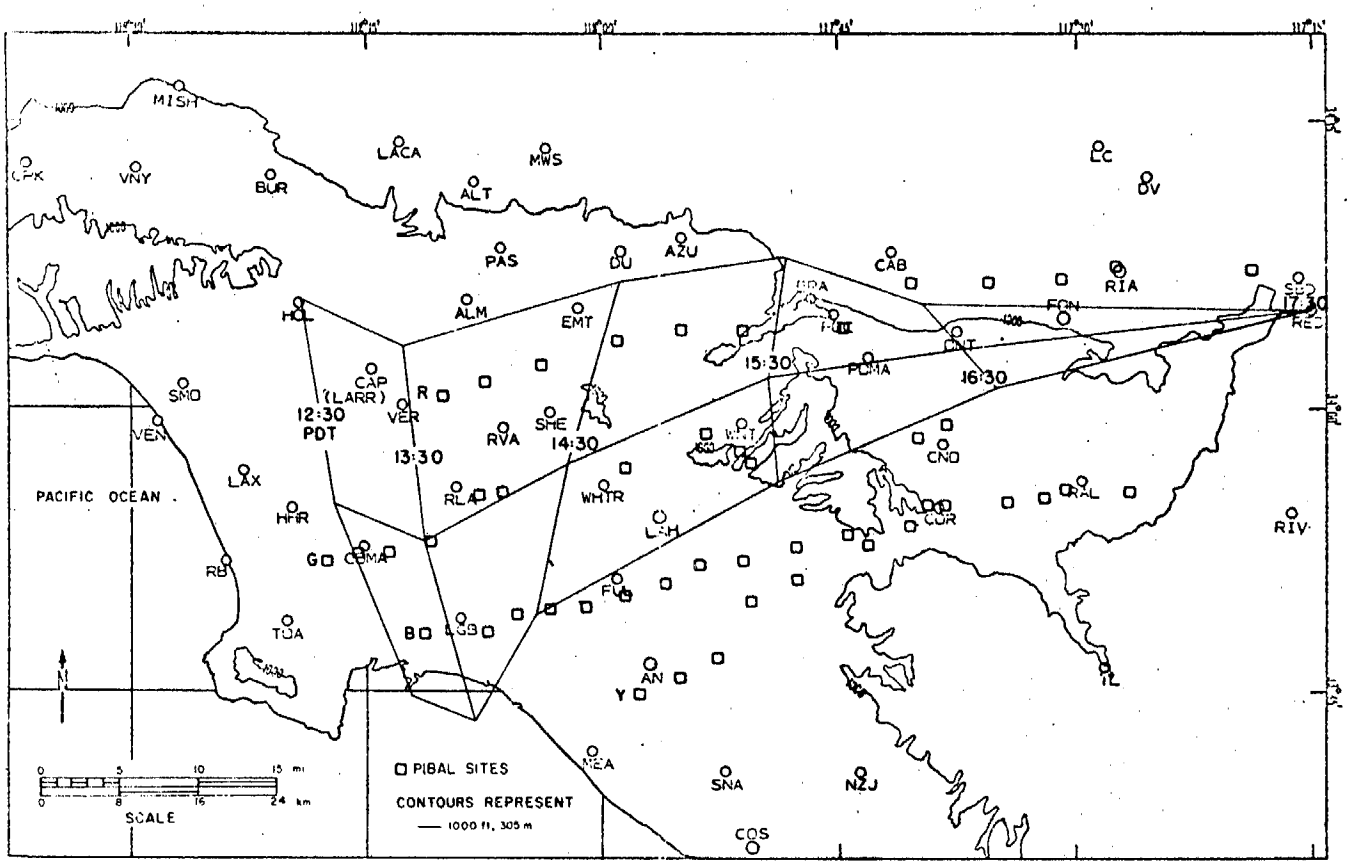

Fig. VIII-6. THE MEAN TRAJECTORY AND TRAJECTORY ENVELOPE OF THE AIR ARRIVING OVER REDLANDS AT 1730 PDT, SEPTEMBER 21, 1972
(Times along the trajectory are the times the air passed that line.)

B. Characteristics of Pollutants Above the Surface Mixed Layer

1. Introduction

During the three-dimensional pollutant gradient study, distinct layers of polluted air were frequently observed above the surface mixed layer. These elevated layers form through a variety of mechanisms which are discussed in Section V. B. In this section, we discuss the pollutant characteristics of these layers.

2. Phenomenology of Elevated Pollutant Layers

The vertical profiles of Figs. VIII-8 and -9 show examples of particularly well defined elevated pollutant layers over Hawthorne and Riverside. Several characteristics are common to both of these profiles:

a. The elevated pollutant layer is separated from the surface mixed layer by a temperature inversion. Between the two polluted layers is a lamina of rather clean air with contaminant levels near background. The elevated pollutant layer is thus clearly isolated from the emissions and reactions taking place within the surface mixed layer. Although it is not always so clearly demonstrated, this isolation is characteristic of elevated pollutant layers, and makes these layers of interest as "outdoor smog chambers" in which pollutant aging can be studied.

b. Contaminant values in the elevated layer show considerable variation with height and are mutually correlated. These features are characteristic of elevated pollutant layers and indicate that there is little vertical interchange of material within the layer. The extent of correlation between contaminants can be quite high; the correlation coefficient for ozone and b_{scat} between 3000 and 5000 feet msl in the Riverside profile is 0.96. Correlations such as this suggest that, although the elevated pollutant layer is not well mixed, it formed from a fairly homogeneous air mass.

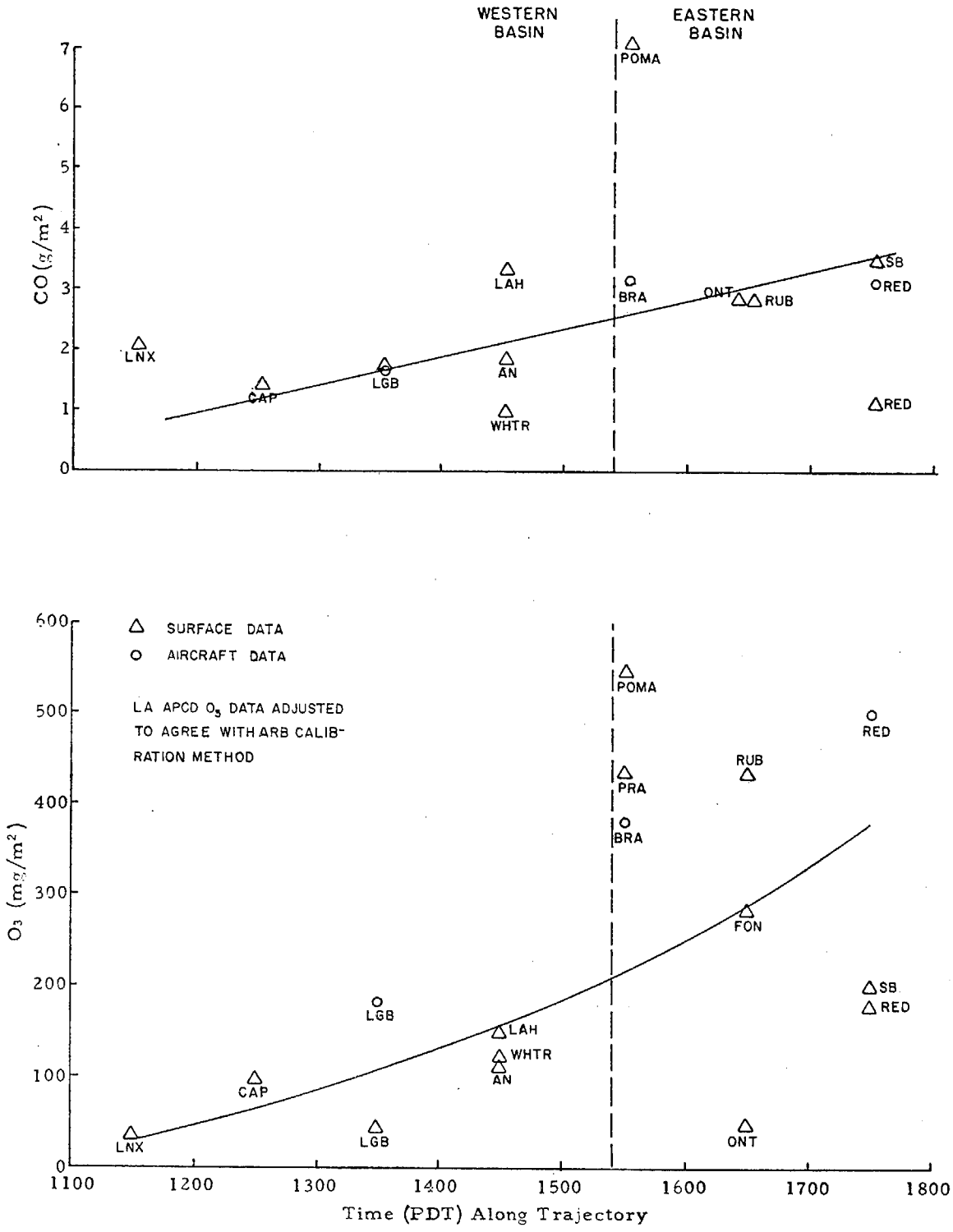

Fig. VIII-7. POLLUTANT LOADINGS IN SURFACE MIXED LAYER ALONG TRAJECTORY ARRIVING AT REDLANDS AT 1730 PDT, SEPTEMBER 21, 1972 (from aircraft measurements plus estimates made from ground data and mixing heights)

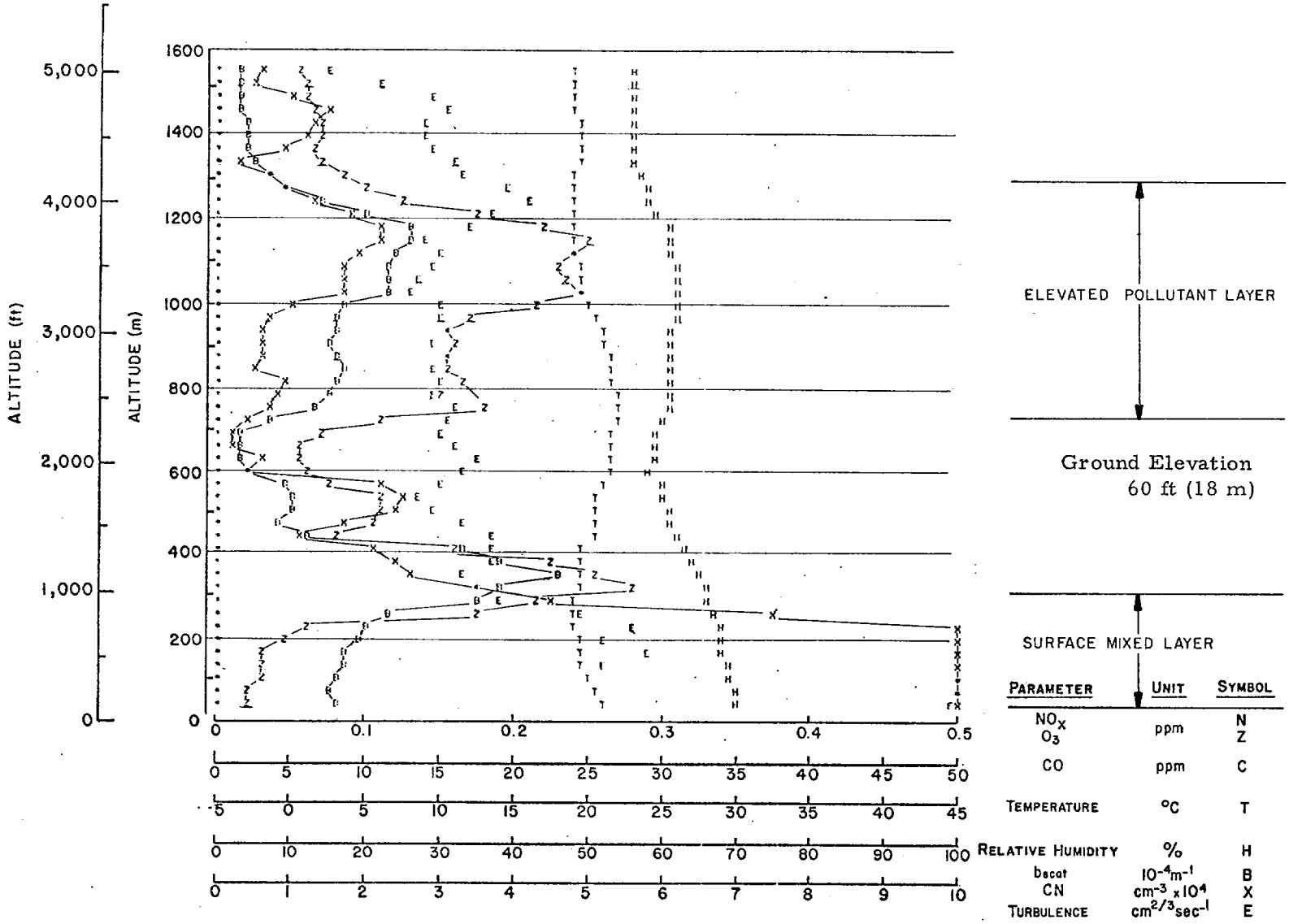

Fig. VIII-8. VERTICAL PROFILE OVER HAWTHORNE (HHR) AUGUST 23, 1973, 1629 PDT

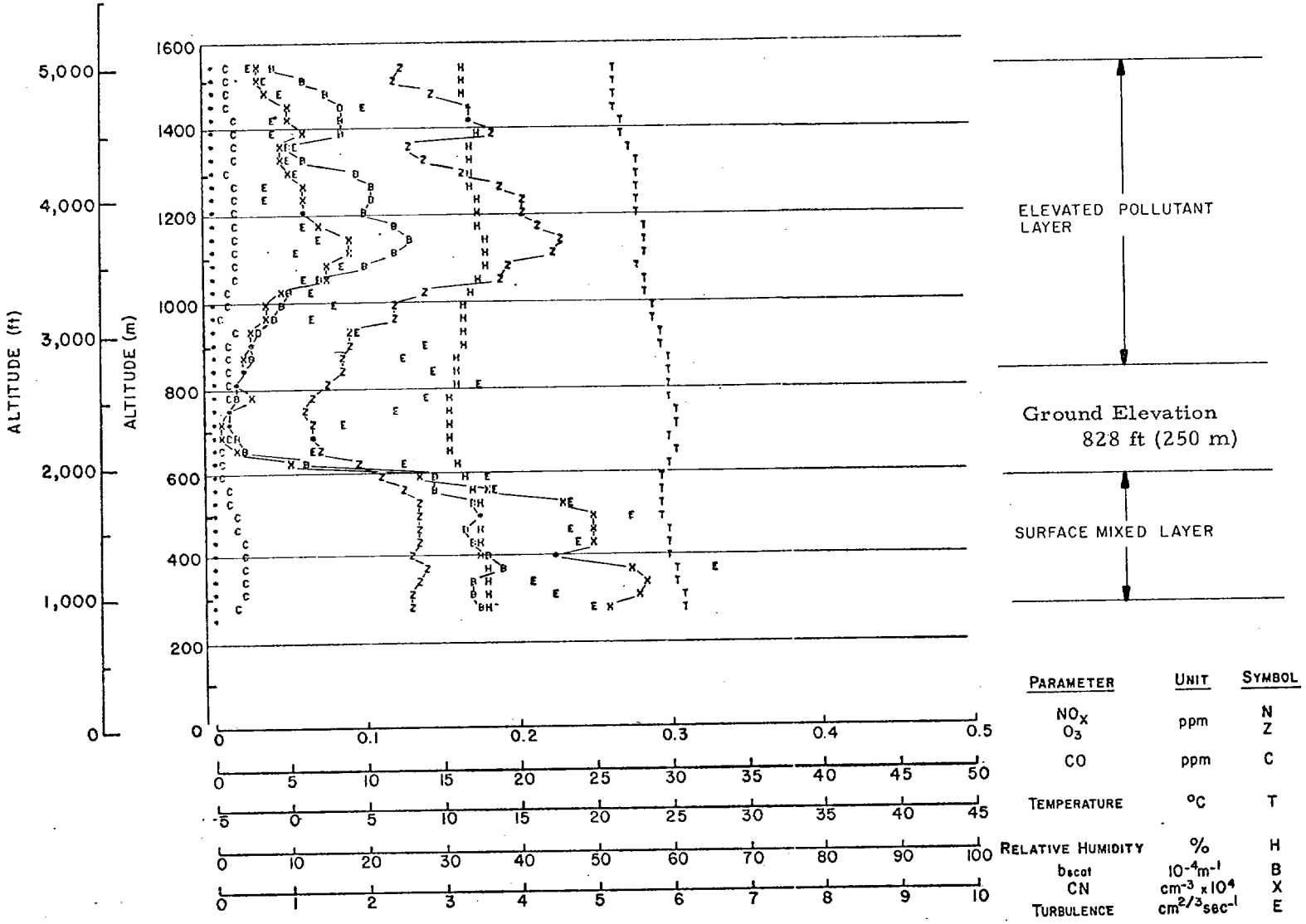

Fig. VIII-9. VERTICAL PROFILE OVER RIVERSIDE (RAL), JULY 19, 1973, 1659 PDT

c. Within the elevated pollutant layer, ozone concentrations are relatively high and condensation nuclei counts are relatively low. The ratio $[O_3]/b_{scat}$, for example, which is less than 0.03 ppm x 10^4 m in the surface mixed layer, is about 0.1 ppm x 10^4 m in the elevated pollutant layer. Similarly, the ratio b_{scat}/CN, which is less than 0.7×10^{-14} m^2 in the surface mixed layer, is about 1.5×10^{-14} m^2 in the elevated pollutant layer. These differences are similar to those observed when the surface mixed layers at Hawthorne and Riverside are compared as in Section V.C.5; in general, pollutants in the surface mixed layer at Riverside have aged longer than those in the surface mixed layer at Hawthorne and pollutants above the surface mixed layer have aged longer than those within it.

3. Statistics of Elevated Pollutant Layers

In order to identify and quantify characteristic features of elevated pollutant layers, a statistical analysis was made of all vertical profiles taken in 1973 at Hawthorne, El Monte, Ontario, and Riverside. For this study, an elevated pollutant layer was identified whenever the maximum light scattering coefficient above the surface mixed layer exceeded 2×10^{-4} m^{-1}, and correlation and regression coefficients within the layer were calculated for each pair of contaminant indices. Table VIII-1 shows the arithmetic averages of the correlation and regression coefficients thus obtained, weighted by the number of data points in each regression.

Elevated pollutant layers were identified in 38 percent of the vertical profiles and occur with about the same frequency at each of the four locations. All variables studied are somewhat correlated and, in general, the regression equations for well correlated variables do not depend strongly upon location. The independence of location shown by elevated pollutant layers contrasts with the dependence on location of surface mixed layer pollutant characteristics and suggests that the elevated layers tend to reflect larger scale phenomena.

TABLE VIII-1

STATISTICAL RELATIONSHIPS AMONG CONTAMINANT INDICES IN ELEVATED POLLUTANT LAYERS

Y-X		Hawthorne	El Monte	Ontario	Riverside	All Four Stations
b_{scat} - O_3						
	A	15.0	22.0	15.0	15.0	16.0
	B	-0.36	-0.67	-0.24	-0.60	-0.45
	R	0.82	0.74	0.75	0.81	0.79
b_{scat} - NO_x						
	A	81.0	85.0	77.0	86.0	82.0
	B	-0.64	-0.41	-0.37	-0.18	-0.27
	R	0.76	0.66	0.63	0.71	0.70
b_{scat} - CN						
	A	0.10	0.30	0.26	0.15	0.18
	B	1.1	0.84	1.1	0.73	0.95
	R	0.59	0.71	0.70	0.71	0.67
O_3 - NO_x						
	A	4.3	3.4	4.2	4.0	4.0
	B	-0.037	-0.012	0.015	0.003	0.026
	R	0.70	0.71	0.65	0.64	0.69
O_3 - CN						
	A	0.0054	0.0048	0.011	0.0060	0.0068
	B	0.011	0.011	0.10	0.10	0.061
	R	0.50	0.54	0.60	0.64	0.58
NO_x - CN						
	A	1.1×10^{-3}	1.9×10^{-3}	1.6×10^{-3}	1.2×10^{-3}	0.0014
	B	0.026	0.037	0.025	0.020	0.025
	R	0.71	0.59	0.71	0.70	0.69
Percent of Vertical Profiles With Elevated Pollutant Layer		42	40	33	39	38
Number of Data Points in Regressions		2242	1068	1881	2534	7725

For each pair of variables, R is the average of the correlation coefficients for individual profiles. A and B are the average coefficients in the regression equation $Y = AX + B$. Units are: b_{scat} (10^{-4} m^{-1}), O_3 (ppm), NO_x (ppm), CN (10^3 cm^{-3}).

The contaminant indices which correlate most closely above the surface mixed layer are ozone concentration and b_{scat}, which have correlation coefficients greater than 0.9 in one quarter of the profiles (Fig. VIII-10). The regression coefficients for ozone and b_{scat} are quite consistent from one profile to the next as shown in Fig. VIII-11.

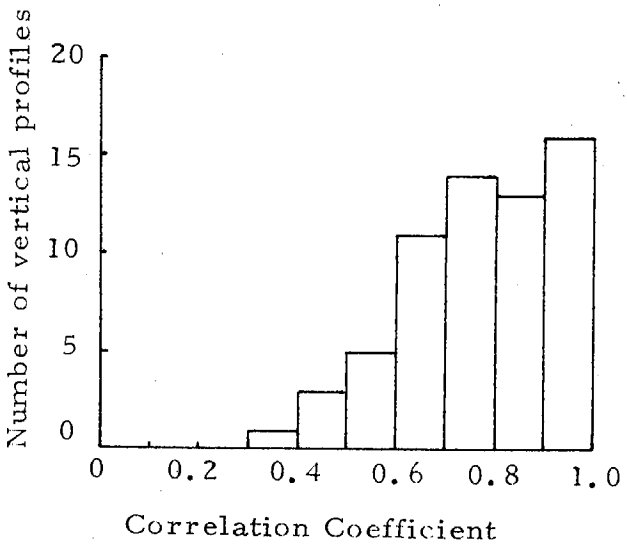

Fig. VIII-10. FREQUENCY DISTRIBUTION OF CORRELATION COEFFICIENTS FOR OZONE CONCENTRATION AND b_{scat} IN ELEVATED POLLUTANT LAYERS

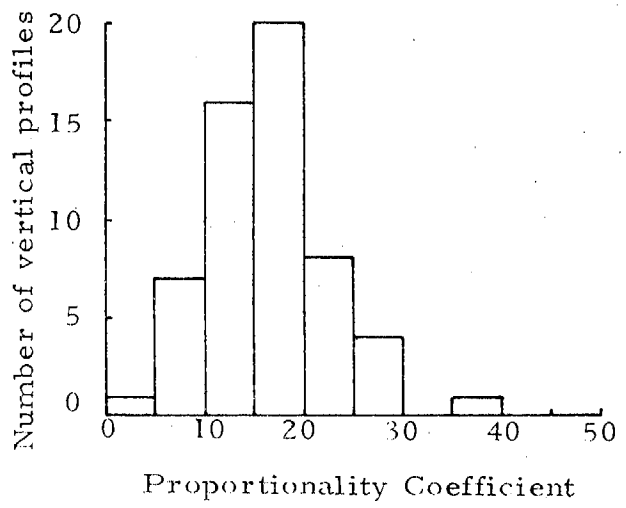

Fig. VIII-11. FREQUENCY DISTRIBUTION OF THE COEFFICIENT OF OZONE IN THE REGRESSION EQUATION FOR b_{scat}, $b_{scat} = A\,[O_3] + B$

C. Additional Observations on the 3-D Distribution of Ozone in California

1. Introduction

A general review of the distribution of ozone in the atmosphere is provided by Junge (1962 and 1963). Ozone in the lower troposphere comes from several sources. Among them, ozone can be mixed down from the stratosphere or can be generated in the troposphere by photochemistry in polluted areas. In clean areas, Junge (1963) reports that the ozone concentration is generally constant through the troposphere with a slight decrease in the immediate vicinity of the ground under stable conditions. Under conditions of strong vertical mixing, however, the mixing ratio of ozone, rather than the absolute concentration, may be constant through the troposphere. Junge reports that an average ozone value in the lower troposphere is about 50 $\mu g/m^3$. In the lower 5000 feet of the atmosphere, this value is about 0.02 to 0.03 ppm.

More recently, Kelly (1970) has reported values of ozone in remote areas of Alaska as high as 0.12 ppm with an average over a three year period of about 0.04 ppm. Likewise, MRI has recently measured ozone in clean areas of Alaska, Colorado, California, and other western states ranging from 0.02 to 0.05 ppm with the high values obtained during periods of strong vertical mixing [Stinson et al., 1972; Stinson and LeBeau, 1972; Blumenthal et al. (MRI 73 FR-1085), 1973; Blumenthal, Anderson, and Sem, 1974].

Numerous studies of the distribution of ozone or oxidant in polluted areas have also been performed. Most of these have been made at ground level and some have examined the vertical distribution at one location, but little data on both the spatial and temporal variations in the distribution of ozone have been available until the present study.

Mosher et al. (1970) examined the seasonal variations in the distribution of ozone maxima in the L. A. Basin. Lea (1968) has studied the vertical distribution of ozone by means of ozone sondes at one location near Los Angeles and has reviewed many of the other ozone studies. As early as 1954, the Air Pollution Foundation made some measurements of the vertical distribution of oxidant using a blimp as a sampling platform (Neiburger et al., 1955). More recently, Edinger et al. (1972) and Edinger (1973) reported the results of a few light aircraft flights in the L. A. Basin during which they measured the oxidant distribution on a vertical section from the coast

to the inland area near San Bernardino. Miller et al. (1972) have discussed the distribution of ozone in the San Joaquin Valley and the Sierra Nevada foothills of California and reported on the results of a few flights during which they measured the ozone distribution. Miller and Ahrens (1970) have used a light aircraft to study spatial and temporal variations of ozone in the San Francisco Bay Area. Blumenthal and Smith (1972) reported the results of a series of vertical profiles of ozone concentration and other pollutant and meteorological parameters made in three major polluted air basins of California as a prelude to the present study.

In polluted areas, the distribution of ozone is often very complicated. In the absence of photochemistry, the ground and the pollutants emitted near the ground can destroy ozone, creating ozone deficits at ground level or in stable layers near the ground. This phenomenon has been observed and commented on by Junge (1963) and mentioned by Kauper (1960). It has been observed and discussed in more detail by Miller and Ahrens (1970) and Miller et al. (1972) and was mentioned by Lea (1968) as a possible cause of his observations of higher ozone concentration in the inversion layer than at ground level. This scavenging effect was also noted by Blumenthal et al., 1974, in the Denver area and has been described elsewhere in this report.

When photochemistry is present, the pollutants act as a source of ozone (Stephens, 1969) and an equilibrium must be established between the formation and destruction rates of ozone (Miller and Ahrens, 1972). In addition, complex meteorological patterns involving the undercutting of polluted air by clean air or the trapping of fresh pollution in layers near the ground while old polluted air remains aloft further complicate the three-dimensional ozone distribution in polluted areas (Edinger et al., 1972, and Edinger, 1973).

The present study has resulted in extensive three-dimensional ozone distribution data. These data are complemented by data on other pollutants and meteorological parameters and by extensive surface wind data and some data on the vertical structure of the winds. In general, the present data agree with, expand upon, and help clarify previously presented data.

2. Data from "Clean" Areas

Figure VIII-12 is a vertical profile taken over the ocean off Point Reyes on an extremely clear and windy day during the preliminary program of November, 1971. The wind was blowing

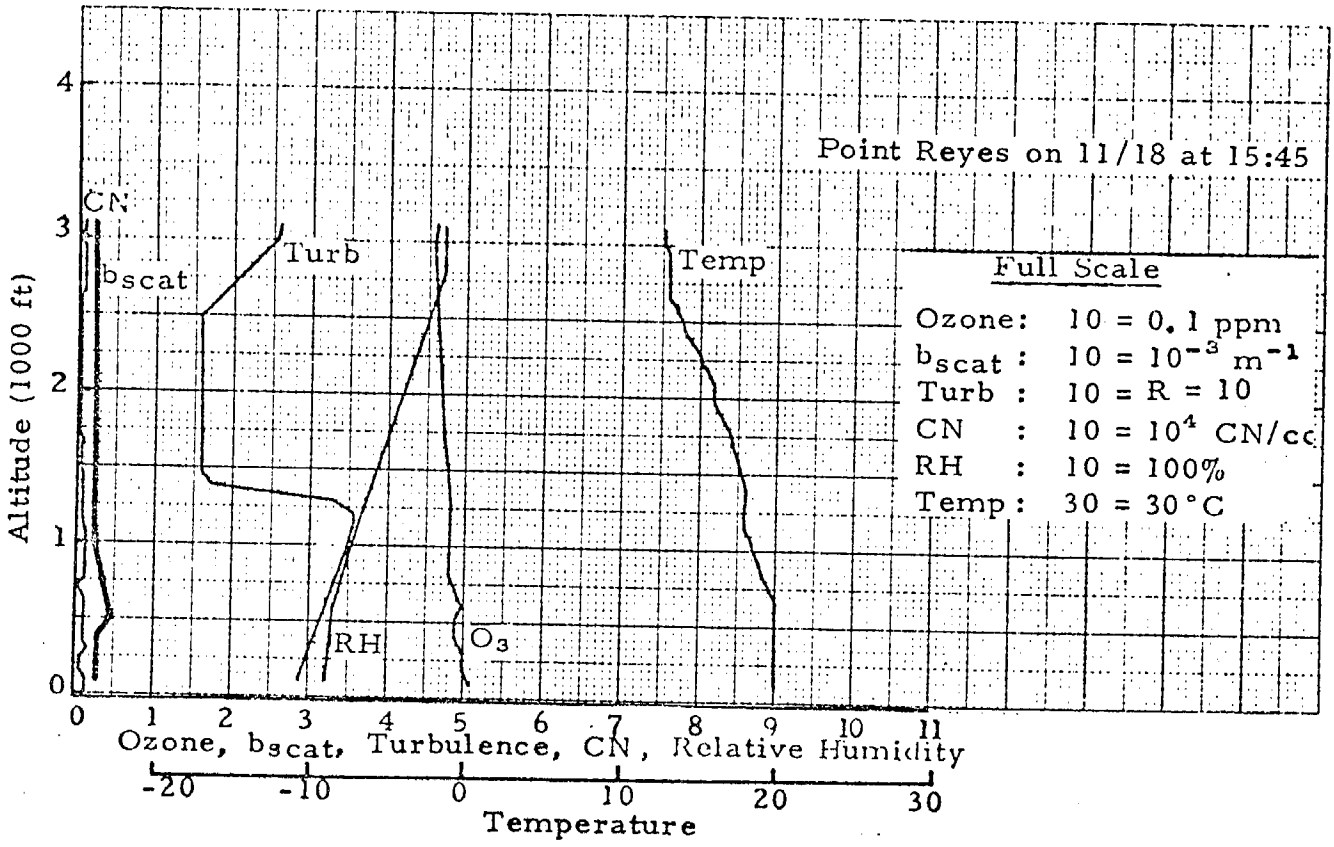

Fig. VIII-12. VERTICAL PROFILE OVER POINT REYES
NOVEMBER 18, 1971

onshore at about 20 knots, the scattering coefficient was approximately at the Raleigh scatter limit, and the condensation nuclei count was only a few hundred per cm^3, all indicating very clean air. The ozone concentration under these conditions is between 0.04 and 0.05 ppm and this level can probably be considered as the background level on that day.

Figure VIII-13 is a vertical profile taken over Avenal at the west edge of the San Joaquin Valley. Although this area is generally considered clean, it is clear from the b_{scat} and condensation nuclei profiles that a well mixed haze layer extends up to a slight inversion at about 5400 feet. A small amount of the pollutant even breaks through the inversion due to the high turbulence levels and finds its way up to about 7400 feet. Above that level, the air is very dry and clean. The condensation nuclei count drops off to a very low level and the scattering coefficient is approximately at the Raleigh scatter limit. In the haze layer, the ozone level is about 0.08 ppm and the level drops to slightly over 0.06 ppm in the clean air.

Figure VIII-14 is a profile taken over the Goldstone tracking station in a remote area of the Mojave Desert. Again, the air is quite clean with visibilities of about 60 miles at ground level but, even in this case without an inversion, a mixing layer exists. At about 5000 feet, the turbulence, condensation nuclei count, scattering coefficient, and ozone all start to drop. By 5500 feet, the air is noticeably cleaner than at ground level. In the mixing layer, the condensation nuclei level is up to several thousand per cm^3 while above it the level is not readable with the instrument set to 10,000 CN/cm^3 full scale. In this clean air, the ozone concentration is about 0.025 ppm.

From the above data, it appears that a substantial background level of ozone exists in Southern California. Our measured ozone levels in clean air throughout the program ranged from 0.02 ppm to about 0.06 ppm. The lower part of this range agrees with the worldwide average given by Junge (1963), but much of our clean air data fell in the 0.04-0.05 ppm range; thus, even in air that is very "clean" by other standards, the ozone level can come close to the federal ambient air standard of 0.08 ppm.

The data from Goldstone also indicate that, even though the area is apparently clean, a mixing layer exists above which the oxidant level drops and, thus, the area is probably influenced to some extent by distant pollution sources which generate photochemical oxidant, such as Los Angeles.

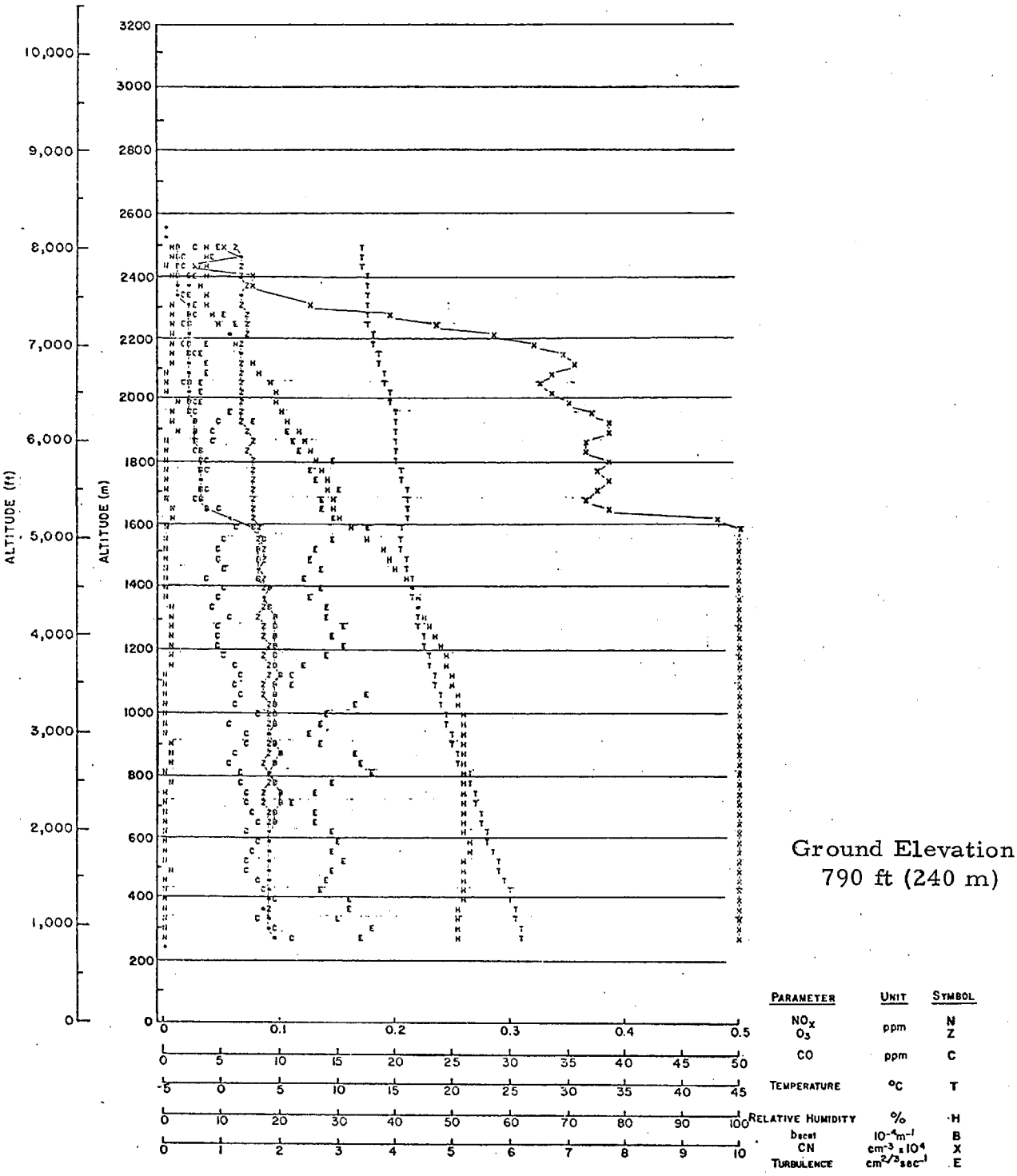

Fig. VIII-13. VERTICAL PROFILE OVER AVENAL SEPTEMBER 13, 1972, 1624 PDT

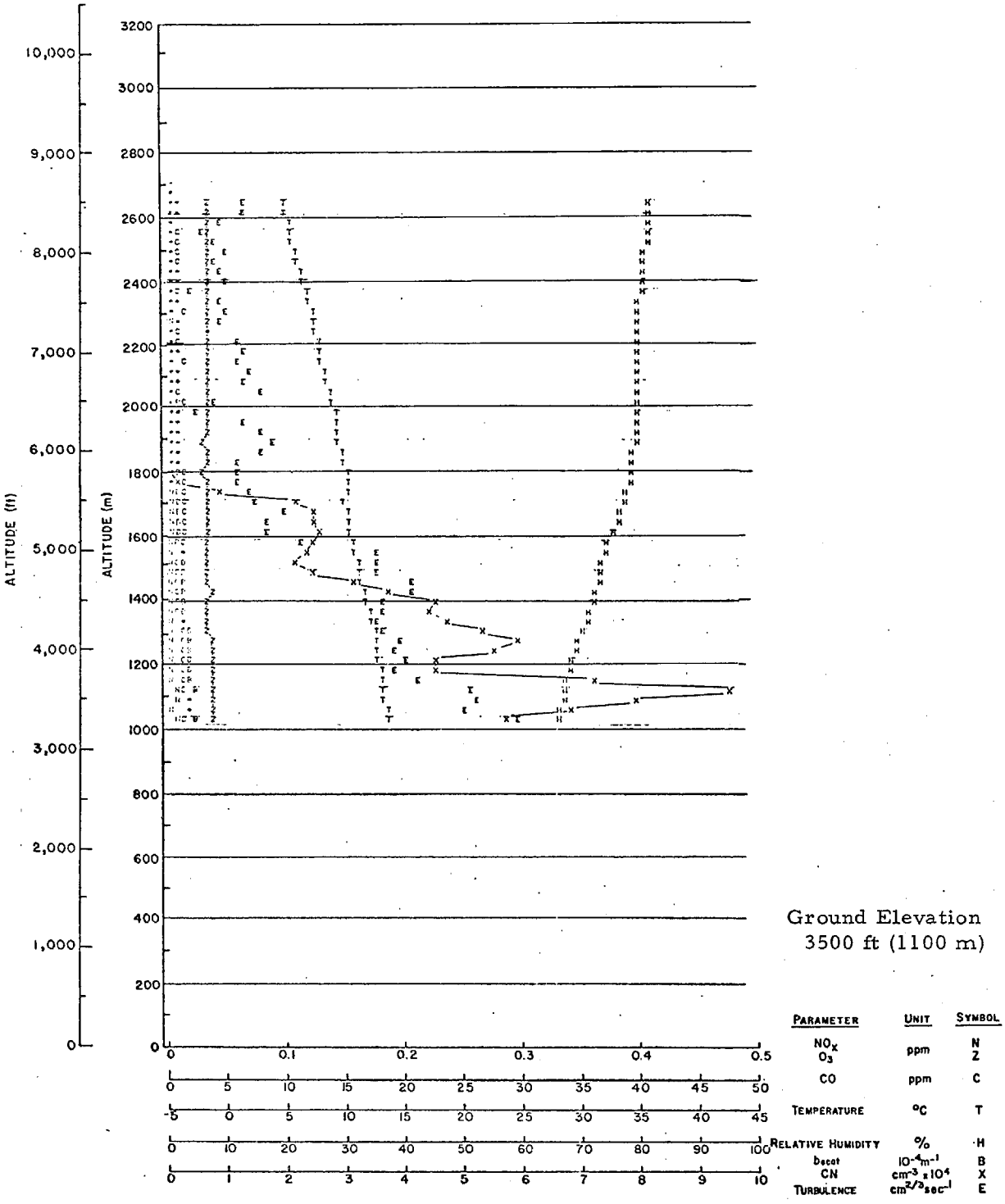

Fig. VIII-14. VERTICAL PROFILE OVER GOLDSTONE NOVEMBER 2, 1972, 1005 PST

3. Spatial and Temporal Variations in the 3-D Distribution of Ozone in the L. A. Basin

Figures VIII-15 and VIII-16 are contour maps of the ozone concentration at the surface and just above the mixing layer in the morning before the period of strongest photochemical activity. This day (September 20, 1972) was representative of late summer conditions in Los Angeles and was chosen since it has already been discussed in detail in Chapter VI. A discussion of the mixing layers, streamlines, and trajectories for September 20, 1972 is included in Chapter VI and will not be repeated here.

The main characteristic of the morning distribution is the low value of the ozone concentration at the surface. These data were taken during the transition from land breeze to sea breeze conditions when the surface winds were relatively calm, the mixing layers shallow, and surface heating and photochemistry still minimal. The ozone levels at the surface are generally well below the level in clean air, yet are at or above the clean air level at the top of the mixing layer. Similar conditions with even higher ozone values aloft were seen for July 25, 1973, also discussed in Chapter VI.

Figure VIII-17 is a vertical profile taken at Fullerton on the morning of the same day. This figure indicates two distinct inversions, the lowest one defining the morning mixing layer and the upper one possibly trapping older pollutants. Below the lower inversion, there is good mixing, the primary pollutant levels are high, and the ozone value is quite low. Above the lower inversion, the primary pollutants are greatly reduced and the ozone level is up.

From Figs. VIII-15 through VIII-17, it appears that in the mixing layer, during the night and early morning hours, the ozone destruction rate from fresh pollutant sources exceeds the photochemical formation rate. Above the mixing layer in the absence of fresh pollutants, the ozone remains at higher concentrations. This is in agreement with the findings of Miller and Ahrens (1970) and Miller et al. (1972).

Figure VIII-18 shows the ground level ozone contours at midday and Fig. VIII-19 is a profile over Fullerton at the same time. By this time, the mixing layer has deepened over much of the basin, photochemistry has become an important factor, and ozone is now being generated throughout the mixing layer faster than it can be destroyed near the ground. The ozone concentrations have thus increased to considerably above clean air values. The air above the

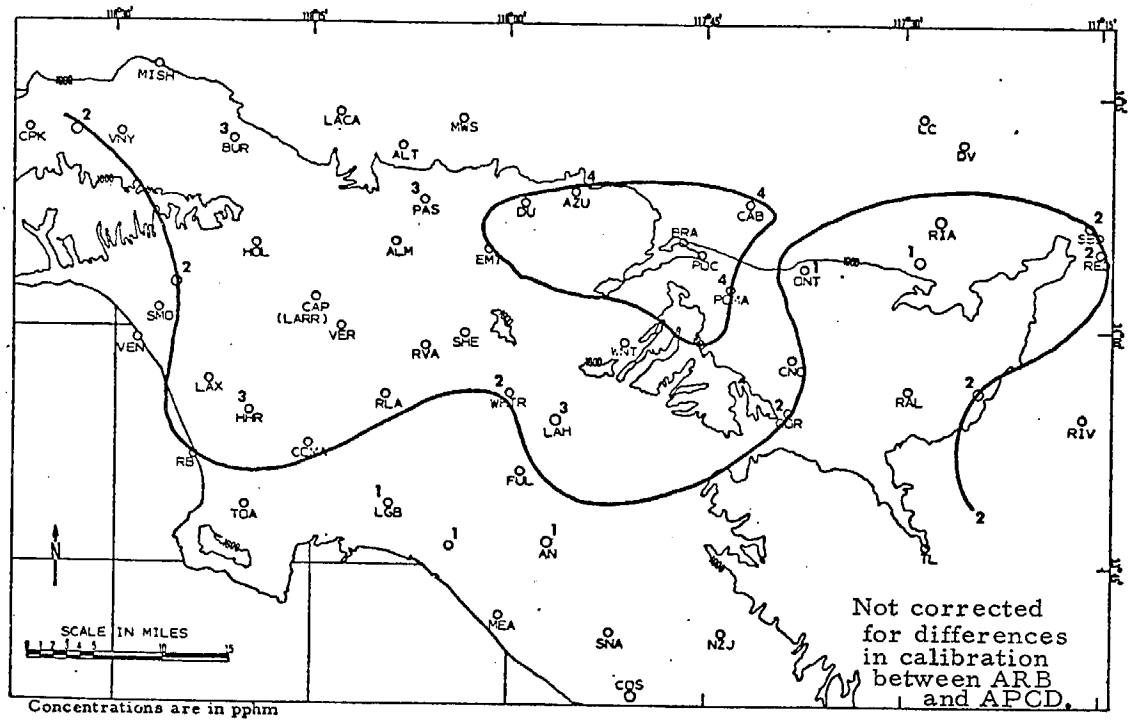

Fig. VIII-15. SURFACE OXIDANT CONCENTRATIONS 0800 PST (0900 PDT) SEPTEMBER 20, 1972

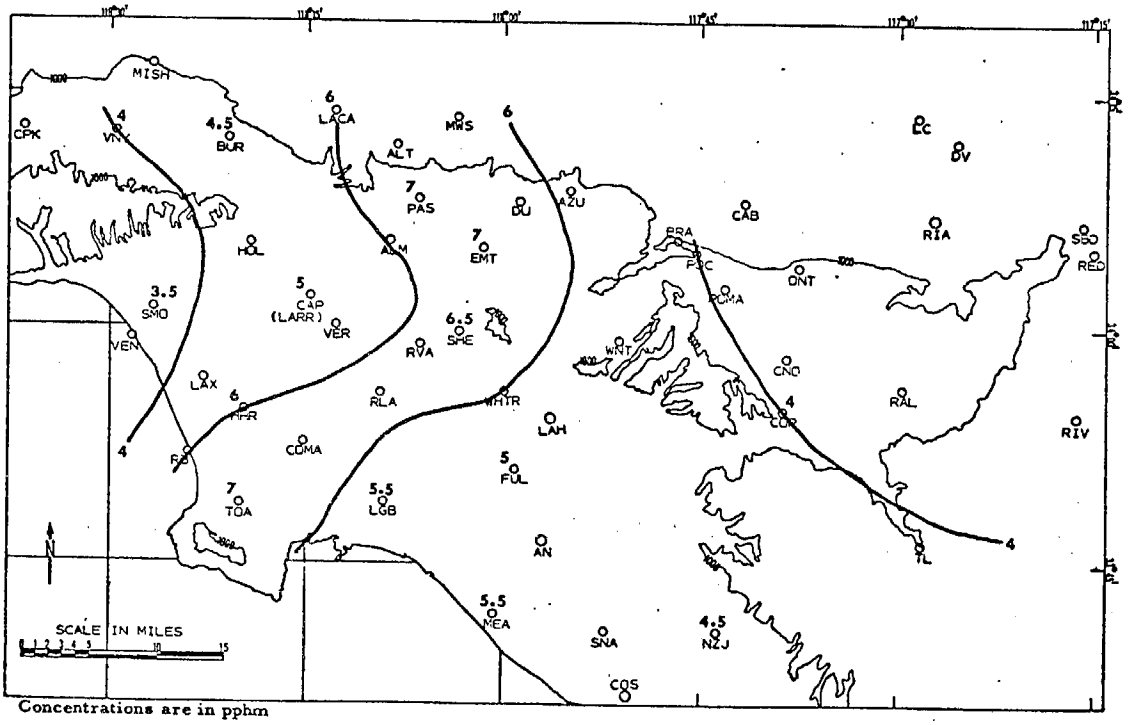

Fig. VIII-16. PEAK OXIDANT CONCENTRATIONS ABOVE MIXING LAYER - MORNING FLIGHT, SEPTEMBER 20, 1972. DATA TAKEN FROM AIRCRAFT SOUNDINGS

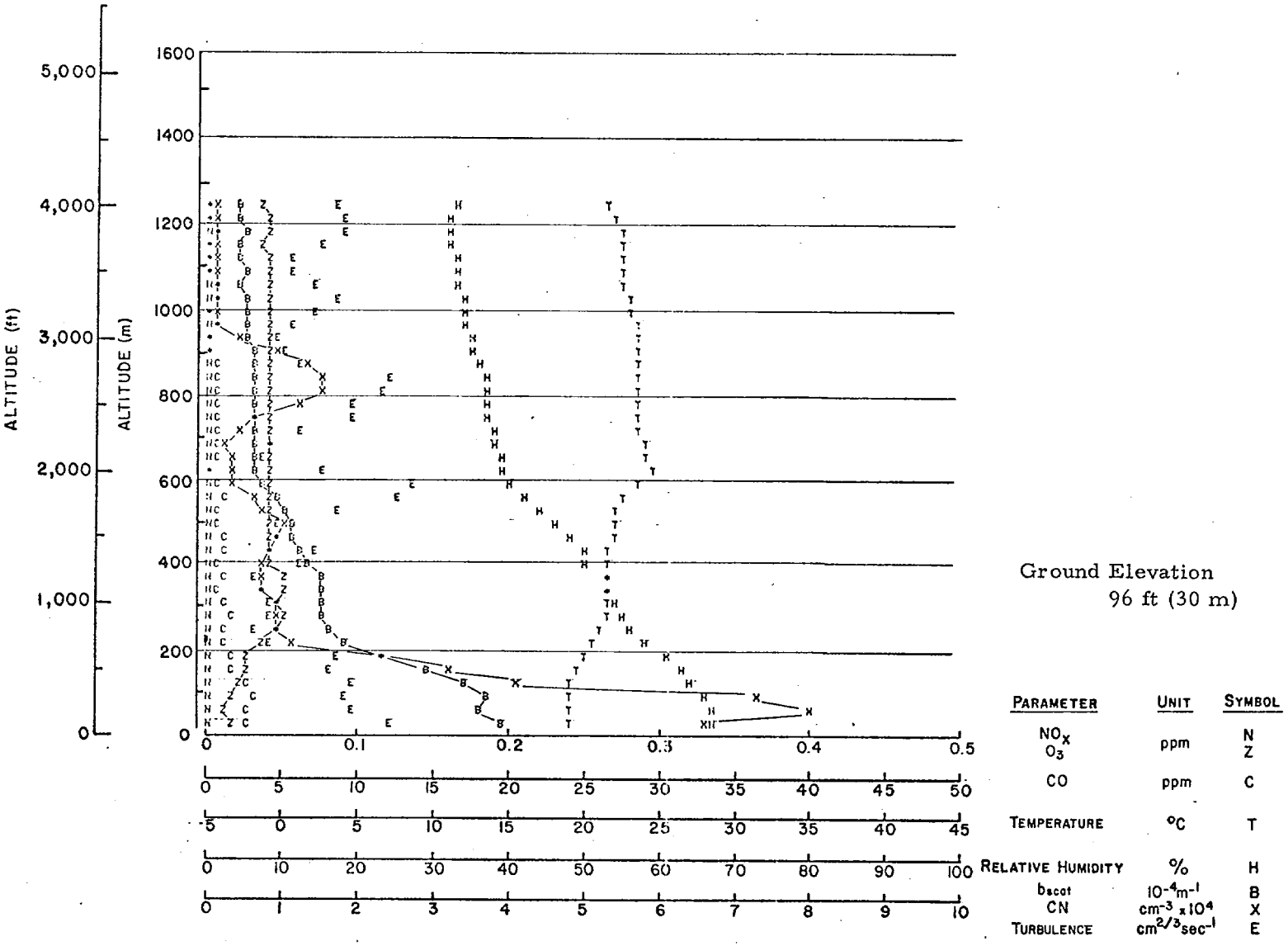

Fig. VIII-17. VERTICAL PROFILE OVER FULLERTON (FUL)
SEPTEMBER 20, 1972, 0900 PDT

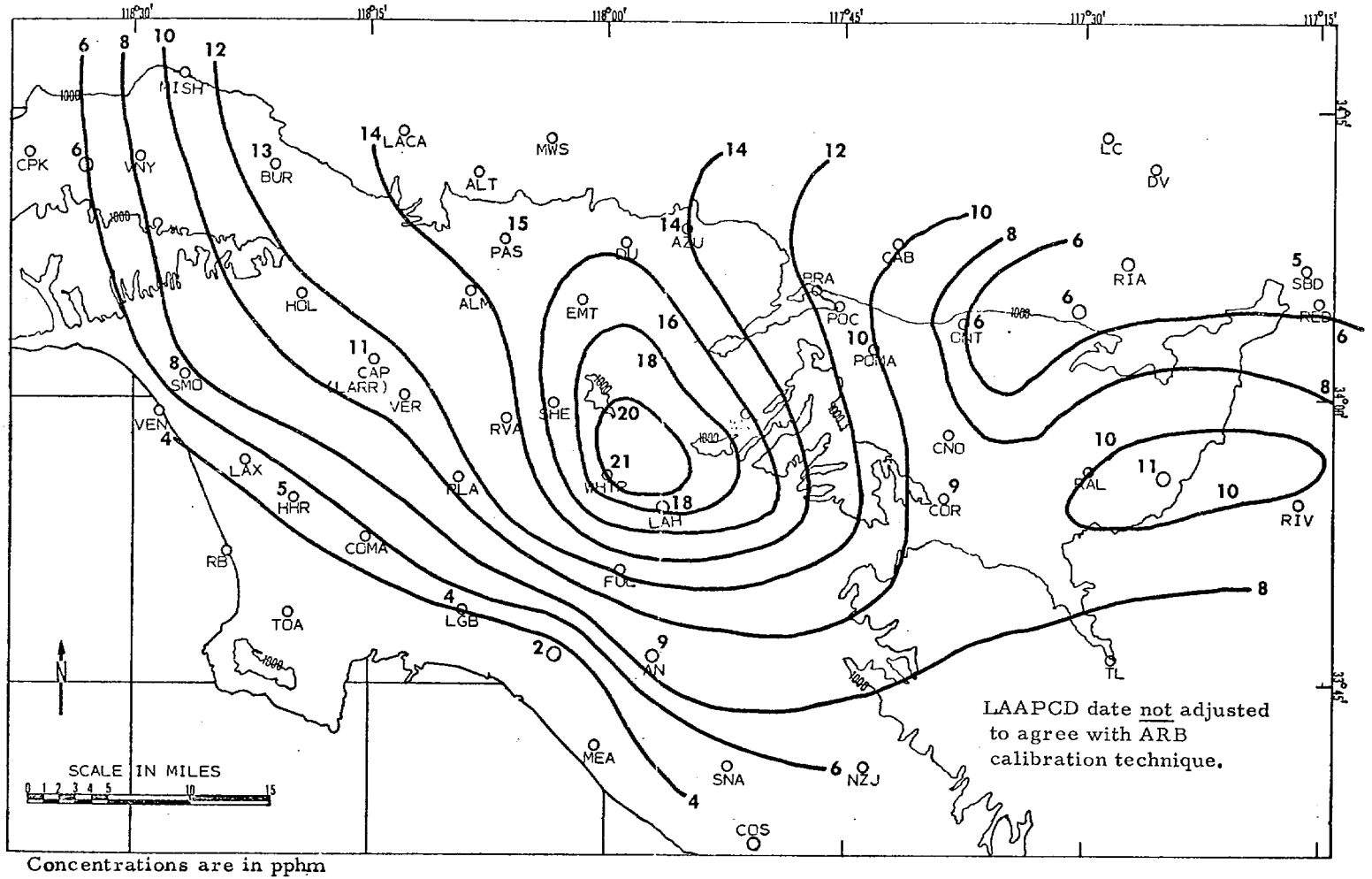

Fig. VIII-18. SURFACE OXIDANT CONCENTRATIONS - 1200 PST (1300 PDT) SEPTEMBER 20, 1972

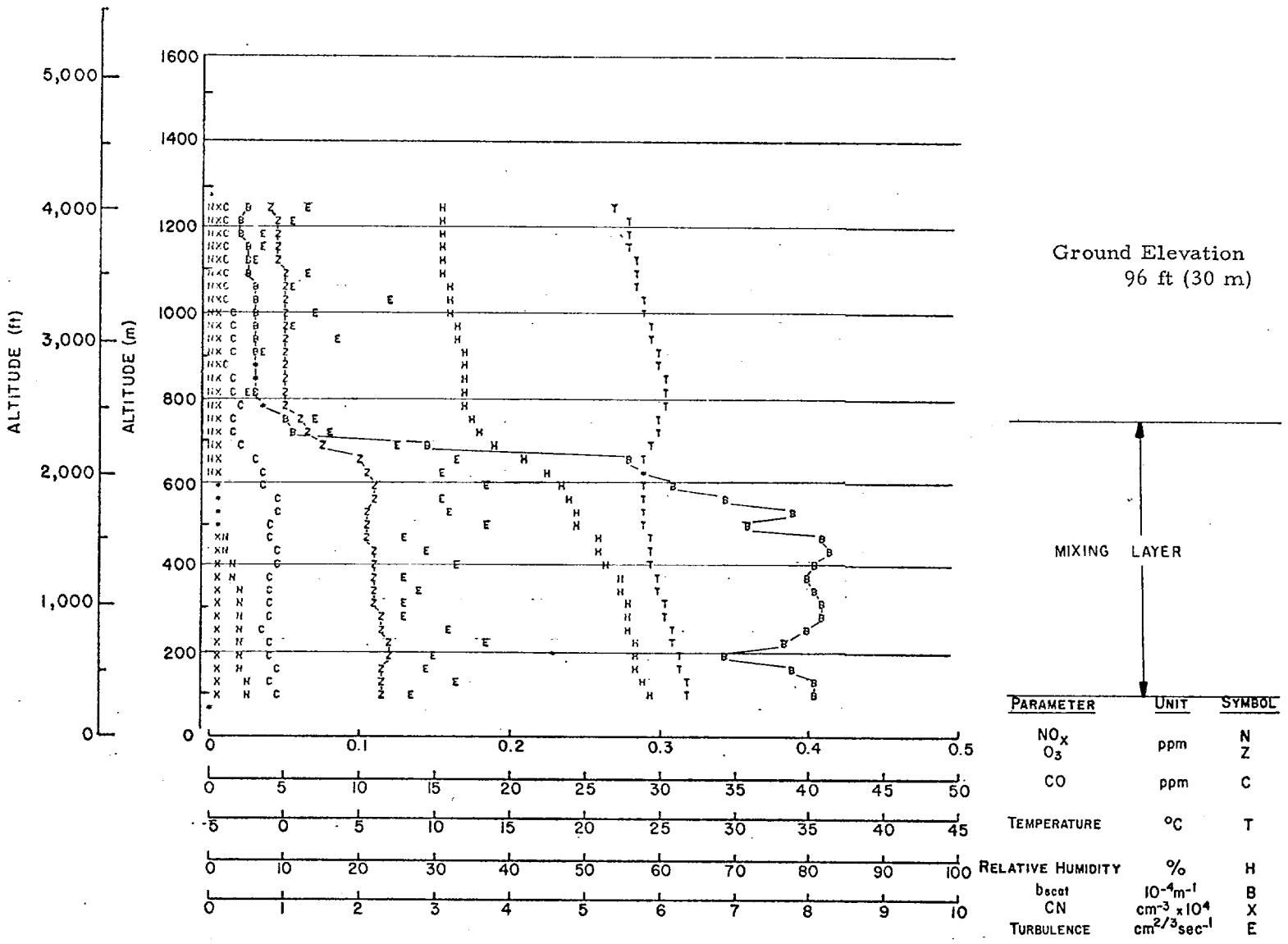

Fig. VIII-19. VERTICAL PROFILE OVER FULLERTON (FUL)
SEPTEMBER 20, 1972, 1240 PDT

mixing layer, however, is relatively clean (about 40 miles visibility) and the ozone level aloft is approximately the same as it was in the morning sounding, about 0.04 ppm, a reasonably clean air value.

Figure VIII-20 shows ground level ozone contours in the afternoon and Fig. VIII-21 is an afternoon vertical profile over Hawthorne near the coast. By this time, a strong onshore flow has developed, bringing in cleaner air which has undercut the older polluted air. In the area affected by the sea breeze, the ozone concentrations at ground level have decreased since midday, while higher concentrations remain in the older air aloft and in the inland areas.

The effect of the afternoon sea breeze is pointed out in the Hawthorne profile (Fig. VIII-21). The overall pollution level is low in the mixing layer as evidenced by the low CO and b_{scat}. Any pollutants which are in the mixing layer are fresh and, since the solar radiation is no longer strong, photochemistry is not a dominant factor. Thus, the ozone level is lower in the mixing layer than it is slightly above the inversion for two reasons: the air in the mixing layer is relatively clean to start with and photochemical ozone formation processes are outweighed by ozone destruction by fresh pollutants, while the air aloft contains ozone formed by photochemistry earlier in the day. Above the older polluted air, however, there is also cleaner air with ozone concentrations near those for clean air. This sea breeze undercutting effect is pointed out even more strongly in Fig. VI-11 for July 25, 1973, discussed previously.

These observations are in agreement with those of Edinger et al. (1972) and Lea (1968). In his paper, Lea wonders at the cause of the ozone peaks above the base of the inversion similar to that in Fig. VIII-21. His measurements were made at Point Mugu, a coastal area, and his data were similar to those obtained at Hawthorne in the present program. Thus, it is possible that the ozone peaks which he saw above the inversion base are really the result of ozone deficits below the inversion caused by ozone destruction processes or by undercutting of polluted air by clean sea air.

It should be mentioned that the three-dimensional ozone distributions are often more complicated than those discussed in this section. For example, layers are often present aloft with clean air between them, especially in the inland areas near the mountains. This type of structure is discussed in Sections V. B. and VIII. B. Even though the interaction of the pollutant sources, the photochemistry, and the meteorology can be extremely complicated,

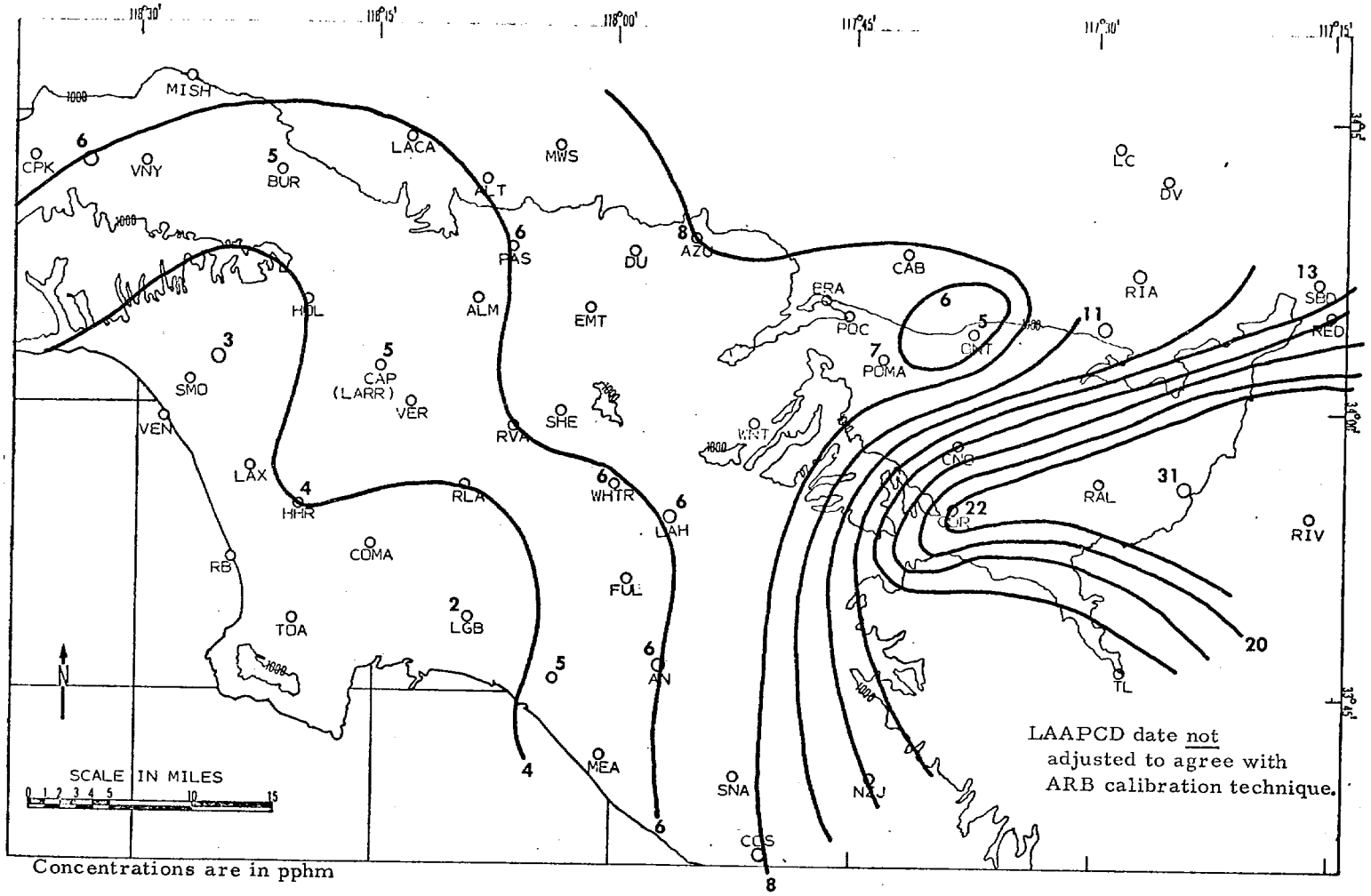

Fig. VIII-20. SURFACE OXIDANT CONCENTRATIONS - 1600 PST (1700 PDT) SEPTEMBER 20, 1972

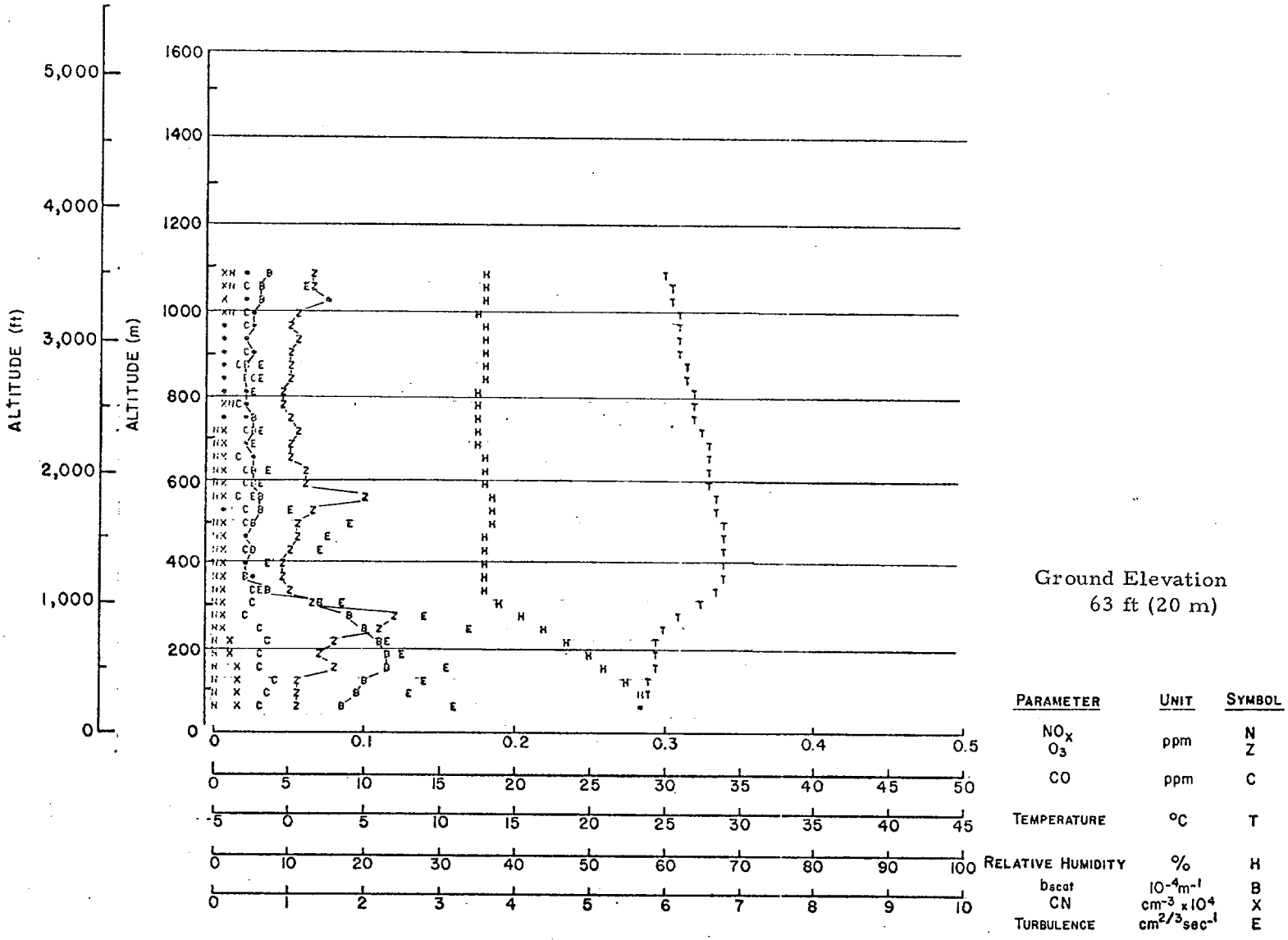

Fig. VIII-21. VERTICAL PROFILE OVER HAWTHORNE (HHR)
SEPTEMBER 20, 1972, 1644 PDT

much can be learned by isolating the various aspects of a complicated structure and examining them one at a time.

We should also note that the ozone deficits in the mixing layer near the ground during the early morning hours were also observed in the San Joaquin Valley. This is in agreement with the observations of Miller et al. (1972).

4. The Vertical Distribution of Ozone in the Absence of Photochemistry

a. Overnight Persistence of Ozone

The ability of ozone to survive in the absence of sunlight is demonstrated by around-the-clock data taken at the end of the July 24-26, 1973, episode discussed in Chapter VI. Throughout the night of July 26-27, aircraft soundings were made at six locations in the San Bernardino-Riverside Air Basin east of Los Angeles. Figures VIII-22 to VIII-25 show vertical profiles taken at Riverside.

The results of the overnight observation of O_3 are summarized in Table VIII-2. Ozone data were studied for an elevated layer free of surface influences. The layer between 3000 and 4500 ft msl was selected so that all soundings would be continuous to the top of the layer and the bottom of the layer would be above the surface inversion on all 24 soundings. Averages of observed ozone were calculated both for this layer and for the first 600 ft above the surface for all soundings. The upper number in each group of three in Table VIII-2 is the mean O_3 concentration for the elevated layer while the lower number is for the surface 600 ft thick layer. The number in parentheses in each group is the difference between the temperature at 3000 ft msl and the temperature near ground, and is an indicator of the stability of the air below 3000 ft msl.

There are many reactions known which can consume O_3 in the lower atmosphere. By far the fastest of these is the following:

$$NO + O_3 \rightarrow NO_2 + O_2$$

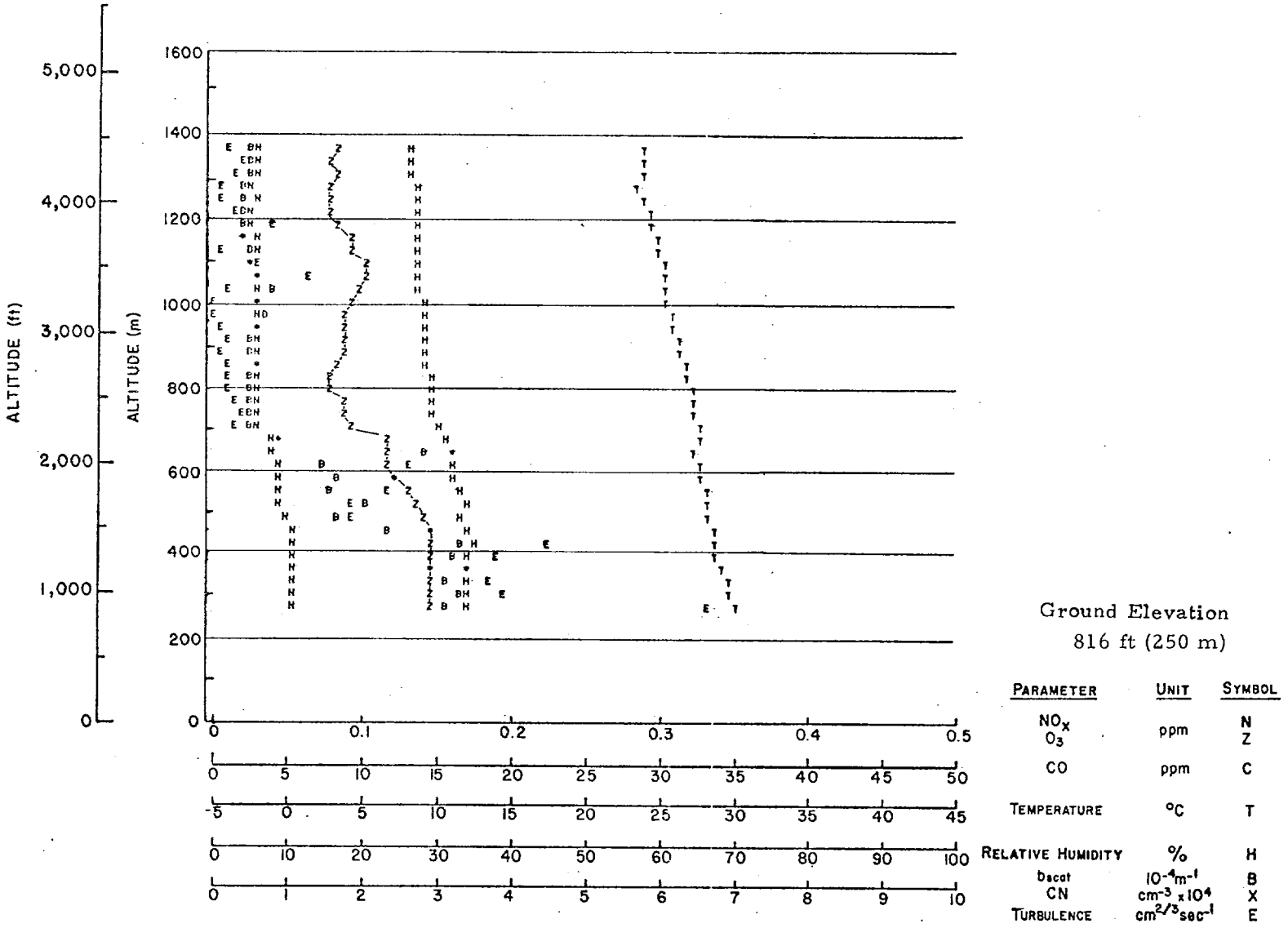

Fig. VIII-22. VERTICAL PROFILE OVER RIVERSIDE (RAL) JULY 26, 1973, 1638 PDT

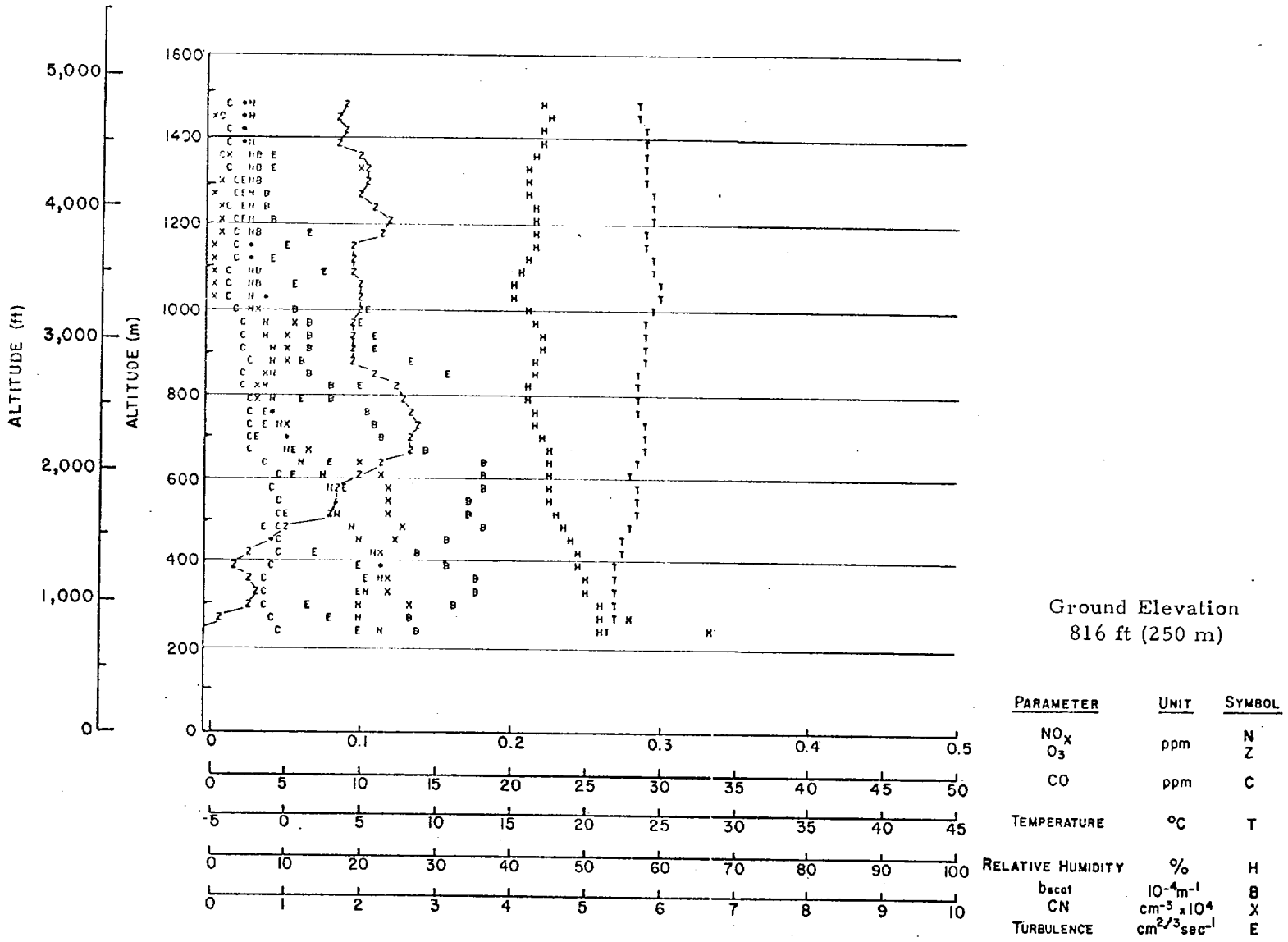

Fig. VIII-23. VERTICAL PROFILE OVER RIVERSIDE (RAL) JULY 26, 1973, 2239 PDT

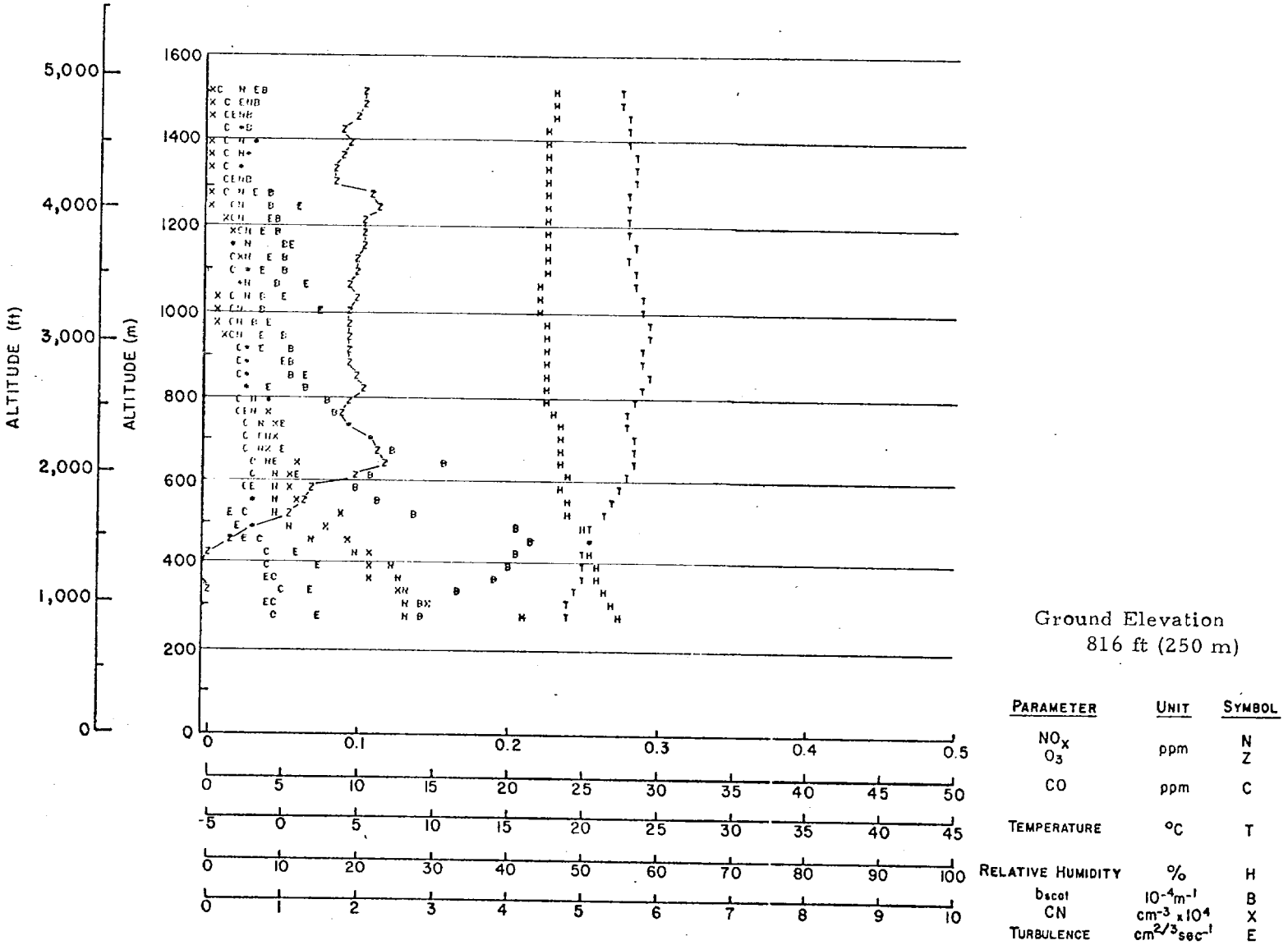

Fig. VIII-24. VERTICAL PROFILE OVER RIVERSIDE (RAL) JULY 27, 1973, 0122 PDT

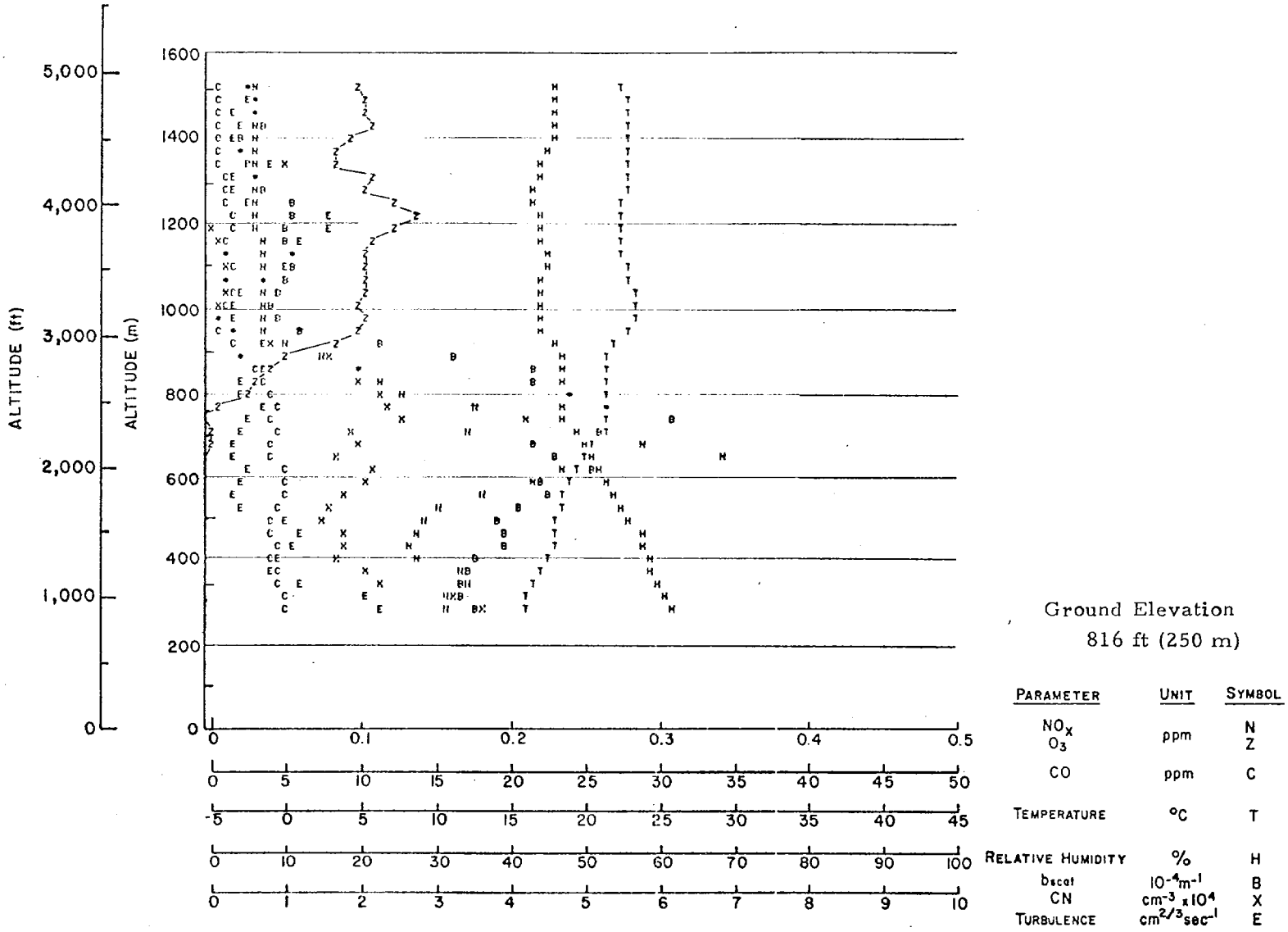

Fig. VIII-25. VERTICAL PROFILE OVER RIVERSIDE (RAL) JULY 27, 1973, 0500 PDT

TABLE VIII-2

OVERNIGHT OZONE CONCENTRATIONS

Location	Times PDT			
	July 26 17 PDT	July 26 23 PDT	July 27 2 PDT	July 27 5 PDT
Ontario (ONT)	9.3 13.8 (-2.5)	11.3 0.6 (3.5)	13.1 1.2 (3.5)	12.0 0.2 (7.5)
Rialto (RIA)	16.4 20.4 (-3.5)	10.7 0.2 (2.5)	12.5 0.4 (2.5)	13.6 0.2 (5)
Redlands (RED)	16.8 16.6 (-4)	13.4 4.8 (1.5)	11.5 3.7 (3.5)	12.1 6.3 (3.5)
Riverside (RAL)	9.8 15.4 (-3.5)	11.0 2.4 (2)	10.6 0.2 (4.5)	11.4 0.1 (6)
Corona (COR)	10.4 12.3 (-2.5)	11.0 0.1 (5)	11.1 0.3 (5)	11.7 0.3 (6)
Bracket (BRA)	9.7 20.7 (-4)	11.9 0.2 (4.5)	13.1 7.2 (2)	14.6 0.1 (6.5)
Average	12.1 16.5 (-3.5)	11.6 1.4 (3)	12.0 2.2 (3.5)	12.6 1.2 (5.5)

The upper left-hand number in each set is the average O_3 concentration (pphm) between 3000 ft and 4500 ft msl. The lower left-hand number is the average O_3 concentration (pphm) in the first 600 ft above ground. The number in parentheses is the temperature ($^\circ$C) at 3000 ft msl minus the average temperature in the first 600 ft above ground.

The rate constant for this reaction is about 0.3 $pphm^{-1}$ min^{-1} (Johnston and Crosby, 1954), which means that, at a constant NO concentration of 1 pphm, the half-life of O_3 for this reaction is less than 3 minutes. In the absence of the solar radiation necessary to produce O_3, NO from the fresh exhaust of combustion sources therefore quickly scavenges O_3. This is seen in Table VIII-2 where O_3 concentrations near the ground fall below the 4 pphm background value during the night due to the continuous introduction of fresh emissions into the surface layer.

As the temperature differentials in Table VIII-2 indicate, air above 3000 ft msl is isolated from the surface layer throughout the night by a strong ground-based temperature inversion that is established at all locations between 1700 and 2300 PDT. Cut off from sources of NO, O_3 at the upper levels appears to be quite stable, as shown by concentrations of 12-13 pphm, well above background, that persist through the night. In all 24 soundings studied, O_3 and b_{scat} were well correlated between 3000 and 4500 ft msl and condensation nuclei (CN) counts at these levels were low. These conditions are typical of well aged pollutant layers, as discussed in Section VIII. B.

These data show that, in the absence of other pollutants to scavenge it, ozone is stable in the atmosphere at high concentrations for many hours, even in the absence of sunlight.

b. Ozone Persistence in Rain

Figures VIII-26 and VIII-27 show profiles made over Shepherd Airport (SHE) in the Los Angeles area. These traverses were made on a fairly clear, rainy day during which photochemical processes should have been minimal. In the absence of photochemistry, the ozone is destroyed by the primary pollutants and the depth to which the polluted air has mixed during the day is indicated by the depth of the ozone deficit. The morning sounding indicates a mixing depth of about 1000 ft (300 m) msl while, by afternoon, the fresh pollutants had mixed up to 3300 ft (1000 m). Note, in Fig. VIII-26, that in the quite clean air at 1600 m the ozone level is between 0.03 and 0.04 ppm (approximately background level), even in the rain.

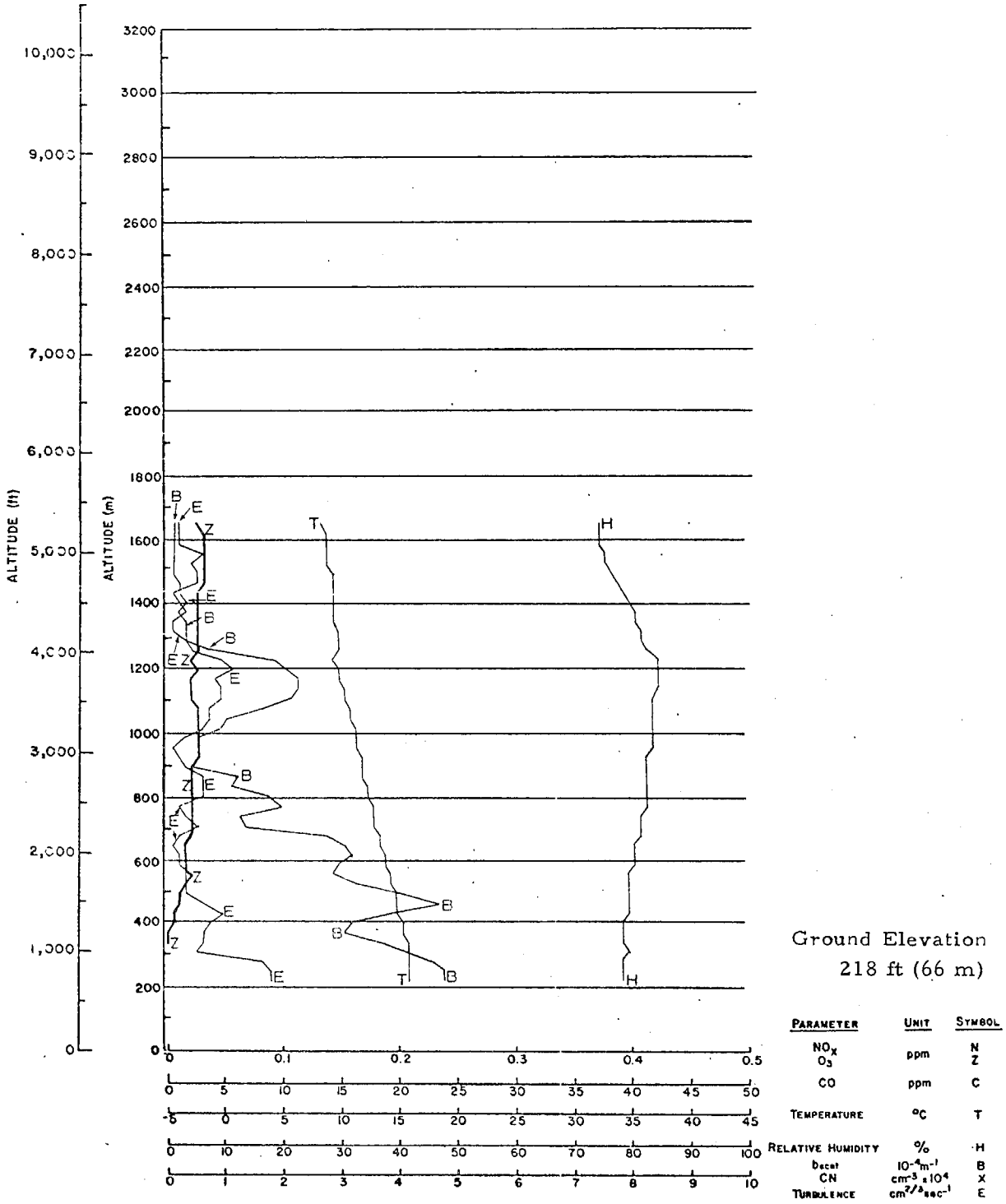

Fig. VIII-26. VERTICAL PROFILE OVER SHEPHERD (SHE) IN THE RAIN OCTOBER 18, 1972, 1020 PDT

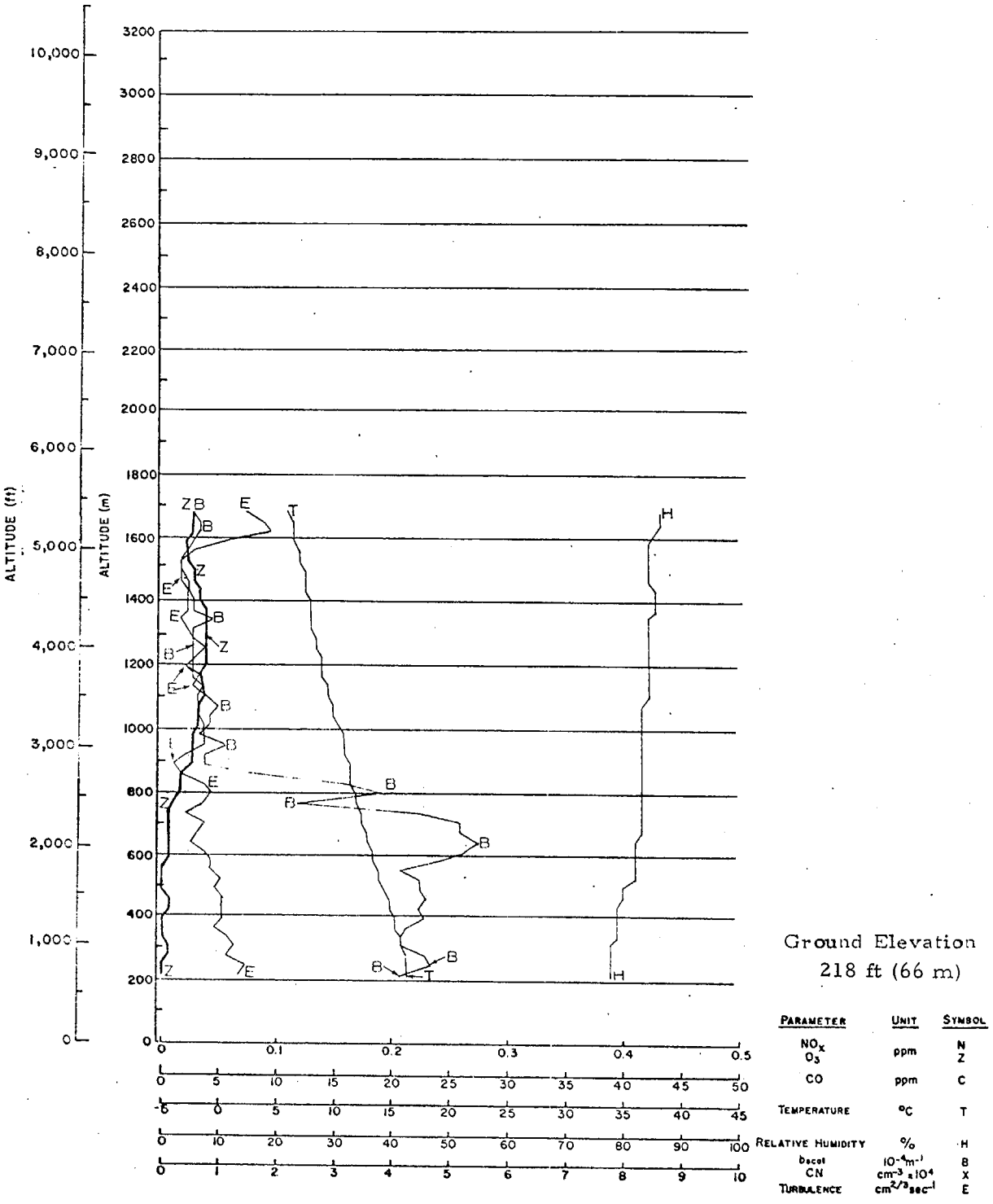

Fig. VIII-27. VERTICAL PROFILE OVER SHEPHERD (SHE) IN THE RAIN OCTOBER 18, 1972, 1357 PDT

Even though ozone is quite reactive, the above data show that, in the absence of other reactants, it is stable and will remain in the atmosphere a long time. This would be in agreement with Junge (1963) who has mentioned that the residence time of ozone in the troposphere should be on the order of one to two months.

5. Conclusions

The present data indicate that ozone is a stable component of the atmosphere and that the lack of ozone in a mixing layer near the surface is indicative of the presence of other pollutants which destroy ozone. In agreement with Miller and Ahrens (1970) and Miller et al. (1972), it appears that the equilibrium between the ozone destroying and ozone formation processes is important in determining the ozone concentration. Since the relative concentrations of old (secondary) and new (primary) pollutants in any volume of air are partially controlled by the meteorology, an understanding of meteorology is necessary to completely understand the chemical processes at work in the atmosphere.

D. Observations on the Spatial Distribution of b_{scat} and CN

1. Spatial Variations in b_{scat}

The occurrence of significant patches of large b_{scat} values in the Los Angeles Basin has been illustrated in Fig. VI-33 for September 20. Figures VIII-28 to VIII-30 show additional examples of this type of b_{scat} pattern occurring in different sections of the Basin. Morning and midday patterns are compared for August 29, 1972, and October 5, 1972, in Figs. VIII-28, and 29. Figure VIII-30 shows the transport of a patch from the Pasadena (PAS) area to the Ontario (ONT) area between midday and afternoon of October 25, 1972. Computed trajectories indicate that the source of the air parcels containing the large b_{scat} values on August 29 may have been in the Long Beach-Torrance-Hawthorne area, while central Los Angeles is a more likely source on the other two days.

It is suggested that these patches of low visibility are indicative of the prolific growth of secondary aerosols, presumably by photochemical action. This is supported by the rapid increase in b_{scat} values in spite of general decreases in the primary constituents as indicated by CO concentrations. The localized nature of the patches may be due to:

1. local concentrations of major sources, or
2. local morning meteorological conditions which are unusually favorable to aerosol growth.

Meteorological factors which might be conducive to the formation of these local patches are light winds, shallow mixing layers, and high humidities.

Patterns such as are shown in Figs. VIII-28 and VIII-30 are not unusual occurrences for pollution in the Basin. However, under other conditions, more of the Basin might be involved in such rapid aerosol growth. It is probable that the patchiness is accentuated under those conditions when a part of the Basin accumulates large amounts of primary pollutants under the meteorological conditions described above.

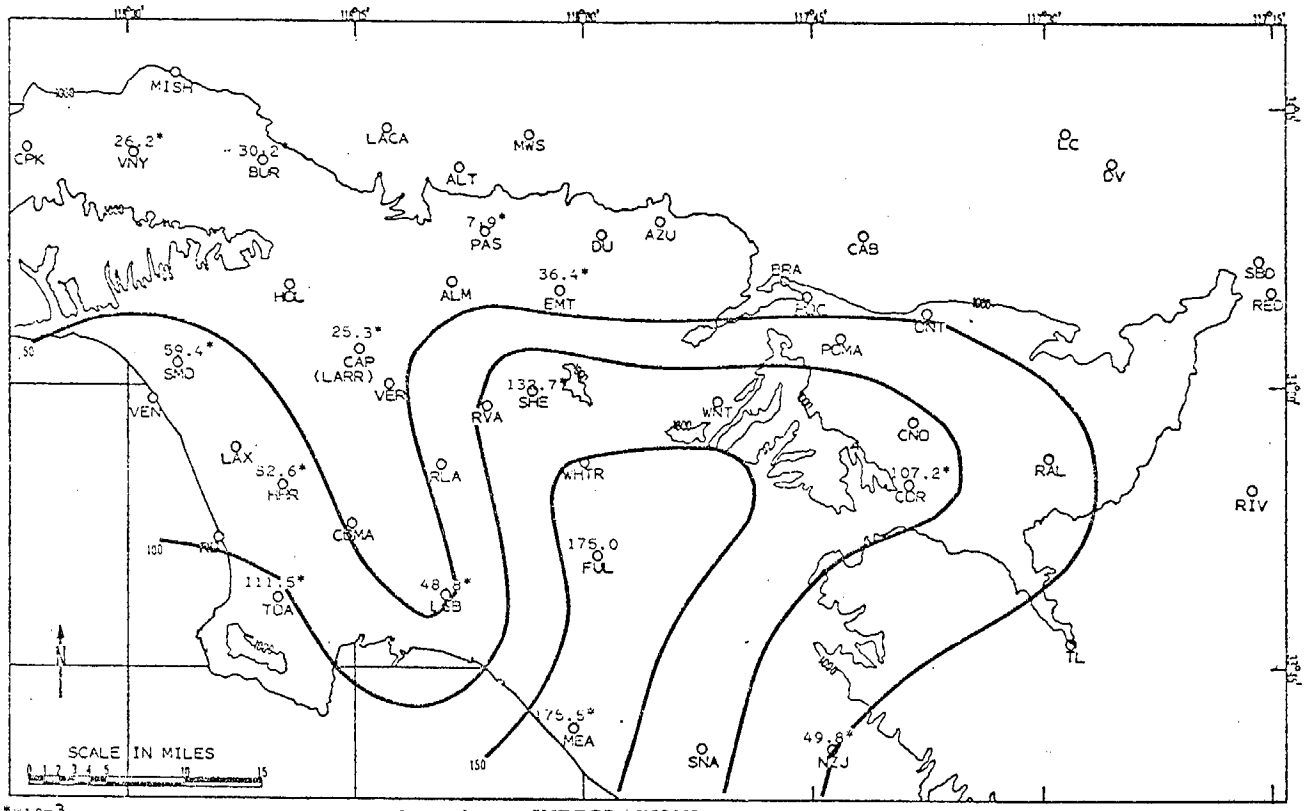

a. b_{scat} INTEGRATIONS - MORNING

August 29, 1972

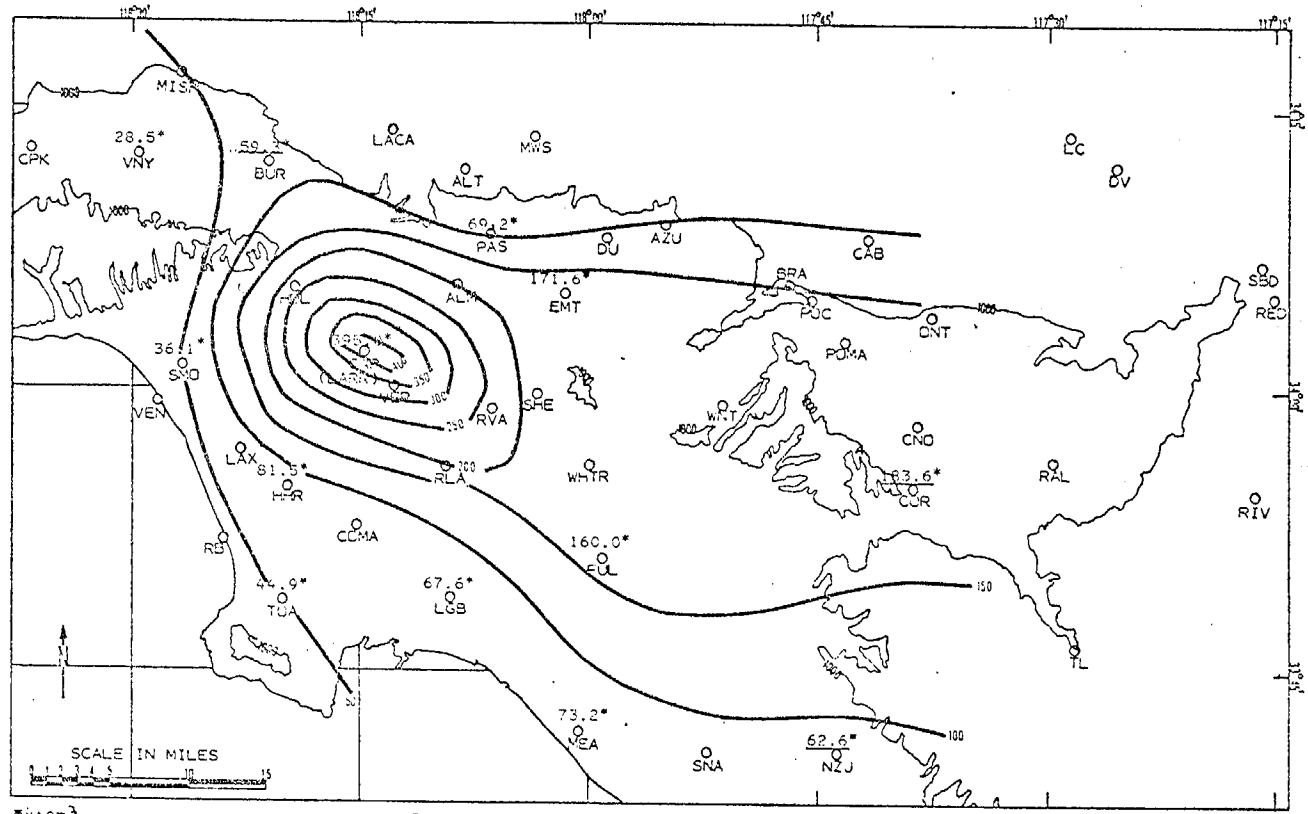

UNDERSCORE INDICATES INVERSION BROKE

b. b_{scat} INTEGRATION - MIDDAY

August 29, 1972

Fig. VIII-28. b_{scat} INTEGRATIONS THROUGH MIXING LAYER FOR AUGUST 29, 1972

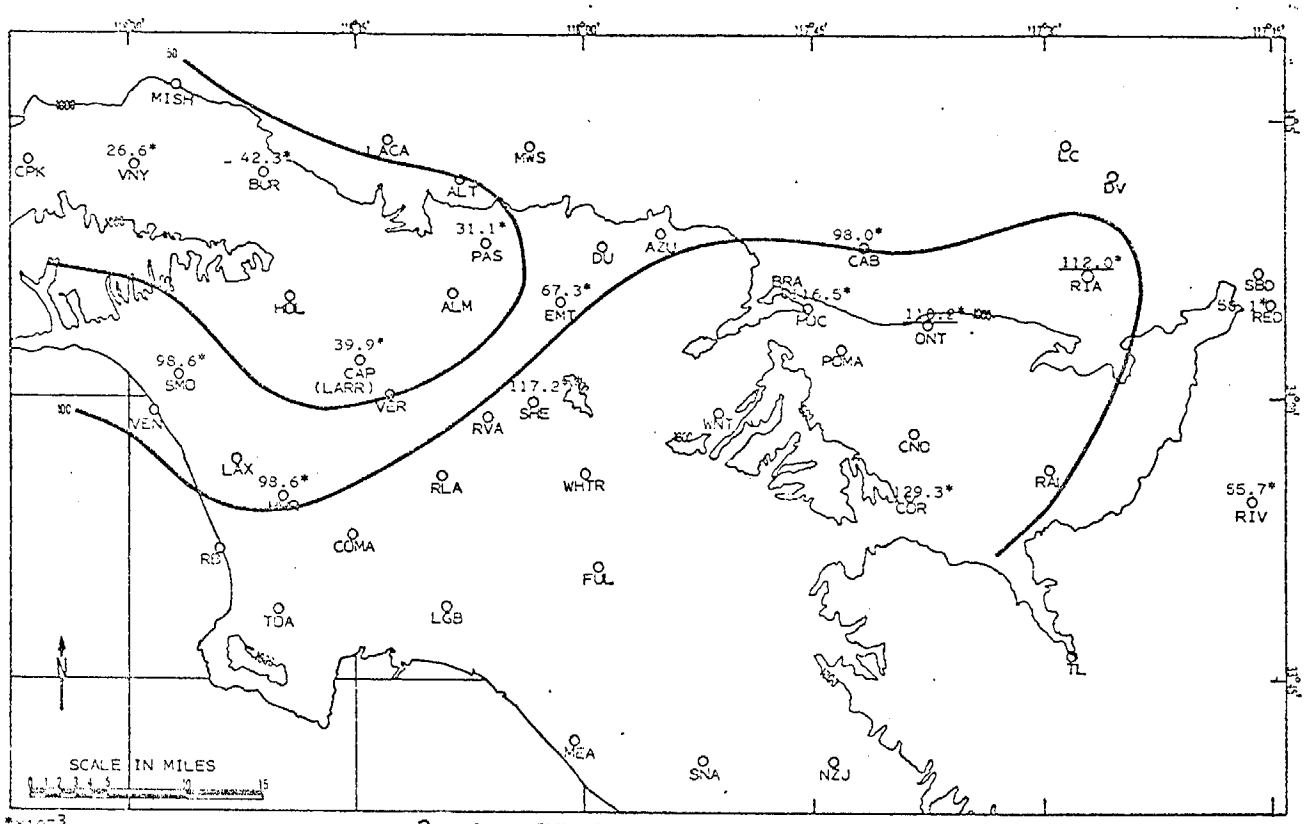

*x10⁻³

UNDERSCORE INDICATES INVERSION BROKE

a. b_{scat} INTEGRATIONS - MORNING

October 5, 1972

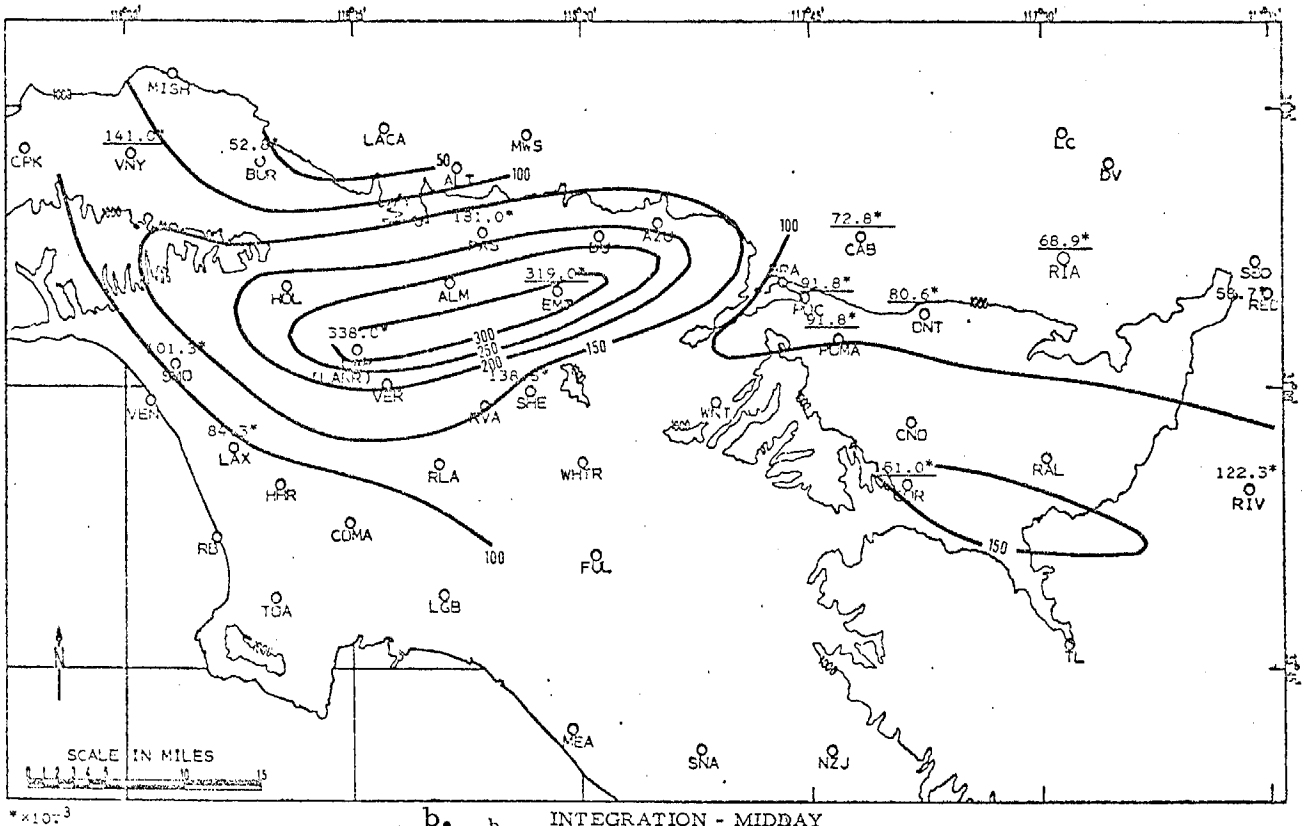

*x10⁻³

UNDERSCORE INDICATES INVERSION BROKE

b. b_{scat} INTEGRATION - MIDDAY

October 5, 1972

Fig. VIII-29. b_{scat} INTEGRATIONS THROUGH MIXING LAYER FOR OCTOBER 5, 1972

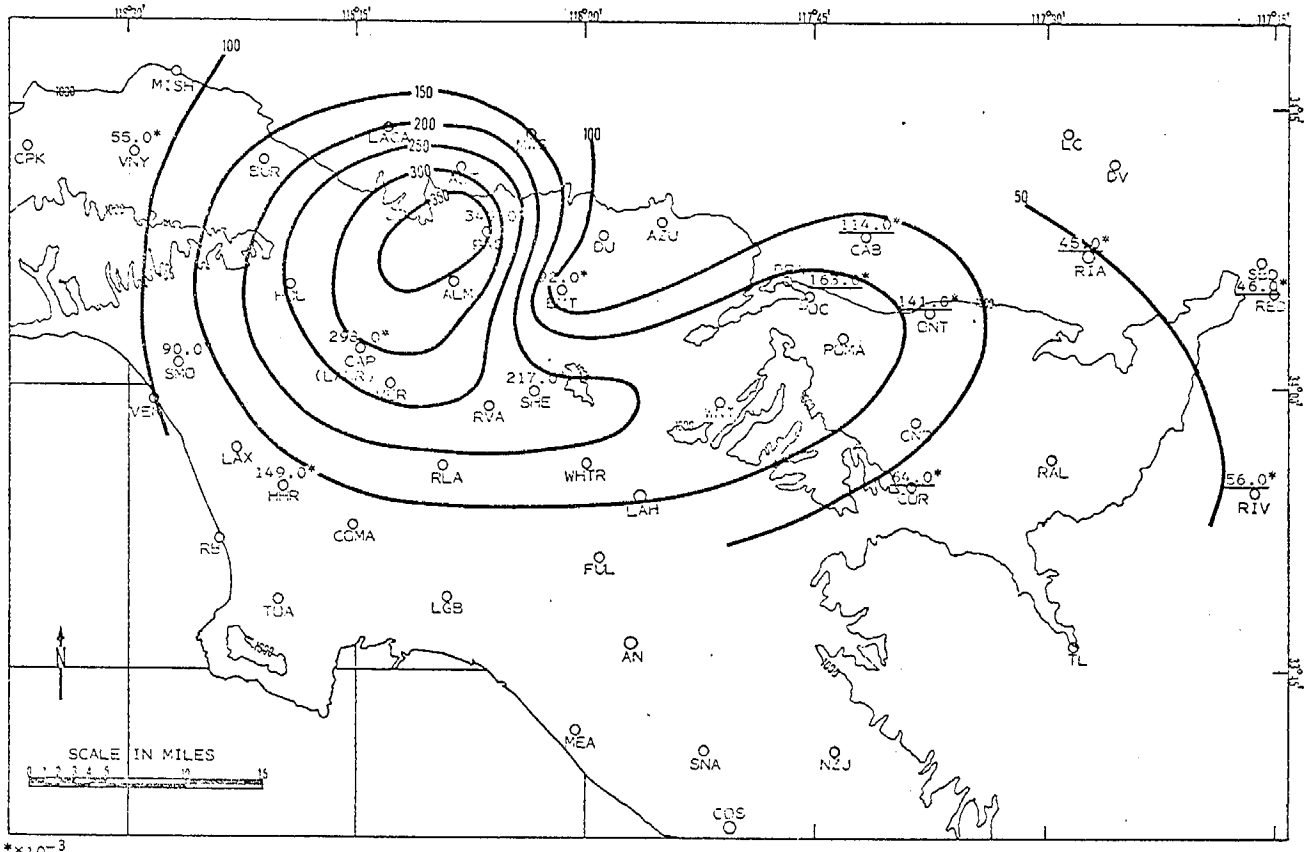

*×10⁻³

UNDERSCORE INDICATES INVERSION BROKE

a. b_{scat} INTEGRATIONS - MIDDAY
October 25, 1972

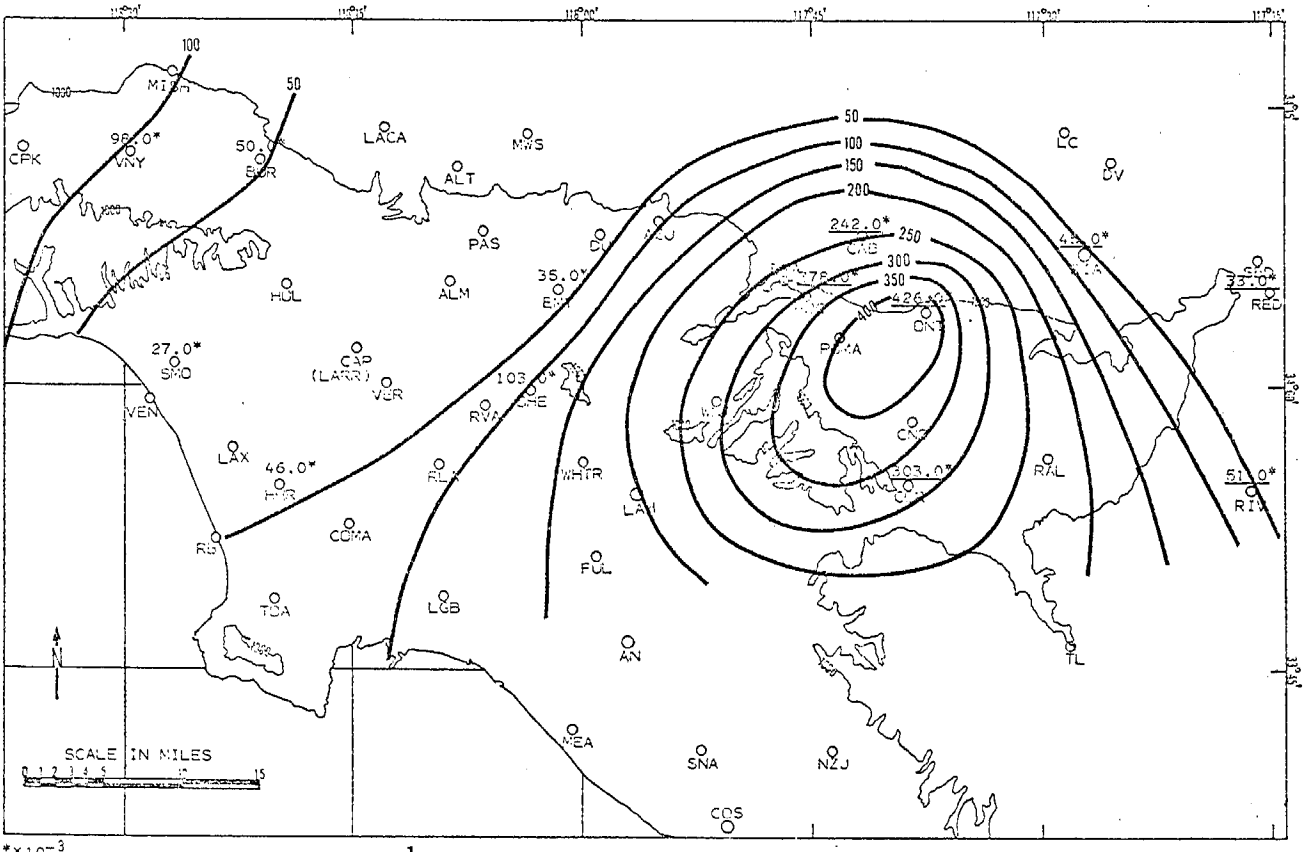

*×10⁻³

UNDERSCORE INDICATES INVERSION BROKE

b. b_{scat} INTEGRATIONS - AFTERNOON
October 25, 1972

Fig. VIII-30. b_{scat} INTEGRATION THROUGH MIXING LAYER FOR OCTOBER 25, 1972

2. Condensation Nuclei (CN) Variations

Figures VIII-31 to VIII-33 show variations in condensation nuclei for September 20, 1972 in the form of contours over the sampling area. Contour values represent peak readings of condensation nuclei within the mixing layer for each sounding. Usually, these peaks occur near the surface. Figure VIII-31 shows that the largest values of condensation nuclei correspond reasonably well with the morning traffic patterns in a manner similar to the CO peaks (Fig. VI-29). The largest CN values appeared near Burbank (BUR). By midday (Fig. VIII-32), the largest CN values occur near Burbank and the eastern San Gabriel Valley area (EMT). Very low values occur near Fullerton where the peak b_{scat} observations were made at this time (Fig. VI-33). Figure VIII-33 shows CN values for the afternoon flights with largest values again in the eastern San Gabriel Valley and near Hawthorne (HHR). Very low CN values occur near Corona which exhibited peak b_{scat} values at this time. High CN values occur in the relatively clear areas of the Basin.

From these and similar observations, it is concluded that CN measurements have considerable value as indicators of fresh combustion sources, but that CN removal processes operate effectively in the presence of large concentrations of particles in the b_{scat} range (0.1 to 1.0 μm). As a consequence, aged aerosols are characterized by low CN values.

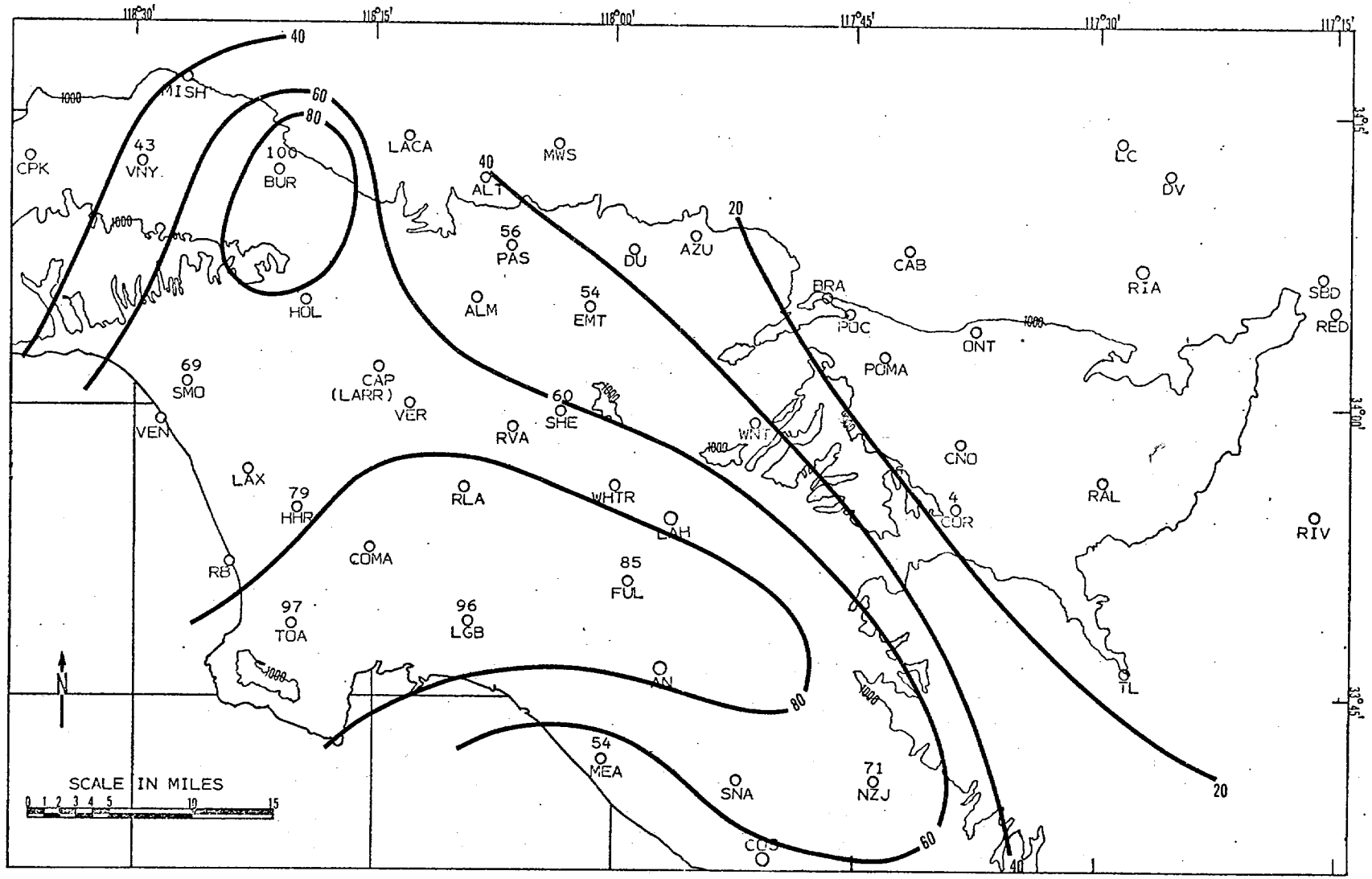

Fig. VIII-31. PEAK CONDENSATION NUCLEI CONCENTRATIONS (x 10^3 CN/CC) WITHIN MIXING LAYER - MORNING, SEPTEMBER 20, 1972

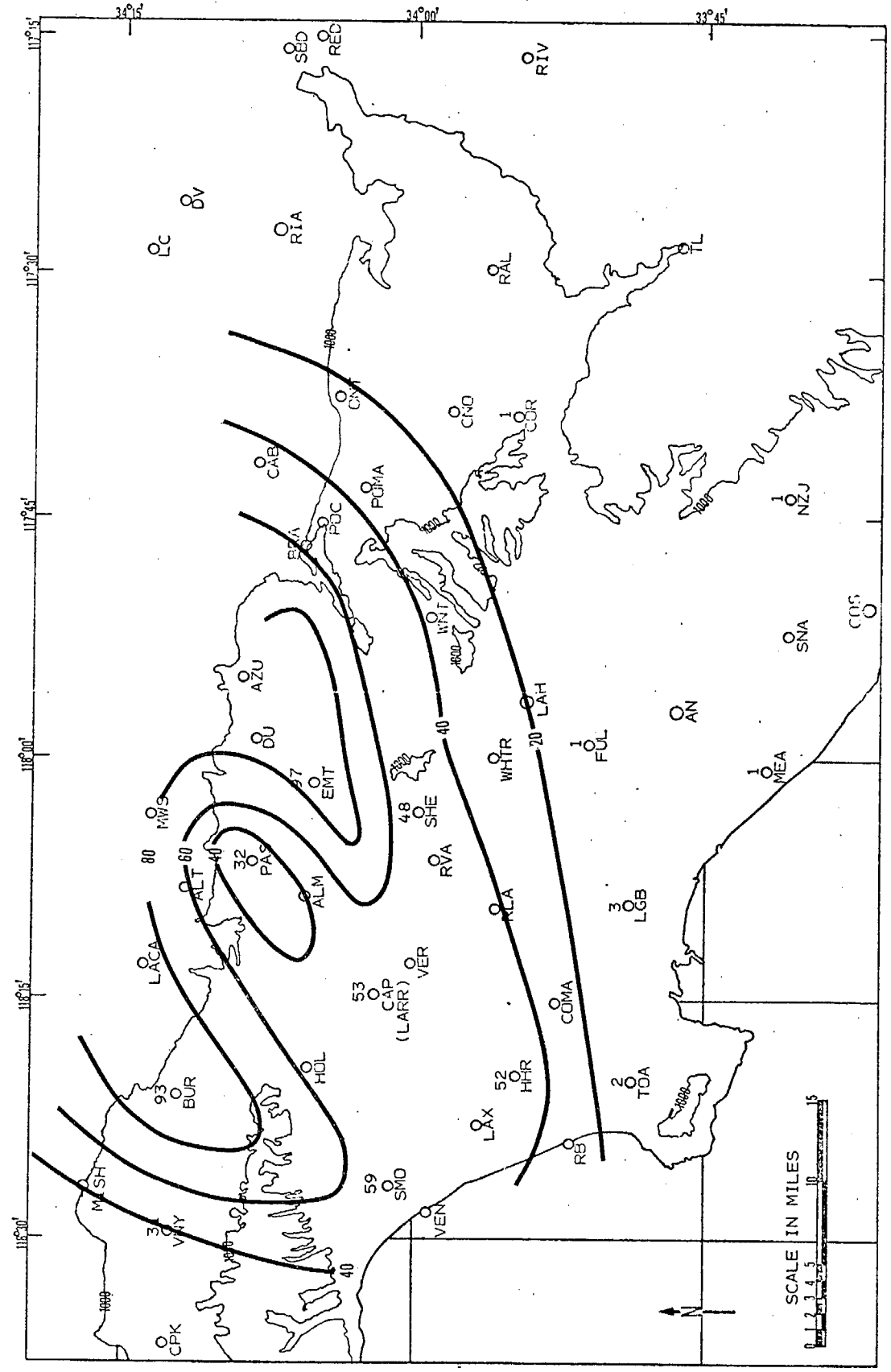

Fig. VIII-32. PEAK CONDENSATION NUCLEI CONCENTRATIONS (x 10^3 CN/CC) WITHIN MIXING LAYER - MIDDAY, SEPTEMBER 20, 1972

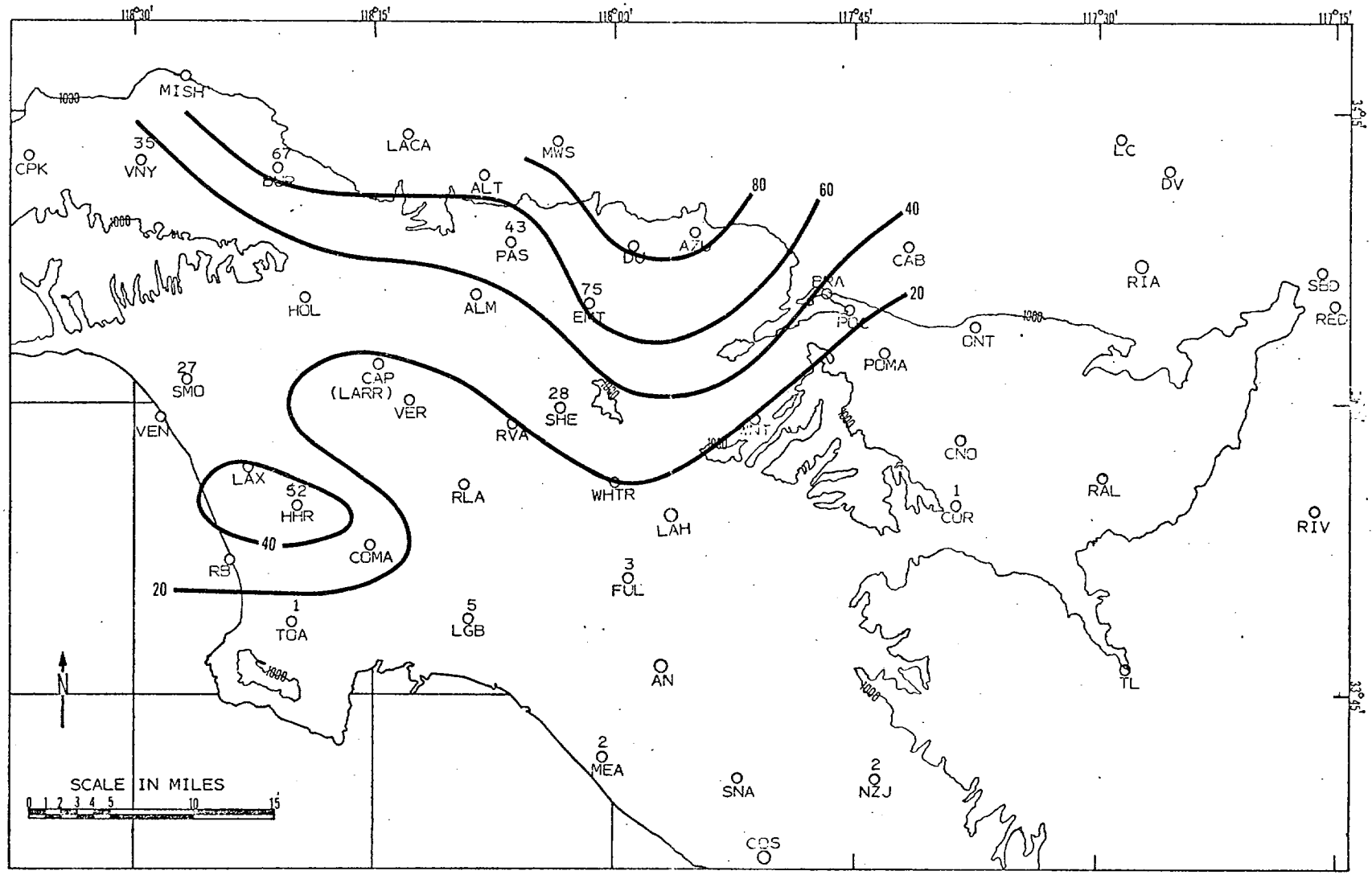

Fig. VIII-33. PEAK CONDENSATION NUCLEI CONCENTRATIONS (x 10^3 CN/CC) WITHIN MIXING LAYER - AFTERNOON, SEPTEMBER 20, 1972

E. The Relationship Between b_{scat}, Relative Humidity, and Automobile Exhaust Concentration - A Statistical Analysis

1. Introduction

The relationship between the aerosol light scattering coefficient and the sources of light scattering aerosols is as yet not well understood. From previous work on the problem of Los Angeles visibility, it is clear, however, that the light scattering fraction of the total aerosol population is influenced by both meteorological parameters (i.e., relative humidity, temperature), as well as by pollution source parameters such as the amount of emitted auto exhaust in an air parcel.

Carbon monoxide is used for the identification of the amount of primary auto exhaust in an air parcel. Since CO is a practically inert species and since over 95 percent of the CO is produced by automobile sources, it may be considered an ideal tracer for auto exhaust.

In this section, we report some preliminary results of statistical data analyses in which we have investigated the relationship between b_{scat}, CO, and relative humidity (RH).

Data for September 20, 1972, obtained from three flights of the Cessna 205, were used for the present analysis. With this aircraft, consistent data were obtained for b_{scat}, CO, and RH.

2. Results

The results of this preliminary data analysis are shown in Fig. VIII-34, in which the data for b_{scat} are plotted against relative humidity. The family of four curves correspond to ranges of carbon monoxide concentration.

At present, it is premature to draw definite conclusions since only data for one day were analyzed. Accordingly, the following statements are to be taken with caution.

For all four ranges of CO (1-2, 2-3, 3-4, and 4-5 ppm), the b_{scat} increases strongly with increasing relative humidity. Qualitatively, the observed increase of b_{scat} with RH is consistent with earlier humidification studies of other investigators. One should note, however, that b_{scat} (in Fig. VIII-34) increases by approximately a factor of three with a humidity increase from 37 to 80 percent, which

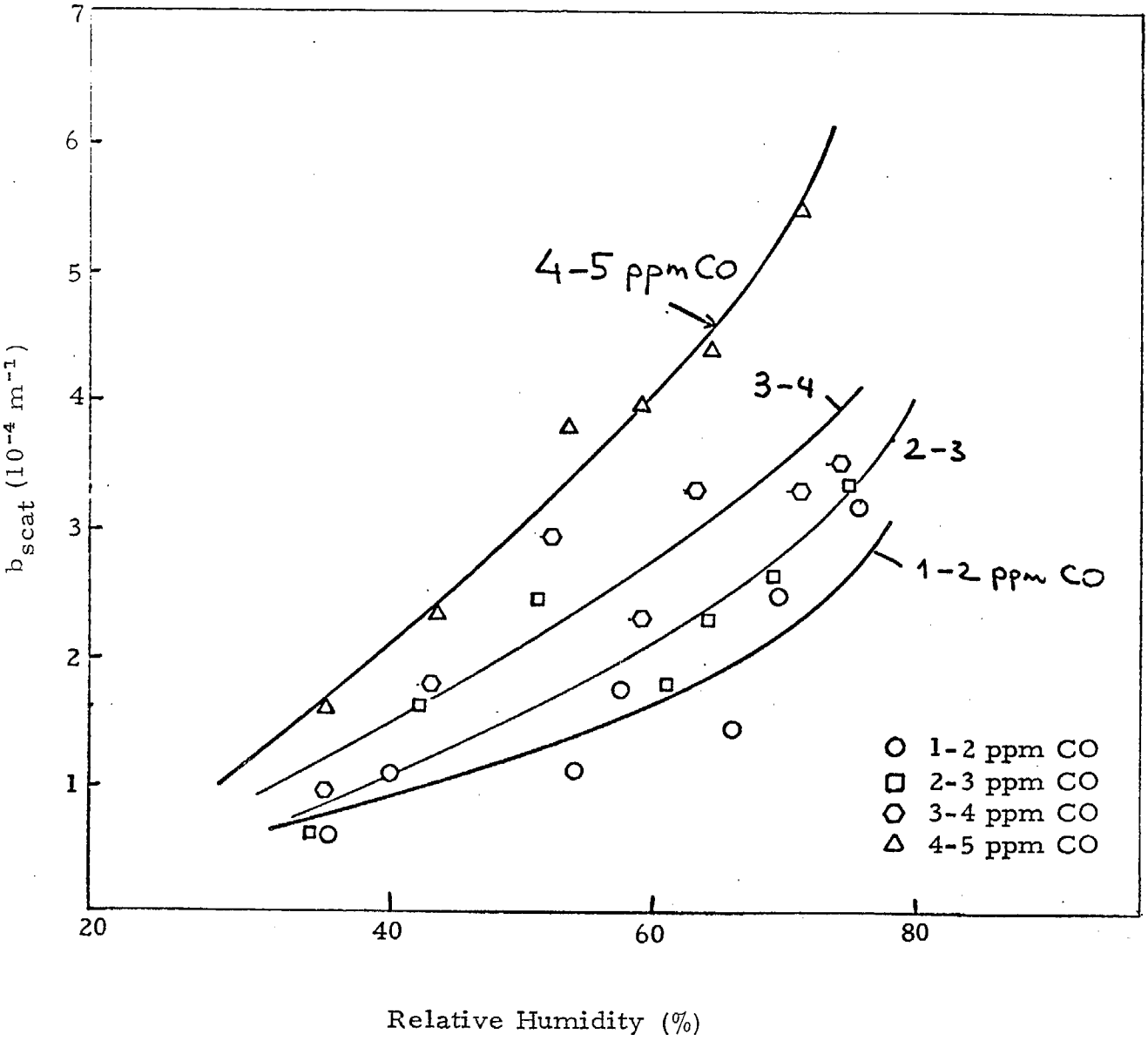

Fig. VIII-34. THE MEASURED LIGHT SCATTERING COEFFICIENT AS A FUNCTION OF RH AND CO FOR SEPTEMBER 20, 1972

is considerably more than the increase observed by humidifying ambient air.

The second observation from Fig. VIII-34 is that the light scattering coefficient also increases consistently with increasing CO concentration (i.e., with auto-exhaust concentration in the air). In fact, for the above data, the increase of b_{scat} is almost linear with CO. This latter statement, if it can be substantiated by further data analysis, is of great significance for developing effective control strategies for visible particulates. The detailed data for Fig. VIII-34 are given in Tables VIII-3 through VIII-6.

It is hoped that further data analyses along these lines could be continued in the future and extended to include ozone, residence time, and other parameters in the statistical analysis.

TABLE VIII-3

INTERVALS FOR RELATIVE HUMIDITY (%)

INTERVAL				
1	0.0	-	2.00E 01	%
2	2.00E 01	-	4.00E 01	
3	4.00E 01	-	5.00E 01	
4	5.00E 01	-	6.00E 01	
5	6.00E 01	-	6.50E 01	
6	6.50E 01	-	7.00E 01	
7	7.00E 01	-	7.50E 01	
8	7.50E 01	-	8.00E 01	
9	8.00E 01	-	8.50E 01	
10	8.50E 01	-	9.00E 01	
11	9.00E 01	-	9.50E 01	
12	9.50E 01	-	1.00E 02	

TABLE VIII-4

INTERVALS FOR CARBON MONOXIDE (ppm)

INTERVAL	RANGE			
A	0.0	-	1.00E 00	ppm
B	1.00E 00	-	2.00E 00	
C	2.00E 00	-	3.00E 00	
D	3.00E 00	-	4.00E 00	
E	4.00E 00	-	5.00E 00	
F	5.00E 00	-	6.00E 00	
G	6.00E 00	-	7.00E 00	
H	7.00E 00	-	8.00E 00	
I	8.00E 00	-	9.00E 00	
J	9.00E 00	-	1.00E 01	

TABLE VIII-5

NUMBER OF POINTS IN INTERVALS

RH/CO →	A	B	C	D	E	F	G	H	I	J
↓ 1	0	0	0	0	0	0	0	0	0	0
2	10	26	59	51	7	0	0	0	0	0
3	120	116	280	161	67	35	18	9	13	8
4	36	109	230	355	388	143	84	44	20	5
5	1	8	15	133	136	90	24	30	22	20
6	0	8	54	51	86	79	57	39	16	5
7	0	2	42	31	42	149	27	5	49	46
8	0	15	102	20	3	0	0	0	0	0
9	8	14	39	19	19	5	13	7	1	0
10	0	0	0	10	51	21	28	30	6	0
11	0	0	0	0	0	0	0	0	0	0
12	0	0	0	0	0	0	0	0	0	0

TABLE VIII-6

AVERAGES OF BSCAT

RH/CO → / ↓	A	B	C	D	E	F	G	H	I	J
1	0.0	0.0	0.0	0.0	0.0	0.0	0.0	0.0	0.0	0.0
2	1.30E 00	7.65E-01	8.27E-01	1.28E 00	1.98E 00	0.0	0.0	0.0	0.0	0.0
3	1.29E 00	1.57E 00	1.88E 00	2.18E 00	2.84E 00	5.68E 00	6.80E 00	6.50E 00	5.01E 00	4.02E 00
4	1.26E 00	1.48E 00	2.82E 00	3.46E 00	4.34E 00	5.60E 00	6.61E 00	5.58E 00	6.54E 00	6.36E 00
5	1.96E 00	1.93E 00	1.86E 00	2.54E 00	4.29E 00	5.82E 00	5.80E 00	6.25E 00	5.40E 00	4.50E 00
6	0.0	1.69E 00	2.39E 00	3.61E 00	4.54E 00	4.69E 00	5.93E 00	6.54E 00	5.33E 00	5.24E 00
7	0.0	2.46E 00	2.72E 00	3.45E 00	5.55E 00	5.34E 00	5.52E 00	5.55E 00	5.60E 00	5.60E 00
8	0.0	3.36E 00	3.54E 00	3.57E 00	3.55E 00	0.0	0.0	0.0	0.0	0.0
9	1.69E 00	2.76E 00	3.45E 00	2.71E 00	3.95E 00	3.58E 00	4.28E 00	4.86E 00	5.83E 00	0.0
10	0.0	0.0	0.0	5.01E 00	5.36E 00	5.21E 00	6.46E 00	6.39E 00	6.60E 00	0.0
11	0.0	0.0	0.0	0.0	0.0	0.0	0.0	0.0	0.0	0.0
12	0.0	0.0	0.0	0.0	0.0	0.0	0.0	0.0	0.0	0.0

ARITHMETIC STD. DEVS. FOR BSCAT

RH/CO → / ↓	A	B	C	D	E	F	G	H	I	J
1	0.0	0.0	0.0	0.0	0.0	0.0	0.0	0.0	0.0	0.0
2	7.38E-01	4.96E-01	3.95E-01	9.69E-01	1.35E 00	0.0	0.0	0.0	0.0	0.0
3	4.55E-01	7.69E-01	9.56E-01	1.32E 00	1.80E 00	1.73E 00	7.80E-01	1.17E 00	1.95E 00	8.76E-01
4	3.96E-01	1.01E 00	1.27E 00	1.82E 00	2.25E 00	1.86E 00	1.64E 00	1.13E 00	3.16E-01	1.24E-01
5	0.0	4.62E-02	9.67E-02	9.22E-01	1.60E 00	1.21E 00	8.57E-01	4.73E-01	9.50E-01	2.45E-01
6	0.0	6.26E-01	6.91E-01	1.53E 00	1.32E 00	1.03E 00	6.60E-01	2.31E-01	2.55E-01	1.16E-01
7	0.0	2.13E-02	5.43E-01	5.42E-01	6.48E-01	4.86E-01	2.88E-01	9.55E-02	1.92E-01	2.00E-01
8	0.0	1.41E-01	2.18E-01	1.01E-01	2.07E-02	0.0	0.0	0.0	0.0	0.0
9	1.95E-02	9.07E-01	4.11E-01	1.11E 00	2.61E 00	1.62E 00	1.12E 00	1.01E 00	0.0	0.0
10	0.0	0.0	0.0	5.33E-01	4.90E-01	4.04E-01	1.98E-01	2.37E-01	5.23E-02	0.0
11	0.0	0.0	0.0	0.0	0.0	0.0	0.0	0.0	0.0	0.0
12	0.0	0.0	0.0	0.0	0.0	0.0	0.0	0.0	0.0	0.0